Studies of the interfacial chemistry of gold, silicon, and an EPDM elastomer.

INFORMATION TO USERS

This manuscript has been reproduced from the microfilm master. UMI films the text directly from the original or copy submitted. Thus, some thesis and dissertation copies are in typewriter face, while others may be from any type of computer printer.

The quality of this reproduction is dependent upon the quality of the copy submitted. Broken or indistinct print, colored or poor quality illustrations and photographs, print bleedthrough, substandard margins, and improper alignment can adversely affect reproduction.

In the unlikely event that the author did not send UMI a complete manuscript and there are missing pages, these will be noted. Also, if unauthorized copyright material had to be removed, a note will indicate the deletion.

Oversize materials (e.g., maps, drawings, charts) are reproduced by sectioning the original, beginning at the upper left-hand corner and continuing from left to right in equal sections with small overlaps.

ProQuest Information and Learning
300 North Zeeb Road, Ann Arbor, MI 48106-1346 USA
800-521-0600

Studies of the Interfacial Chemistry of Gold, Silicon, and an EPDM Elastomer

By

Mong-Tung Lee

A Dissertation

Presented to the Graduate and Research Committee

of Lehigh University

in Candidacy for the Degree of

Doctor of Philosophy

in

Department of Chemistry

Lehigh University

December 3rd, 2001

CERTIFICATE OF ACCEPTANCE

Approved and recommended for acceptance as a dissertation in partial fulfillment of the requirements for the degree of Doctor of Philosophy.

Dec 3, 2001
Date

Dec 7, 2001
Accepted Date

Dissertation Director

Committee Members:

Dr. Gregory S. Ferguson, Chair

Dr. James E. Roberts

Dr. Gary W. Simmons

Dr. Richard P. Vinci

Acknowledgements

I would like to express my sincere gratitude to Prof. Gregory Ferguson for his continuous support and guidance during the course of this research. It has been a very rewarding experience for me to work with him. I also want to thank Dr. Michael Freund and Dr. Chen-Chan Hsueh for their suggestions, discussions, and help during the collaborative work in the Bunte salt project. Thanks also go to Prof. Gary Simmons for his helpful comments and suggestions. I would like to thank my other committee members, Professor James Roberts and Richard Vinci for valuable suggestions in my work. Permission from Prof. Chaudhury for using the metal evaporator is greatly appreciated. I also wish to thank Dr. A. C. Miller for his technical assistance and helpful discussions on ECSA experiments. Help from Dr. D. J. Wang on NMR and other instruments is also appreciated. The kind support from the Polymer Interface Center at Lehigh University and Office of Naval Research is acknowledged.

I enjoyed the extensive period of time working with members of the Ferguson group (Jason, Fon, Steve, Barb, Maki, Jon, Elaine, and Paul) and wish them the best. I also thank Steve Grunzinger for helpful discussions in the synthesis of the branched, semifluorinated alkanethiol. Editorial assistance from Jane Derbenwick is also greatly appreciated.

Finally, very special thanks to my family and friends for their patience and encouragement during the course of my education.

Table of Contents

List of Figures

List of Tables

Abstract

Modern device technology involves a variety materials including--metals, semiconductors, and polymers-- each with characteristic interfacial behavior. This thesis addresses important issues relating to each of these types of material. For example, self-assembled monolayers (SAMs) of alkanethiolates on gold are of interest as a model system for fundamental surface science, as well as for technological applications. We have studied the stability of alkanethiolates in self-assembled monolayers (SAMs) on gold in air and found that the rate of oxidation increases dramatically with decreasing size and amount of Au (111) grains on the surface.

We also report an electrochemical method for the preparation of self-assembled monolayers by oxidizing alkylthiosulfates, or "Bunte salts," and trapping the resulting intermediates or products at gold electrodes. Selective preparation of self-assembled monolayers on gold was accomplished by electrolysis of alkylthiosulfates in THF in the presence of tetrafluoroborate anion.

We have used molecular self-assembly to prepare highly ordered monolayer films on silicon (oxide) substrates, to prepare well-defined Si/SiO_2/polymer interfaces for studies of device-failure mechanisms. Chemical synthesis was used to introduce amine groups capable of forming covalent bonds to polyimide coatings. Formation of the monolayer adhesion promoter was confirmed by infrared and X-ray photoelectron spectroscopy, and adhesion tests showed that this structurally well-defined adhesion promoter greatly enhanced the adhesion of polyimide films to silicon.

Finally, in the area of self-assembled monolayers, a branched alkanethiol having one hydrocarbon chain and one fluorocarbon chain was synthesized as part of a collaboration study on 2-D phase behavior in self-assembled monolayers on gold.

The surface of the crosslinked terpolymer of ethylene, propylene, and diene (EPDM) was oxidized using water plasma. This hydrophilic surface became hydrophobic when heated against air, thus minimizing its interfacial free energy. However, the surface showed an unusual reconstruction, becoming more hydrophilic, when the substrate was equilibrated against air at room temperature, contrary to the behavior of most other modified polymer surfaces. These changes in surface wettability depended on the extent of modification, annealing temperature, cooling temperature, and bulk crosslinking density.

Chapter 1

Air Oxidation of Self-Assembled Monolayers on Polycrystalline Gold: The Role of the Gold Substrate

This chapter includes material that has been modified with permission from: Mong-Tung Lee, Chen-Chan Hsueh, Michael S. Freund, and Gregory S. Ferguson *Langmuir* **1998**, *14*, 6419-6423.

1.1 Abstract

Alkanethiolates in self-assembled monolayers on gold oxidize in air, in the dark, to form sulfinates and sulfonates. The kinetics of oxidation, however, vary depending on the morphology of the underlying gold, with the rate of oxidation increasing dramatically with a decrease in the size of the grains and the amount of Au (111) on the surface. This difference in kinetics of oxidation is sufficiently great to explain discrepancies among previous reports in the literature regarding the inertness of these SAMs in air. The oxidized products also desorb readily, and these species decompose under prolonged x-ray irradiation in ultrahigh vacuum.

1.2 Introduction

Self-assembled monolayers (SAMs) of alkanethiols on gold have been studied extensively because they have ordered structures and are easy to prepare, and thus allow convenient control of surface composition.[1-3] During the past several years, a number of groups have reported mass spectrometric evidence for the air oxidation of the thiolates in these SAMs to produce alkyl sulfinates and sulfonates.[4-6] The possibility of oxidation has been confirmed by other methods and attributed to photochemical processes.[7-8] A report from Fritsch and coworkers, however, provided evidence that the degree of oxidation can be extensive and fast in the *absence* of light![9] This result raises several interesting questions, primary among which is why extensive oxidation had not been evident in x-ray photoelectron (XPS) spectra in earlier reports.[2,10,11] A possible explanation for this discrepancy is that the kinetics of oxidation may vary from laboratory to laboratory, leading to different assessments of inertness. We hypothesized that the kinetics of oxidation in the systems would depend not only on the concentration of oxidants (e.g., ozone) in the ambient atmosphere, but also, and perhaps more importantly, on the size of ordered domains within the SAM. We expected that oxidation would be more facile at defect sites, for example at interfacial grain boundaries between gold crystallites, and therefore that the degree of polycrystallinity of the gold could strongly influence the kinetics of oxidation. Such defect sites are known to enhance reactivity locally in these systems.[12] Finally, it is also possible that in some instruments, particularly those without monochromators, the flux of low-energy secondary electrons

from the gold substrate is sufficient to reduce the oxidized sulfur species back to thiolates.[13]

To test these hypotheses, we have studied the oxidation of SAMs of alkanethiolates using XPS to determine the composition of monolayers and the oxidation state of their constituent sulfur atoms on gold films having different surface-grain sizes. Scanning tunneling microscopy provided images of the gold surfaces and allowed quantitative assessment of grain sizes. We have examined thermally evaporated gold films supported on both glass and on silicon supports. This chapter reports evidence for vast differences in rate of oxidation by air in the dark –i.e., complete oxidation over periods of a few days *versus* no oxidation over two weeks– for samples having different average grain sizes. Furthermore, these two types of sample were prepared by methods that initially appeared similar. Although we did not control the amount of ozone in the atmosphere above our samples, we did our experiments with both types of gold substrate in the same laboratories, and at least in one case, at the same time. This finding is important because SAMs of alkanethiols on gold have been widely used in fundamental studies of surface science, as well as for a basic platform for building sensors. Furthermore, one could image the possibility that a controllable-release medical device could be designed using SAMs of alkanethiol on gold having a rough surface.

1.3 Results and Discussion

In 1997 Ingrid Fritsch and her coworkers reported evidence using Fourier transform mass spectrometry that the degree of oxidation of dodecanethiolate SAMs on sputtered

gold can be extensive in the *absence* of light, and can even be complete within 9 h![9] In 1998, Schoenfisch and Pemberton reported fast oxidation of SAMs of octadecanethiol on mechanically and electrochemically polished polycrystalline gold.[14] Their surface Raman spectra showed that sulfonate, sulfonite, sulfate, and sulfite species were formed at the surface after 6 h of exposure to air. X-ray photoelectron spectroscopy results also confirmed the rapid and complete loss of the intensity of the thiolate sulfur 2p peak at 162 eV.[14] Futhermore, their work identified ozone as the oxidant in air responsible for this reactivity. Subsequently, oxidation of octadecanethiolate overlayers on gold clusters[15] by O_3 within an hour has also been reported.[16]

Obviously, this extensive oxidation reported by Fritsch could not be due to the known photochemical processes, and thus the speed of the oxidation posed a huge apparent discrepancy in the kinetics of oxidation between Fritsch's laboratory and those of others. To resolve this discrepancy, our hypothesis was that the gold substrates themselves might play an important role in determining the quality of SAMs adsorbed on them. The quality of the SAMs, we expected, would in turn at least partially determine their level of inertness toward oxidation. There are several factors that influence the texture of gold films during the their preparation, and we expected that differences in this texture, specifically grain sizes, would give monolayers having different levels of inertness.

1. *The method of deposition*: Evaporated gold films are usually considerably smoother than sputtered gold films.[17,18] In the sputtering technique, energetic target atoms or clusters of atoms are ejected and condensed onto a substrate to form

a film. The sputtered atoms have a much higher kinetic energy than those in an evaporation and thus are more likely to become embedded within the substrate surface and have limited surface mobility. In addition to surface damage caused by such energetic impacts, the formation of a high areal density of nucleation centers results in a rough surface. As a result, sputtering generally fails to produce large and oriented crystallites on substrates.[17,18] Because grain boundaries in SAMs are known to be more reactive than regions within ordered domains,[12] we expected that the rough surface or less oriented crystallites of Fritsch's sputtered gold films might be responsible for the unusually fast oxidation. Similar to the sputtering process, polishing polycrystalline gold also results in a rough surface.

2. *Rate of Deposition*: In general, higher deposition rates produce gold films with rougher surfaces. Rechelt and Lutz used X-ray diffraction to study gold films deposited at various rates and found a strong dependence of the evaporation rate on the transition temperature required to obtain a given crystal quality.[19] At higher evaporation rates, the substrate temperature necessary to obtain well-oriented surfaces increased.[19]

3. *Substrates*: Evaporation of gold on mica produces gold films with larger grains than on silicon wafers (100) because its crystal-packing parameters are close to those of gold, so that near-epitaxial growth is possible. Epitaxial growth of gold films on mica has been extensively studied using scanning tunneling microscopy.[20-24] DeRose demonstrated that baking mica before the evaporation of gold helped reduce the surface roughness and suggested that heating the mica helped to

eliminate contamination by outgasing.[25] Nonetheless, in our studies we found that silicon wafers and glass microscope slides provided convenient substrates that allowed us to vary the quality of deposited gold films widely.

4. *Temperature during the evaporation.* Evaporation of gold onto unheated substrates tends to result in gold films with larger numbers of small grains than evaporations onto heated substrates.[26] Scanning tunneling microscopy (STM) of gold films have shown that during a room temperature evaporation, nuclei do not fuse together into larger single crystallites as the films coalesce.[26] X-ray diffraction has also shown that weak epitaxial growth of gold was deposited on mica near room temperature, resulting in a highly textured film and the presence of (200), (220), and (311) reflections from atomic planes normal to the substrate.[26] An increase in the substrate temperature during the thermal evaporation resulted in flatter and smoother gold films.[22,23,25] Dishner and coworker reported that the surface of gold on mica became rough again if the substrate temperature was greater than 380 °C, and they attributed this effect to three-dimensional growth being favored over two-dimensional growth at such a high temperature.[21] Höpfner and coworkers, however, have reported that evaporation at 500 °C gave large crystalline areas with a moderate number of defects.[27] The stability of substrates at high temperature also has an important effect on the quality of resulting films in heated evaporations. Mica, for example, starts to decompose when it exceeds 600 °C, and of course, glass microscope slides soften at ~ 720 °C.[28]

5. *Annealing.* Annealing provides thermal energy for atoms that have been

deposited to rearrange and form larger and energetically favored crystals. It can therefore produce smoother surfaces.[19] These larger grains are produced as smaller grains merge as the substrate temperature increases. In addition, annealed films approach complete [111] termination.[21] Little change of surface morphology, however, would be expected for samples that had originally been deposited at high temperature.[23]

6. *Film Thickness*: Chidsey et al. compared gold films on mica that were either thickness on surface morphology.[23] Holes between grains were observed on the 500-Å sample, though no holes were found in the thicker sample.

In our studies, gold films were prepared using thermal evaporation onto silicon and onto glass substrates, and we varied the rate of evaporation to control the surface morphology. Gold was evaporated at a rate of approximately 1.5 Å/s onto glass and onto silicon substrates that had been treated with (3-mercaptopropyl)trimethoxysilane as an adhesion promoter to produce gold films for adsorption of SAMs (films **1/glass** and **1/silicon**).[29] Likewise, evaporation onto substrates at a slower rate, approximately 0.5 Å /s, produced a second set of films for comparison (films **2/glass** and **2/silicon**). Scanning tunneling microscopy (STM) in air revealed differences in the morphologies of the films deposited at different rates (Figure 1.1): films **1/glass** and **1/silicon** had smaller average grain sizes than the corresponding samples, **2/glass** and **2/silicon**.[30]

A standard intercept method was used to estimate the average surface-grain size (a) from the STM images using equation 1.1, where the mean intercept distance (l) is determined by

Figure 1.1. STM images of thermally evaporated gold films grown at: a) 1/glass; b) 1/silicon; c) 2/glass; and d) 2/silicon. The sample bias was 20 mV *versus* the tip with a constant tunneling current of 2 nA.

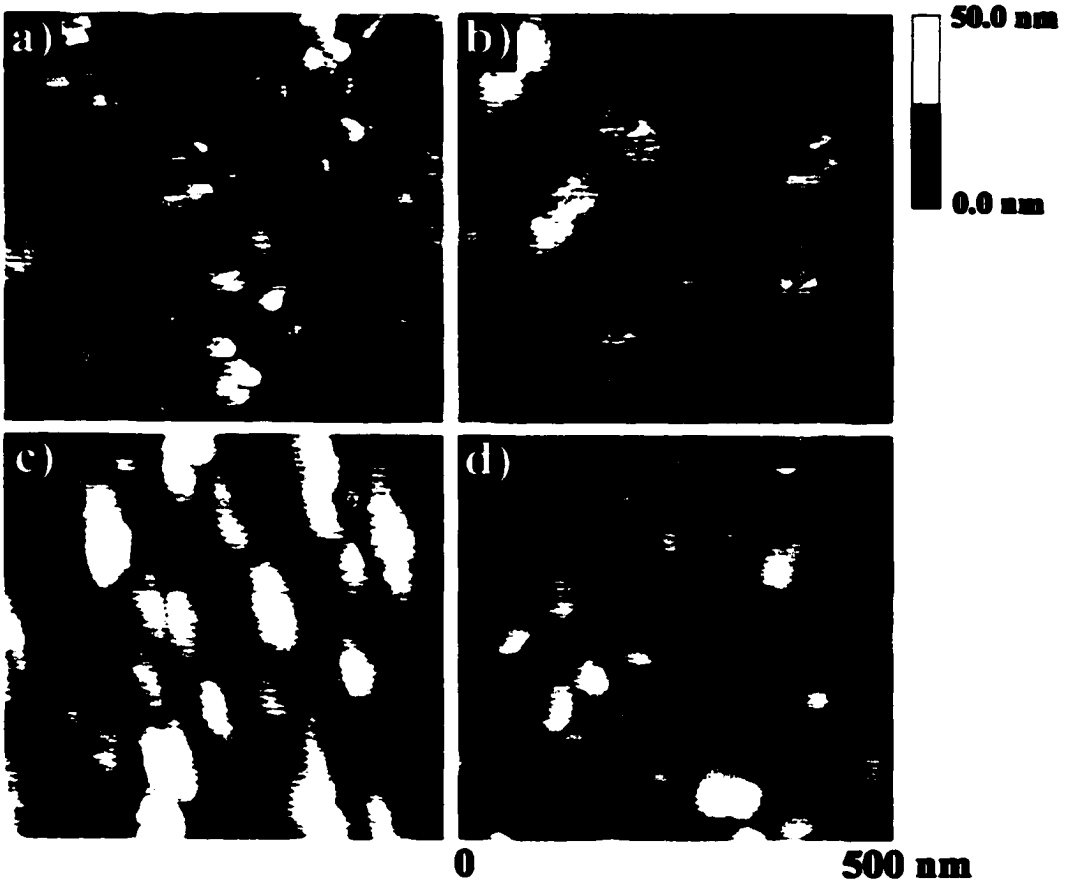

$$a = (4l^2)/\pi \qquad (1.1)$$

dividing the length of a trace across the image by the number of grain boundaries that intersect the trace.[31] The results of this analysis for diagonal lines across 1-μm x 1-μm images of the samples in Figure 1.1, presented in Table 1.1, demonstrate a significant change in surface-grain size (or areal density of grain boundaries) as a function of evaporation rate.[32] For each substrate, the slower growth rate resulted in approximately a six-fold increase in the average surface-grain size. We note this analysis gives only an approximate measurement of grain sizes, as it assumes that the grains are symmetric ("equiaxed").[31]

We also found that, in general, gold films on glass had larger grains than those on silicon wafers, even though the surface of silicon wafers appear to be smoother than glass by STM.[33] A possible explanation is that the heat generated during the thermal evaporation was dissipated faster onto a silicon wafers due to its higher thermal conductivity.[34] Gold atoms deposited onto a silicon surface could thus quickly lose thermal energy and become less mobile and unable to form grains with larger areas. We don't believe the crystallinity of silicon to be of direct importance because the native oxide overlayer is amorphous. Furthermore, the (3-mercaptopropyl)trimethoxysilane adhesion promoter on the glass slides and silicon wafers likely left both the surfaces undifferentiated chemically.

X-ray diffractometry (XRD, $\theta/2\theta$ scan in the range of 2-90° 2θ) of samples **1/glass** and **2/glass** as seen in Figure 1.2, revealed the expected predominance of preferred (111) orientation of the gold crystallites, with smaller (200), (220), and (311) reflections.[35]

Table 1.1. Average Surface-Grain Size for Gold Films Grown at Different Evaporation Rates, Determined Using a Standard Intercept Method.

	1/glass	2/glass	1/silicon	2/silicon
N*	45	19	73	31
l (nm)	31	74	19	46
a (nm^2)	1200	7000	460	2700

* The grain-boundary intercepts were determined along diagonal traces 1-μm x 1-μm STM images of the samples in Figure 1.1.

Figure 1.2. The X-ray Diffractograms (XRD, θ/2θ scan in the range of 2-90° 2θ) of samples (a) gold evaporated on glass at 0.5 Å/s; (b) gold evaporated on glass at 0.5 Å/s.

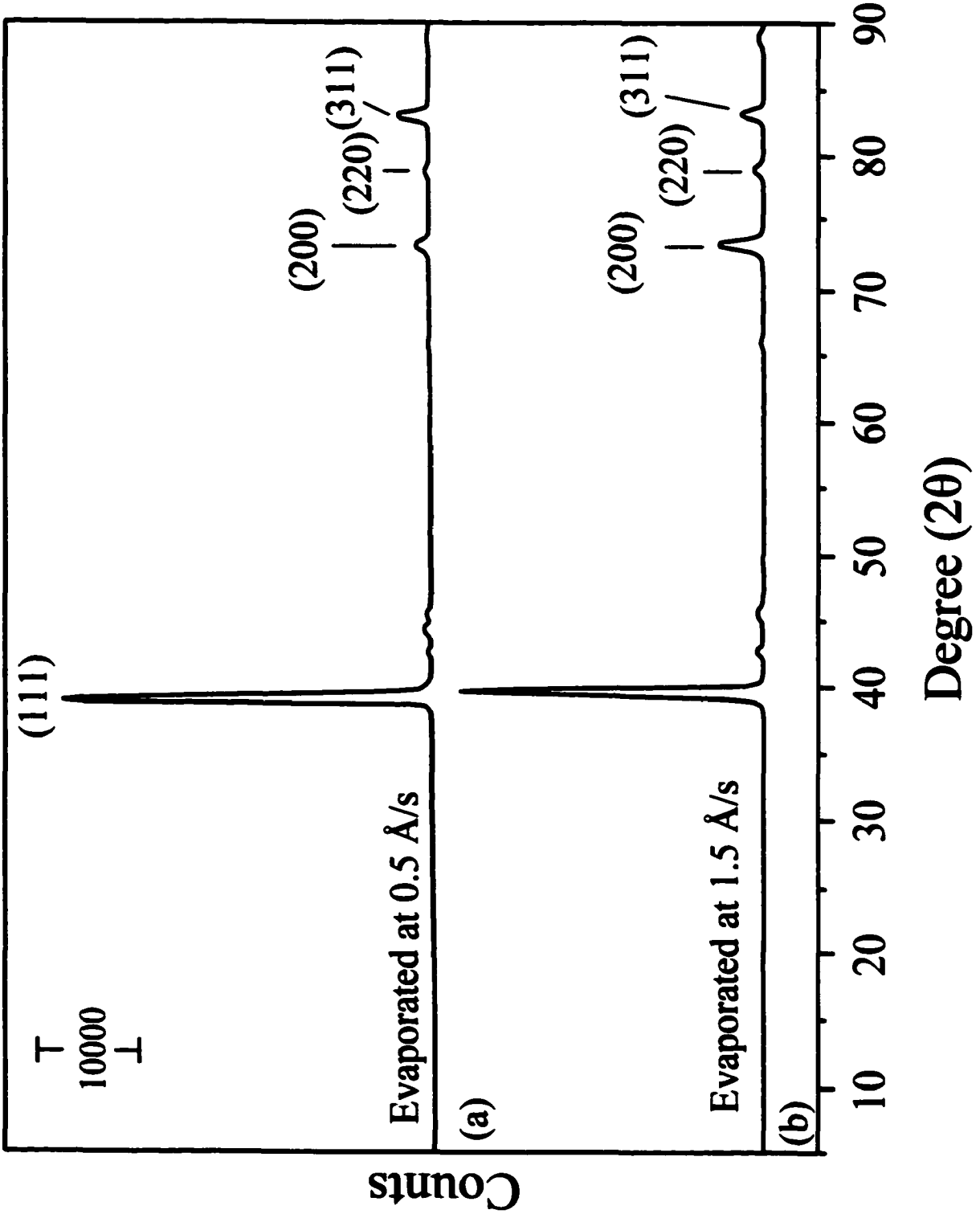

Sample **1/glass**, grown at the faster rate, showed more intense reflections due to these minor components than did sample **2/glass** by factors of about 3-5 (Table 1.2). The fraction of the surface displaying the crystal faces corresponding to these reflections may be important because at least one of them, Au (100), is associated with an incommensurate arrangement of the monolayer lattice and correspondingly weaker thiol-gold bonding, relative to the commensurate monolayer on Au (111).[36] We have focused in this study on the effect of the differences elucidated by STM and XRD on the propensity of SAMs grown on these surfaces to oxidize in air.[37]

Several samples were cut from gold films **1/glass** and **2/glass** and immersed into a 50 mM solution of dodecanethiol in ethanol at room temperature. After a minimum of 48 h in this solution, duplicate samples of each type were removed, rinsed with ethanol, and dried with a stream of nitrogen. One of these samples was used to measure contact angles of water and of hexadecane; the other was stored under ambient conditions in the dark for specific periods of time prior to XPS analysis. Samples **1a/glass**, **1a/silicon**, **2a/glass**, and **2a/silicon** were transferred from the thiol solutions, following rinsing and drying, into the spectrometer within 20 min to minimize their exposure to air. Samples **1b/glass**, **1b/silicon**, **2b/glass**, and **2b/silicon** were stored in air in the dark for 12 h prior to XPS analysis. Samples **1c/glass**, **1c/silicon**, **2c/glass**, and **2c/silicon** were stored in air in the dark for 6 d prior to analysis by XPS.[38]

Survey XPS scans of SAMs on the gold films having small surface-grain sizes showed an increase in the amount of oxygen and decrease in the amount of carbon, relative to gold, as a function of the amount of time the sample had been exposed to air

Table 1.2. Normalized Peak Areas from θ/2θ X-ray Diffractograms of Evaporated Gold Films.

reflection (hkl)	normalized peak areas (%) for sample **1/glass**	reflection (hkl)	normalized peak areas (%) for sample **2/glass**
111	100	**111**	100
200	3.51	**200**	1.23
220	1.56	**220**	0.323
311	4.09	**311**	1.39

(Figure 1.3). atomic ratios of oxygen : gold and carbon : gold, taken from the survey scans of these samples, are reported in Table 1.3. Little or no oxygen was present in the survey scans of the samples that were exposed to air for only a short time (**1a/glass** and **1a/silicon**). The samples that had spent several hours to days in air, in contrast, showed much larger amounts of oxygen. High-resolution spectra of the sulfur 2p region of samples **1a-c/glass** and of samples **1a-c/silicon** showed a corresponding decrease in the amount of thiolate sulfur (162.0 eV, $2p_{3/2}$; 163.2 eV, $2p_{1/2}$) and the appearance of a broad emission characteristic of oxidized sulfur as the amount of time samples had spent in air increased (Figure 1.4). The high-resolution scans of the sulfur 2p region of sample **1c/glass** and of sample **1c/silicon**, in fact, revealed only a broad doublet centered at approximately 168.0 eV and no doublet due to thiolate sulfur, indicating complete oxidation of these monolayers. The range of binding energy spanned by this photoemission is consistent with the presence of both sulfonate (ca. 168.4 eV) and sulfinate (ca. 166.5 eV) species.[40]

The dramatic decrease in carbon photoemission (C : Au ratio, Table 1.3) as samples were exposed to air for longer periods of time is consistent with partial desorption of the monolayers as a result of their storage in air. To assess the possibility of decomposition or desorption during the XPS measurement, we conducted a separate control experiment in which a sample was prepared in the same way as **1c/glass**, and after 6 d in air in the dark, an XPS spectrum of this sample also showed complete oxidation of the thiolate species in the SAM. Figure 1.5 displays high-resolution XPS spectra of this sample taken over the course of 16 h of x-ray irradiation in ultrahigh vacuum and shows a decrease of

Figure 1.3. Survey XPS spectra of self-assembled monolayers that had been stored in air in the dark for approximately 20 min **(1a/glass** and **1a/silicon),** 12 h **(1b/glass** and **1b/silicon),** and 6 d **(1c/glass** and **1c/silicon).** These SAMs were formed by adsorption of dodecanethiol on gold films that had been evaporated at a rate of 1.5 Å/s onto either glass or silicon substrates. The spectrum for sample **1c/silicon** has been normalized to the same peak height for the Au $4f_{7/2}$ peak as found in spectra **la/silicon** and **lb/silicon.**[39]

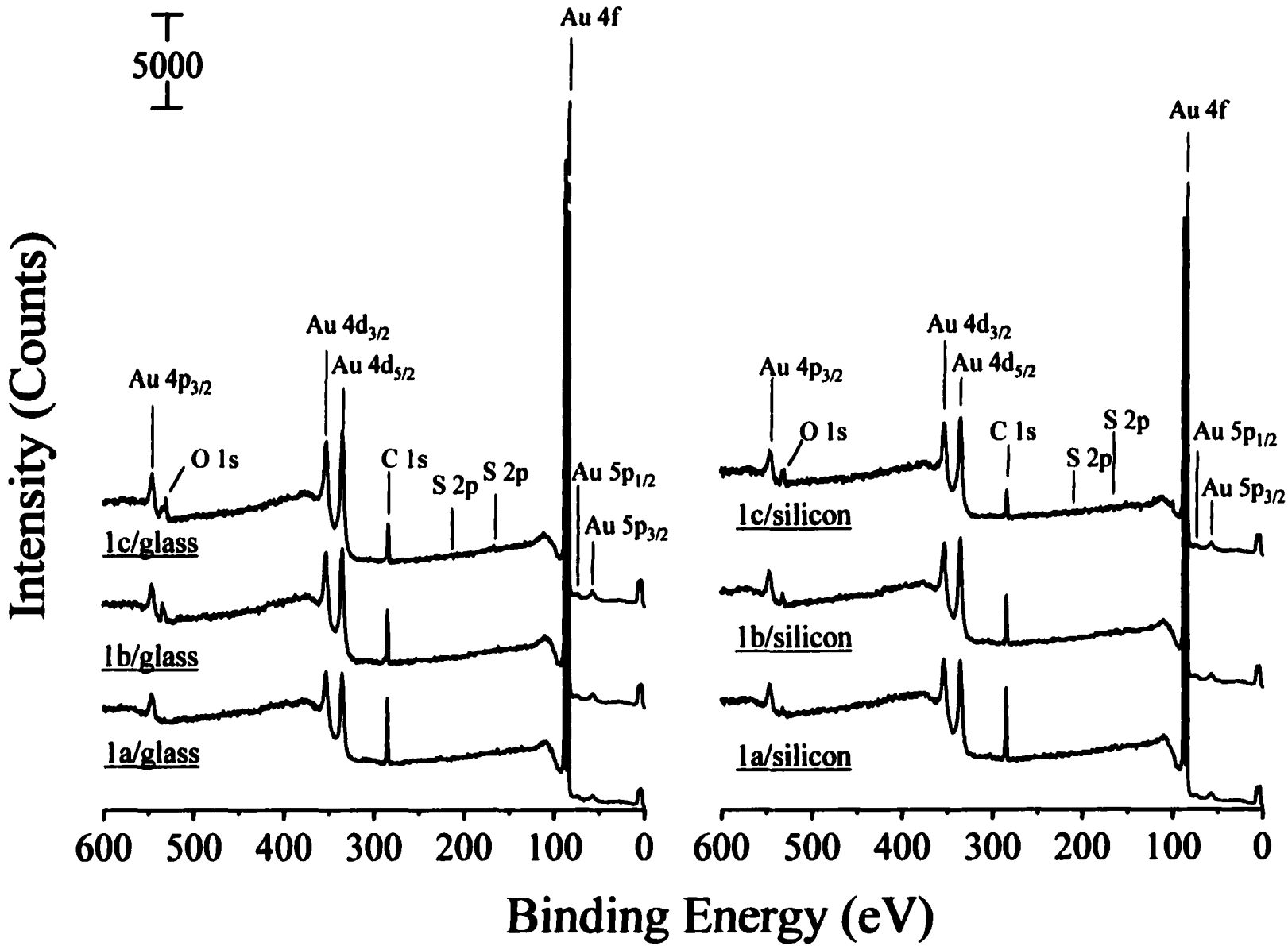

Table 1.3. Ratios of Corrected[40] Photoemission Intensity from Survey XPS Spectra of Samples **1a-c/glass** and **1a-c/silicon.**

Element / Sample	O/Au	C/Au
1a/glass	< 0.05‡	2.6
1b/glass	0.41	1.5
1c/glass	0.50	0.95
1a/silicon	0.11	2.5
1b/silicon	0.16	1.7
1c/silicon	0.50	0.96

‡ The height of the O 1s peak was less than twice the standard deviation of the noise in this spectrum.

Figure 1.4. High-resolution XPS spectra of the sulfur 2p region for samples **la-c/glass** and **la-c/silicon).**

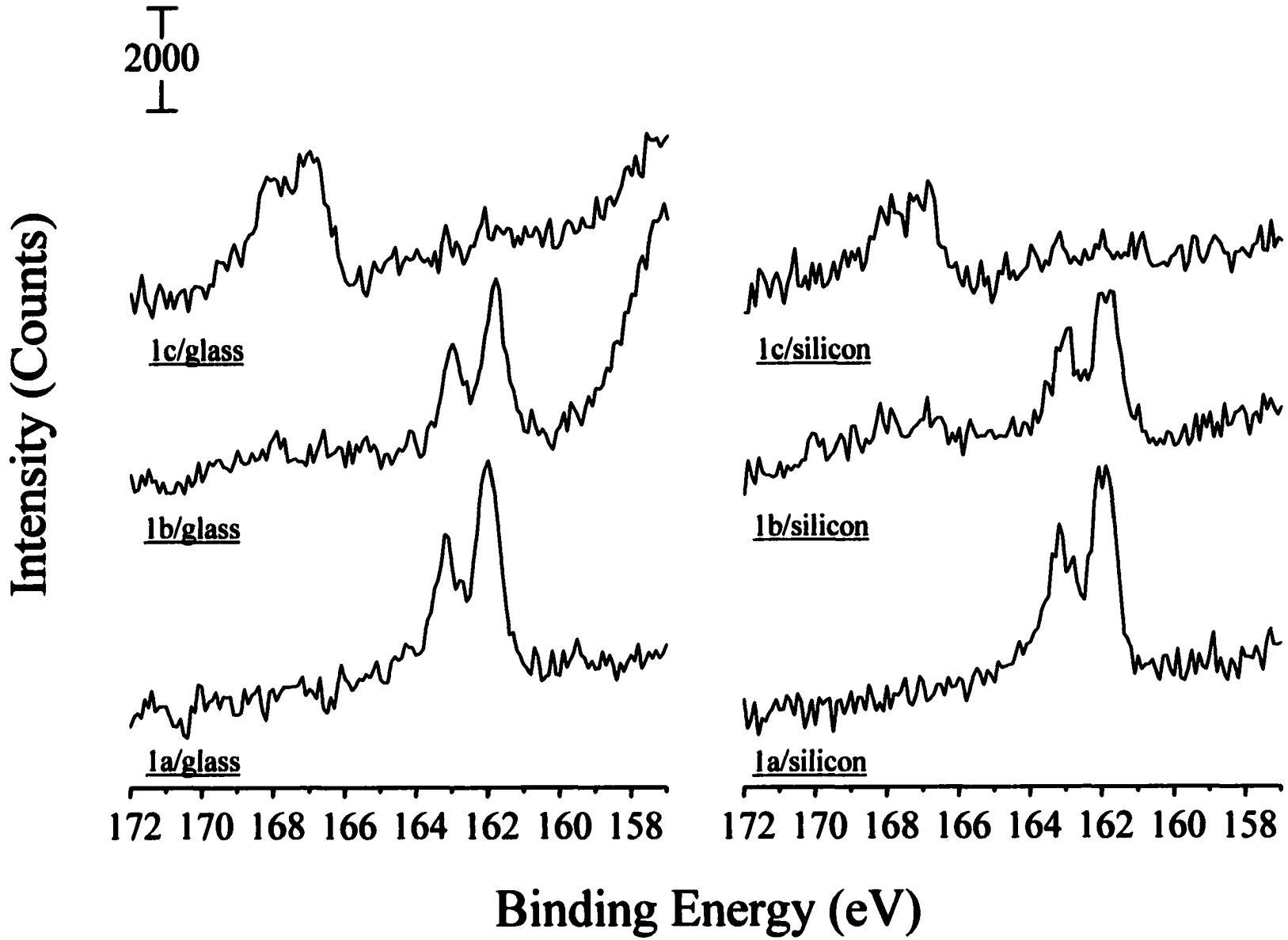

Figure 1.5. High-resolution XPS spectra of the sulfur 2p region for a sample prepared and treated in the same way as **1c/glass** as a function of time of exposure to x-rays in the spectrometer: a) initial spectrum; b) I h; c) 3 h; d) 6.5 h; and e) 16 h.

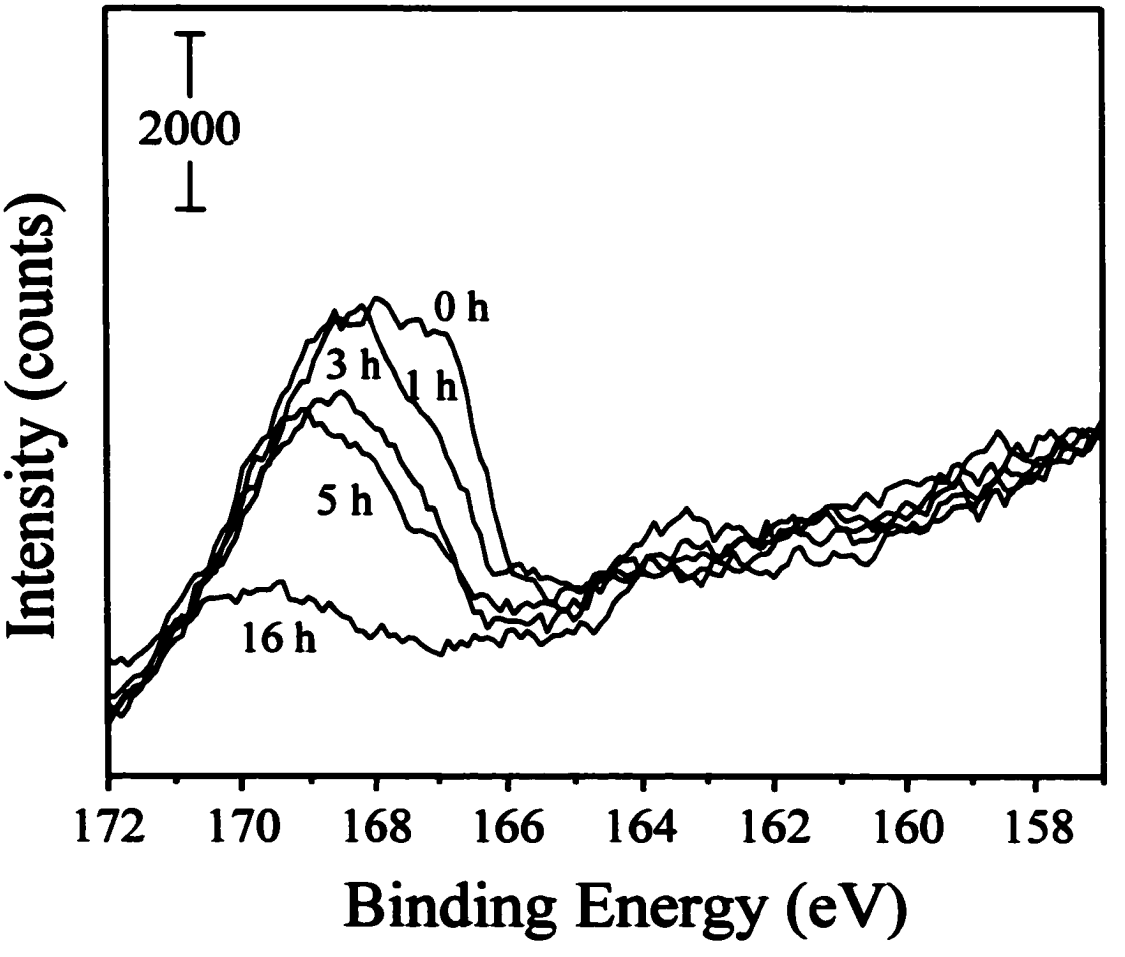

approximately 71% of the sulfur 2p signal during that period. The loss of this signal could be due to damage of the film resulting from exposure to x-rays over this extended time,[13] for example by extrusion of SO_2 or SO_3. This explanation is consistent with the fact that over same period of time the carbon signal did not decrease. As the sulfur 2p photoemission decreased in intensity, it shifted to higher binding energy, suggesting that the sulfinate species desorb or decompose preferentially to the sulfonates. This loss of oxidized sulfur may explain why some have observed oxidation by mass spectrometry but not by XPS.[41] Finally, we did not find evidence for reduction of the oxidized sulfur species back to thiolates, despite the flux of low-energy secondary electrons from the gold substrate.[13]

Analogous samples prepared on the gold films that had been evaporated at a slower rate (**2/glass** and **2/silicon**) contrasted starkly in their behavior in air in the dark: they were inert to oxidation over the same periods of time studied for samples **1a-c/glass** and **1a-c/silicon**. Although survey XPS scans of these samples showed small amounts of oxygen (Figure 1.5), high-resolution spectra of the sulfur 2p region showed no evidence for oxidation of the thiolate species in the SAM (Figure 1.6). An additional sample that was allowed to age in air for two weeks in the dark showed a large increase in the amount of oxygen in the survey scan (**2d/glass**, Figure 1.5 and Table 1.4), but again failed to show evidence for oxidation of the thiolate species in the high-resolution spectrum of the sulfur 2p region (Figure 1.7). We attribute the added oxygen to adventitious contamination. Our evidence was further supported by the STM data from Poirier and his coworkers that the oxidation of decanethiolate monolayer under ozone initiated at

Figure 1.6. Survey XPS spectra of self-assembled monolayers that had been stored in air in the dark for approximately 20 min **(2a/glass** and **2a/silicon),** 12 h **(2b/glass** and **2b/silicon),** 6 d **(2c/glass** and **2c/silicon)** and 2 weeks **(2d/glass).** These SAMs were formed by adsorption of dodecanethiol on gold films that had been evaporated at a rate of 0.5 Å/s onto either glass or silicon substrates. The spectra for samples **2a/glass** and **2a/silicon** were collected at a take-off angle of 57°; the others were collected at 20°.

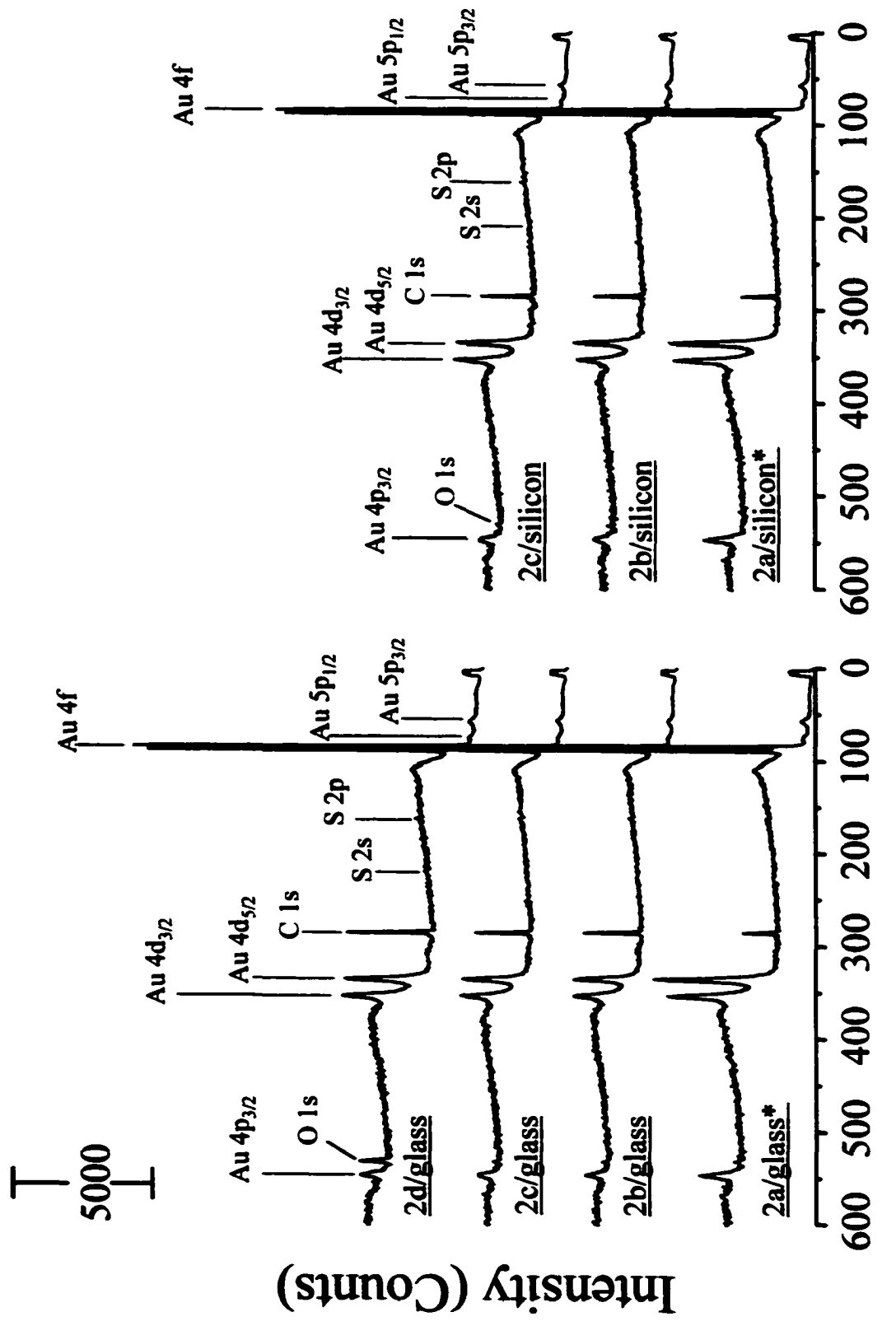

Figure 1.7. High-resolution XPS spectra of the sulfur 2p region for samples **2a-d/glass** and **2a-c/silicon.**

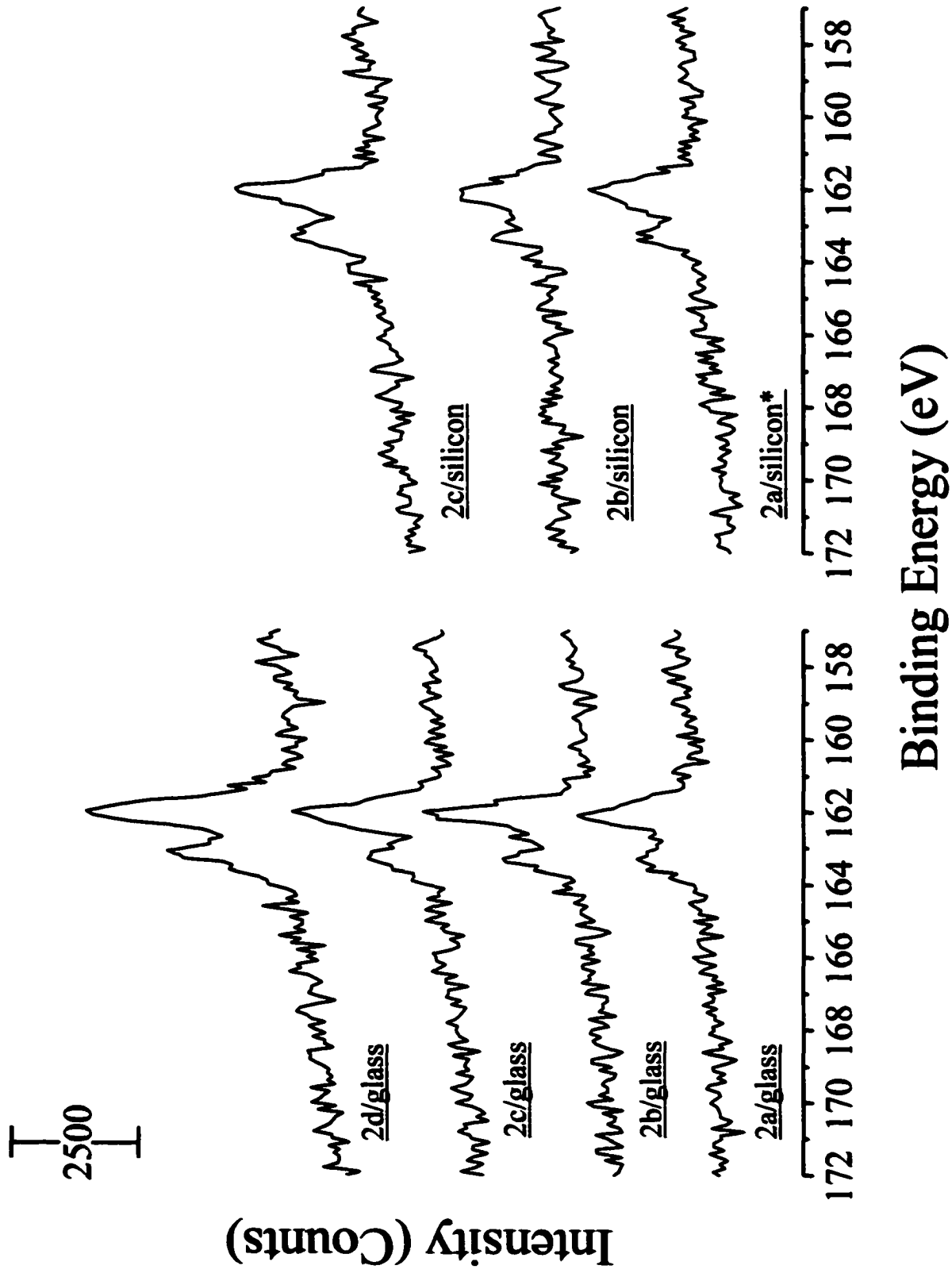

Table 1.4. Ratios of Corrected[23] Photoemission Intensity from Survey XPS Spectra of Samples **2a-d/glass** and **2a-c/silicon**.

Element / Sample	O/Au	C/Au
2a/glass*	< 0.09‡	1.1
2b/glass	0.12	3.0
2c/glass	0.10	2.5
2d/glass	0.64	3.8
2a/silicon*	< 0.06‡	1.1
2b/silicon	0.08	2.4
2c/silicon	0.15	2.8

* These spectra were collected at a take-off angle of 57°; the others were collected at 20°.

‡ The height of the O 1s peak was less than twice the standard deviation of the noise in this spectrum.

domain boundary and propagated into the domains.[42]

1.4 Conclusions

In summary, our results confirm that alkyl thiolates in self-assembled monolayers on gold can oxidize extensively in air, in the dark, to form the corresponding sulfinates and sulfonates. The rate at which this oxidation occurs, however, depends critically on the morphology of the gold surface: surfaces with higher areal densities (Table 1.1) of grain boundaries oxidized within hours to days, whereas those having lower areal densities showed no apparent oxidation after two weeks. Such a wide variability in rate, resulting from subtle differences in formation of the gold films, may be responsible for differences among reports by various other groups. We cannot rule out, however, that in some cases differences in the composition of the air (e.g., the concentration of ozone or other oxidants) in contact with the sample may also play a role. We assume that grain boundaries evident in the STM images correspond to defects (e.g., line defects between ordered domains) in the SAMs adsorbed at these sites, and as such give rise to enhanced reactivity.[30] In addition, XRD of a gold film evaporated at the faster rate indicated the presence of more Au (100), which binds alkyl thiolates less strongly than does Au (111).[36]

The oxidized products appear to desorb as a result of exposure to air under ambient conditions over a period of days, consistent with these species being less strongly bound to the gold than are thiolates. Analysis by XPS results in loss of sulfonate sulfur and oxygen atoms under x-ray irradiation in ultrahigh vacuum over a period of hours. In addition to providing direct evidence and quantification of the extent of

oxidation of SAMs by air in the dark, our studies provide practical guidance regarding how to prepare samples with desired reactivity, or lack thereof, in air. Future studies and applications that use SAMs of alkyl thiolates on gold must account for the possibility and the kinetics of this chemistry.

1.5 Experimental Methods

1.5.1 *Materials.* The dodecanethiol was obtained from Aldrich and was distilled under vacuum prior to use. Absolute ethanol was obtained from McCormick Distilling Co. and used as received. Hexadecane used in contact-angle measurements was obtained from Aldrich and was purified by percolation twice through activated alumina. Gold (99.99%) was obtained from Refining System Co.

1.5.2 *Sample Preparation.* Silicon wafers and glass microscope slides were treated with (3-mercaptopropyl)trimethoxysilane (Union Carbide) according to a published procedure to act as an adhesion promoter for a gold overlayer.[29] Gold films were then deposited by thermal evaporation of the metal at two different rates, approximately 1.5 Å/s (films **1/glass** and **1/silicon)** or 0.5 Å/s (films **2/glass** and **2/silicon)** at a background pressure of approximately $1x10^{-6}$ Torr, to a final thickness of about 1000 Å. Several samples cut from the same evaporated gold film were immersed into the same unstirred solution of dodecanethiol (50 mM) in ethanol at room temperature. Samples were removed and stored under ambient conditions in the dark for various amounts of time prior to analysis.

1.5.3 *X-ray Photoelectron Spectroscopy.* The XPS spectra in this paper were obtained using a Scienta ESCA-300 spectrometer, equipped with a rotating anode (Al

Kα) source producing 6.0 kW of x-ray power, a monochromator, and 300-mm (diameter) hemispherical analyzer. All spectra were collected at a take-off angle of 20° (unless noted otherwise) between the plane of the surface and the detector, a slit width of 0.8 mm, and were referenced to the Au $4f_{7/2}$ peak set at 84.0 eV. The background pressure in the sample chamber was $2x10^{-9}$ Torr. Survey scans were collected with a pass energy of 75 eV and a step energy of 1.0 eV, and took 19 min to complete. High-resolution spectra were the sum of five scans collected with a pass energy of 150 eV and a step energy of 0.1 eV. Under these conditions, a single scan took 1.67 min to complete. For quantitative analysis, the sensitivity factors used to correct the number of counts under each peak (or envelope) were: O 1s, 2.8370; C 1s, 1.000; S 2p (both components), 2.1735; and Au $4f_{7/2}$, 9.5800. The sensitivity factors for oxygen, carbon, and sulfur photoemission are based on data in reference 42 and were verified by A. C. Miller with the Scienta ESCA-300 at Lehigh University. The value for gold is the Scofield value.[40]

1.5.4 *Scanning Tunneling Microscopy (STM).* STM images were taken with a NanoScope (Digital Instruments). Platinum-iridium wires were used as tunneling tips, and the sample bias was set at 20 mV *versus* the tip. The STM was operated in height mode, with a scan rate of 1.97 Hz and a constant tunneling current of 2 nA. All images were corrected for tilt and curvature.

1.5.6 *X-ray Diffraction (XRD).* X-ray diffractometry was performed using a Philips APD 3720 powder diffractometer. The samples of gold deposited on glass at different evaporation rates were broken to approximately 1.5 cm x 1 cm to fit into the well in the sample mount. The diffractometer was operated in θ/2θ mode using

monochromatized CuKα radiation (λ = 0. 154 nm) from an anode operating at 45 kV and 30 mA. Data were obtained using a 0.05° step and 3 s/step collection time.

1.5.7 *Contact-Angle Measurements.* Contact-angle measurements were made with hexadecane and with water using a Rame-Hart NRL Model 100 goniometer. A minimum of three independent measurements were made for each sample. The advancing contact angles of water on the surfaces analyzed were in the range 112-114°; the advancing angles of hexadecane were 43-45°. These angles are in accord with values reported for well-ordered monolayers.[2]

1.5.8 *Ellipsometric Measurements.* Ellipsometric measurements were made using a null ellipsometer (Rudolph Auto-EL III) equipped with helium-neon laser (X = 632.8 nm) set at a 70° incident angle. Measurements were made from three arbitrarily chosen spots on the samples. Data were analyzed using the manufacturer's program, and calculations of film thickness assumed a refractive index of the monolayer of 1.5. The ellipsometric thickness of these SAMs was approximately 10 Å, consistent with contamination physisorbed on the gold surface prior to treatment with the thiol being displaced during the adsorption of the SAM.[2]

1.6 Acknowledgements

We gratefully acknowledge the National Science Foundation and industrial partners for support of this research through the Polymer Interfaces Center, an Industry/University Cooperative Research Center at Lehigh University. In addition, we thank Lehigh University for support of the Scienta ESCA facility, and Gary W. Simmons

and A. C. Miller for technical assistance and helpful discussions. We also thank Katayun Barmak for helpful discussions.

1.7 Reference

1. Nuzzo, R. G.; Allara, D. L. *J. Am. Chem. Soc.* **1983**, *105*, 4481-4483.
2. Bain C. D.; Troughton, E. B.; Tao, Y.-T.; Evall, J.; Whitesides, G. M.; Nuzzo, R. G. *J. Am. Chem. Soc.* **1989**, *111*, 321-335.
3. Ulman, A. *An Introduction to Ultrathin Organic Films: From Langmuir-Blodgett to Self-Assembly;* Academic Press: New York, 1991.
4. Li, Y.; Huang, J.; McIver, R. T. Jr.; Hemminger, J. C. *J. Am. Chem. Soc.* **1992**, *114*, 2428-2432.
5. (a) Tarlov, M. J.; Newman, J. C. *Langmuir* **1992**, *8*, 1398-1405. (b) Burroughs, J. A.; Hanley, L. *J. Am. Soc. Mass Spectrom.* **1993**, *4*, 968-970. (c) Huang, J.; Hemminger, J. C. *J. Am. Chem. Soc.* **1993**, *115*, 3342-3343. (d) Beulen, M. W. J.; Huisman, B.-H.; van der Heijden, P. A.; von Veggel, F. C. J. M.; Simons, M. G.; Biemond, E. M. E. F.; de Lange, P. J.; Reinhoudt, D. N. *Langmuir* **1996**, *12*, 6170-6172.
6. (a) Scott, J. R.; Baker, L. S.; Everett, W. R.; Wilkins, C. L.; Fritsch, I. *Anal. Chem.* **1997**, *69*, 2636-2639. Very recent papers have identified ozone as the primary atmospheric oxidant in this and related systems: (b) Schoenfisch, M. H.; Pemberton, J. E. *J. Am. Chem. Soc.* **1998**, *120*, 4502-4513. (c) Zhang, Y.; Terrill, R. H.; Tanzer, T. A.; Bohn, P. W. *J. Am. Chem. Soc.* **1998**, *120*, 2654-2655. (d) Norrod, K. L.; Rowlen, K. L. *J. Am. Chem. Soc.* **1998**, *120*, 2656-2657. (e) Zhang, Y.; Terrill, R. H.; Bohn, P. W. *Chem. Mater.* **1999**, *11*, 2191-2198.

7. (a) Tarlov, M. J.; Burgess, D. R. F.; Gillen, G. *J. Am. Chem. Soc.* **1993**, *115*, 5305-5306. (b) Rieley, H.; Price, N. J.; White, R. G.; Blyth, R. I. R.; Robinson, A. W. *Surf. Sci.* **1995**, *331-333*, 189-195. (c) Rieley, H.; Price. N. J.; Smith, T. L.; Yang, S. *J. Chem. Soc., Faraday Trans.* **1996**, *92*, 3629-3634. (d) Garrell, R. L.; Chadwick, J. E.; Severance, D. L.; McDonald, N. A.; Myles, D. *J. Am. Chem. Soc.* **1995**, *117*, 11563-11571. (e) Hutt, D. A.; Leggett, G. J. *J. Phys. Chem.* **1996**, *100*, 6657-6662.

8. For related work on the oxidization of SAMs on silver, see: Lewis, M.; Tarlov, M. J. *J. Am. Chem. Soc.* **1995**, *117*, 9574-9575 and references therein. For oxidization of SAMs on copper, see: (a) Laibinis, P. E.; Whitesides, G. M.; Allara, D. L.; Tao, Y.-T.; Parikh, A. N.; Nuzzo, R. G. *J. Am. Chem. Soc.* **1991**, *113*, 7152-7167. (b) Beecher J. F. *Surf. Interface Anal.* **1991**, *17*, 245-250. (c) Laibinis, P. E.; Whitesides, G. M. *J. Am. Chem. Soc.* **1992**, *114*, 9022-9028. (d) Nishihara, H.; Aramaki, K. *J. Electrochem. Soc.* **1995**, *142*, 1839-1846. (e) Feng, Y.; Teo, W-K.; Siow, K-S.; Gao, Z.; Tan., K-L.; Hsieh, A-K. *J. Electrochem. Soc.* **1997**, *144*, 55-64. For Oxidization of thiolates on nickel, see: Mekhalif, Z.; Riga, J.; Pireaux, J.; Delhalle, J. *Langmuir* **1997**, *13*, 2285-2290.

9. Scott, J. R.; Baker, L. S.; Everett, W. R.; Wilkins, C. L.; Fritsch, I. *Anal. Chem.* **1997**, *69*, 2636-2639.

10. Bain C. D.; Troughton, E. B.; Tao, Y.-T.; Evall, J.; Whitesides, G. M.; Nuzzo, R. G. *J. Am. Chem. Soc.* **1989**, *111*, 321-335.

11. (a) Castner, D. G.; Hinds, K.; Grainger, D. W. *Langmuir* **1996**, *12*, 5083-5086. (b) Huang, J.; Dahlgren, D. A.; Hemminger, J.C. *Langmuir* **1994**, *10*, 626-628. (c) Tsao,

M.-W.; Pfeifer, K.-H.; Rabolt, J. F.; Castner, D. G.; Haussling, L. *Macromolecules* **1997**, *30*, 5913-5919. (d) Kwan, W. S. V.; Atanasoska, L.; Miller, L. L. *Langmuir* **1991**, *7*, 1419. (e) Sun, F.; Grainger, D. W.; Castner, D. G. *J. Vac. Sci. Technol. A* **1994**, *12*, 2499. (f) Sun, F.; Castner, D. G.; Grainger, D. *W. Langmuir* **1993**, *9*, 3200-3207. (g) Sun, F.; Grainger, D. W.; Castner, D. G.; Leach-Scampavia, D. K.; *Macromolecules* **1994**, *27*, 3053-3062.

12. For examples, see: (a) Nuzzo, R. G.; Fusco, F. A.; Allara, D. L. *J. Am. Chem. Soc.* **1987**, *109*, 2358-2368. (b) Bain, C. D.; Biebuyck, H. A.; Whitesides, G. M. *Langmuir* **1989**, *5*, 723-727. (c) Laibinis, P. E.; Whitesides, G. M.; Allara, D. L.; Tao, Y.-T.; Parikh, A. N.; Nuzzo, R. G. *J. Am. Chem. Soc.* **1991**, *113*, 7152-7167. (e) Laibinis, P. E.; Bain, C. D.; Whitesides, G. M. *J. Chem. Phys.* **1991**, *95*, 7017-7021. (f) Evans, S. D.; Goppert-Beraducci, K. E.; Urankar, E.; Gerenser, L. J.; Ulman, A.; Snyder, R. G. *Langmuir* **1991**, *7*, 2700-2709. (g) Biebuyck, H. A.; Whitesides, G. M. *Langmuir* **1993**, *9*, 1766-1770. (h) Lenk, T. J.; Hallmark, V. M.; Hoffmann, C. L.; Rabolt, J. F.; Castner, D. G.; Erdelen, C.; Ringsdorf, H. *Langmuir* **1994**, *10*, 4610-4617. (i) Sun, F.; Castner, D. G.; Mao, G.; McKeown, P.; Grainger, D. W. J. *Am. Chem. Soc.* **1996**, *118*, 1856-1866. (j) Ning, Y.; Xie, H.; Xing, H.; Deng, W.; Yang, D. *Surf. Interface Anal.* **1996**, *24*, 667-670. (k) Buck, M.; Grunze, M.; Eisert, F.; Fisher, J.; Trager, F. *J. Vac. Sci. Technol. A.* **1992**, *10*, 926-929.

13. (a) Chidsey, C. E. D.; Bertozzi, C. R.; Putvinski, T. M.; Mujsce, A. M. *J. Am. Chem. Soc.* **1990**, *112*, 4301. (b) Collard, D. M.; Fox, M. A. *Langmuir* **1991**, *7*, 1192-1197. (c) Stranick, S. J.; Parikh, A. N.; Tao, Y.-T.; Allara, D. L.; Weiss, P. S. *J. Phys.*

Chem. **1994**, *98*, 7636-7646. (d) Schlenoff, J. B.; Li, M.; Ly, H. *J. Am. Chem. Soc.* **1995**, *117*, 12528-12536.

14. Schoenfisch, M. H.; Pemberton, J. E. *J. Am. Chem. Soc.* **1998**, *120*, 4502-4513.
15. Sandhyarani, N.; Resmi, M. R.; Unnikrishnan, R.; Ma, S.; Vidyasagar, K.; Antony, M. P.; Selvam, P.; Visalakshi, V.; Chandrakumar, N.; Pandian, K.; Tao, Y.-T.; Pradeep, T.; *Chem. Mater.* **2000**, *12*, 104.
16. Sandhyarani, N; Pradeep, T. *Chem. Phys. Lett.* **2001**, *338*, 33-36.
17. Golan, Y.; Margulis, L.; Rubinstein, I. *Surf. Sci.* **1992**, *264*, 312-326.
18. Guo, L.-H.; Facci, J. S.; McLendon, G.; Mosher, R. *Langmuir* **1994**, *10*, 4588-4593.
19. Reichelt, K.; Lutz, H. O. *J Cryst. Growth* **1971**, *10*, 103-107.
20. Emch, R.; Nogami, J.; Dovek, M. M.; Lang, C. A.; Quate, C. F. *J. Appl. Phys.* **1989**, *65*, 79-84.
21. Dishner, M. H.; Ivey, M. M.; Gorer, S.; Hemminger, J. C.; Feher, F. J. *J. Vac. Sci. Technol.* A **1998**, *16*, 3295-3300.
22. Putnam, A.; Blackford, B. L.; Jericho, M. H.; Watanabe, M. O. *Surf. Sci.* **1989**, *217*, 276-288.
23. Chidsey, C. E. D.; Loiacono, D. N.; Sleator, T.; Nakahara, S. *Surf. Sci.* **1988**, *200*, 45-66.
24. Vancea, J.; Reiss, G.; Schneider, F.; Bauer, K.; Hoffmann. M. *Surf. Sci.* **1989**, *218*, 108-126.
25. DeRose, J. A.; Thundat, T.; Nagahara, L. A.; Lindsay, S. M. *Surf. Sci.* **1991**, *256*, 102-108.

26. (a) Buchhloz, S.; Fuchs, H.; Rabe, J. P. *J. Vac. Sci. Technol. B* **1991**, *9*, 857. (b) Golan, Y.; Margulis, L.; Rubinstein, I. *Surf. Sci.* **1992**, *264*, 312. (c) Chidsey, C. E. D.; Loiacono, D. N.; Sleator, T.; Nakahana, S. *Surf. Sci.* **1988**, *200*, 45.

27. Hopfner, U.; Hehl, H.; Brehmer, L. *Appl. Surf. Sci.* **1999**, *152*, 259-265.

28. Discussion with manufactorer.

29 Gross, C. A.; Charych, D. H.; Majda, M. *Anal. Chem.* **1991**, *63*, 85-88.

30. We use the term "surface grain" to describe regions delineated by surface features in our STM images. These regions do not necessarily correspond to the faces of crystallites within the bulk of the gold film. For example, see: Files-Sesler, L. A.; Hogan, T.; Taguchi, T. *J. Vac. Sci. Technol. A* **1992**, *10*, 2875.

31. "Standard Test Methods for Determining Average Grain Size," ASTM Designation: E 112-88.

32. The differences in film topography and morphology, observed by STM and XRD, could be due to differences in the rate of evaporation itself (relative to the rates of surface diffusion and crystal growth) or could also involve differential, radiative heating of the samples at the two evaporation rates.

33. Pashley, D. W. *Adv. Phys.* **1956**, *5*, 173, and references therein.

34. The thermal conductivity of silicon varies as a function of temperature: it is 49.8 w/mK at 20 °C and then decreases as the temperature increases. The thermal conductivity of glass varies as its composition and temperature change. In general, the conductivity of glass is between 0.6 to 1.2 W/mK from 0 to 100 °C. These data

were obtained from *CRC Handbook of Chemistry and Physics*, 74th Ed, CRC Press, Ann Arbor, 1993.

35. International Centre for Diffraction Data (ICDD); CD ROM Database PCPDFWIN v. 20 (September, 1996); Newtown Square, PA 19073, USA.
36. Camillone III, N.; Chidsey, C. E. D.; Liu, G.-y.; Scoles, G. *J. Chem. Phys.* **1993**, *98*, 4234.
37. The differences in film topography and morphology, observed by STM and XRD, could be due to differences in the rate of evaporation itself (relative to the rates of surface diffusion and crystal growth) or could also involve differential, radiative heating of the samples at the two evaporation rates.
38. As a result of this procedure, the total length of immersion in the thiol solution for samples **1a/glass, 1a/silicon, 2a/glass,** and **2a/silicon** was 8.0 d; samples **1b/glass, 1b/silicon, 2b/glass,** and **2b/silicon** were immersed in the thiol solution for 7.5 d; and samples **1c/glass, 1e/silicon, 2c/glass, 2c/silicon,** and **2d/glass** were immersed for 48 h.
39. This normalization was necessary due to an apparent difference in sample positioning relative to the focal point of X-rays on the sample. This procedure does not affect the quantitative ratios reported in Table 1.3.
40. Scofield, J. H. *J. Electron Spectrosc.* **1976**, *8*, 129.
41. Lindberg, B. J.; Hamrin, K.; Johansson, G.; Gelius, U.; Fahlman, A.; Nordling, C.; Siegbahn, K. *Phys. Scr.* **1970**, *1*, 286-298.

42. Li, Y.; Huang, J.; McIver, R. T. Jr.; Hemminger, J. C. *J. Am. Chem. Soc.* **1992**, *114*, 2428-2432.

43. Poirier, G. E.; Herne, T. M.; Miller, C. C.; Tarlov, M. J. *J. Am. Chem. Soc.* **1999**, *121*, 9702-9711.

Chapter 2

Electrochemically Directed Self-Assembly of Monolayers on Gold

2.1 Abstract

We report an electrochemical method for the preparation of self-assembled monolayers (SAMs) by oxidizing alkylthiosulfates, or "Bunte salts," and trapping the resulting intermediates or products at gold electrodes. Selective preparation of self-assembled monolayers (SAMs) on gold was accomplished by electrolysis of alkylthiosulfates (Bunte salts) in THF in the presence of tetrabutylammonium tetrafluoroborate as the supporting electrolyte. Tetrafluoroborate ions inhibited the spontaneous chemisorption of alkylthiosulfates to form monolayers, so that monolayers formed only on gold electrodes at a sufficiently oxidative potential. This oxidative potential was applied using square-wave pulses, and as expected, the degree of completeness of the monolayers depended upon both the voltage and the length of the period during which it was applied. The monolayers produced are very similar to those prepared in the conventional way, by chemisorption of alkanethiols, though this approach allows SAMs to be formed selectively in less than a minute.

X-ray photoelectron spectroscopy (XPS) and infrared spectroscopy supported our hypothesis that this process involved formation of stable gold-thiolate bonds at the gold surface and that (bi)sulfate is a side-product under our experimental conditions. Unlike the preparation of SAMs from alkanethiols, clean gold was not required for forming complete monolayers from alkylthiosulfates. We demonstrated the selectivity of this process by chemically modifying one electrode in the close proximity (76 μm) of another on a microelectronic device.

2.2 Introduction

Molecular self-assembly of monolayers (SAMs) provides a simple method to form highly ordered two-dimensional organic assemblies. Among the various systems that display this behavior, SAMs formed by the chemisorption of alkanethiols on gold to produce strong gold-thiolate bonds is particularly convenient because of the ease of their preparation.[1-3] Well-ordered SAMs form spontaneously on gold surfaces within a short period upon immersion of the surface in either a dilute solution or the vapor of an alkanethiol of interest. These monolayers have been used as model systems for fundamental studies of wettability,[4] adhesion,[5] biocompatibility,[6] fouling,[7] as well as serving as the basis for building multilayers[8] and bio- and analytical sensors,[9] for the immobilization of biomolecules,[10] and for preparing patterned surfaces.[11]

One of the most attractive characteristics of self-assembled monolayers (SAMs) is the facility of their preparation —simply exposing a substrate surface to an appropriate adsorbate-[1-3] though this facility prevents selective formation at particular surfaces in the presence of others of the same composition. While contact printing of SAMs has proven useful in preparing mesoscale patterns on various substrates,[12] formation of monolayers on only particular features of a pre-existing pattern —such as an electrode array, an integrated circuit, or a MEMS device— has remained an elusive synthetic challenge. Hence, treating an array of identical gold electrodes with a solution of an alkanethiol or alkyl disulfide would result in formation of a monolayer on all of the electrodes. One approach to controlling self-assembly in these systems has focused on the inability of thiolate ions to covalently bind the gold surface directly, without concomitant oxidation.[13] Hence, gold electrodes immersed in a solution of thiolate ions will only

adsorb a SAM if held at a sufficiently high potential. Electrochemistry, in this case reduction, can also be used to *remove* SAMs that had previously been adsorbed.[14] Hence, an alternative strategy for producing patterns involves allowing indiscriminate self-assembly to occur, followed by articulation of a pattern by the selective removal of the SAM from certain substrates.

Alkylthiosulfates, also known as Bunte salts, can be used to synthesize disulfides by oxidation,[15] acidic hydrolysis,[16-17] or alkaline degradation.[18] Disulfides also can be formed from Bunte salts electrochemically.[19-20] This method has been extended to form polysulfides from "double" Bunte salts, molecules carrying two thiosulfate groups, using electrochemistry with gold electrodes.[21]

At the outset of this work, we hypothesized that if oxidation of Bunte salts occurred at a gold electrode, trapping of the intermediates or products of the oxidation could provide a selective method for driving self-assembly only at electrodes held a sufficiently high potential. Our hypothesis, summarized in Figure 2.1, is that oxidation would lead to formation of an alkylsulfide radical by release of SO_3.[19,20] This radical could then combine directly with a dangling bond at the gold surface, or could couple to form disulfide. Either of these pathways would be expected to lead to formation of SAMs, as disulfides readily oxidatively add to gold surfaces.[22] Finally, SO_3 would be expected to react with any water in the solvent to form sulfate ion. Sulfuric acid produced in this way could also be involved in monolayer formation, via acid hydrolysis of the Bunte salt to give thiol.

The monolayers produced in this way are very similar to those prepared in the conventional method, by chemisorption of alkanethiols. One focus of the present study

Figure 2.1. Schematic Representation of the Proposed Electrochemical Synthesis of Self-Assembled Monolayers on Gold.

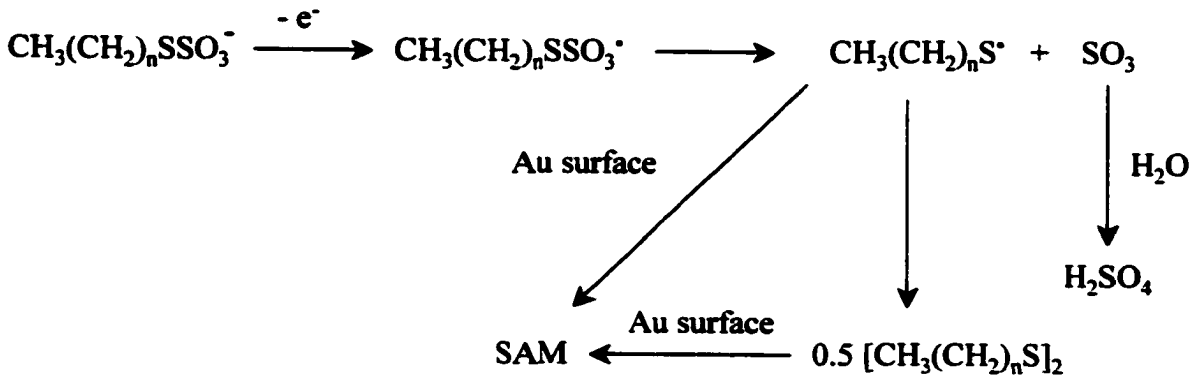

was to address aspects of the mechanism of the electrochemical synthesis of monolayers in this way, including the inhibition of spontaneous chemisorption of alkylthiosulfates in the presence of tetrabutylammonium tetrafluoroborate, and identification of the side-product(s) of the process.

We also demonstrate the *selective* formation by oxidation of alkylthiosulfates selectively in specific locations on a set of closely spaced microelectrodes.[23] The resulting chemical differentiation at small scales of length is a feature we expect to be very useful in microelectronic and sensor applications. For example, one could potentially use this method to build a sensor that has SAMs with different functionalities on an each member of an electrode array. This alternative approach to the synthesis of SAMs also offers several attractive features: it allows control of the degree of coverage, requires only short adsorption times (< 1 min), does not require clean substrates,[23] and uses precursors that do not have unpleasant odors (for *n*-alkyl chains greater than about 10 carbons in length).

2.3 Results and Discussion

Oxidation of Alkylthiosulfates

Alkylthiosulfates, $CH_3(CH_2)_nS_2O_3Na$ (n = 15, 13, 11, 9, and 7) were synthesized by nucleophilic displacement reactions between sodium thiosulfate and the corresponding alkyl bromides, and purified by recrystallization in ethanol, according to a reported procedure.[17] Our initial studies of the electrochemistry of these alkylthiosulfates were carried out using cyclic voltammetry in various solvents, e.g. acetonitrile, water, ethanol, and ethanol/water (50:50), but oxidation was only observed in the THF. Different

supporting electrolytes were also used, with widely varying results. For example, the cyclic voltammogram (–0.9 V to 1.6 V) of *n*-hexadecylthiosulfate in THF using $LiClO_4$ as the supporting electrolyte contained an oxidation peak at 0.95 V in the first anodic scan, which then decreased significantly in the following scans (Figure 2.2). The sample became more hydrophobic after 3 cycles, but an ordered monolayer did not form: contact angles of hexadecane on the surface after 200 scans (16-18°) indicated that the monolayer was incomplete. Cycling to a lower potential (1.2 V) did produce a nearly complete monolayer with contact angles of hexadecane of 42-44° (Figure 2.3). Control experiments, however, suggested that formation of this monolayer could have been due primarily to the spontaneous chemisorption of *n*-hexadecylthiosulfate, rather than to the electrochemical process (vide infra). Nonetheless, cycling to the low positive potential in these experiments apparently avoided the oxidative desorption found at potentials approaching ~ 1.6 V.

In contrast, the voltammogram of *n*-hexadecylthiosulfate in THF with 0.1 M Bu_4NBF_4 as the supporting electrolyte contained a large oxidation peak in the first anodic scan, which decreased only gradually in subsequent scans (Figure 2.4). The current rose sharply and reached a maximum at approximately 0.95 V before decreasing again, consistent with a decrease in the concentration of Bunte salt near the gold electrode or blocking of the electrode by the resulting monolayer at the gold surface. The peak current due to oxidation of Bunte salt gradually decreased in each successive scan until about the sixth scan, after which it remained unchanged. This decrease in current in each successive scan was likely due to the decrease of free gold surface after each scan, arising

Figure 2.2. Cyclic voltammograms for a 10 mM solution of sodium *n*-hexadecylthiosulfate in THF from –0.9 to 1.6 V (0.1 M $LiClO_4$, 100 mV/s) using a gold working electrode and a $Ag/AgNO_3$ reference electrode (3 mM in CH_3CN).

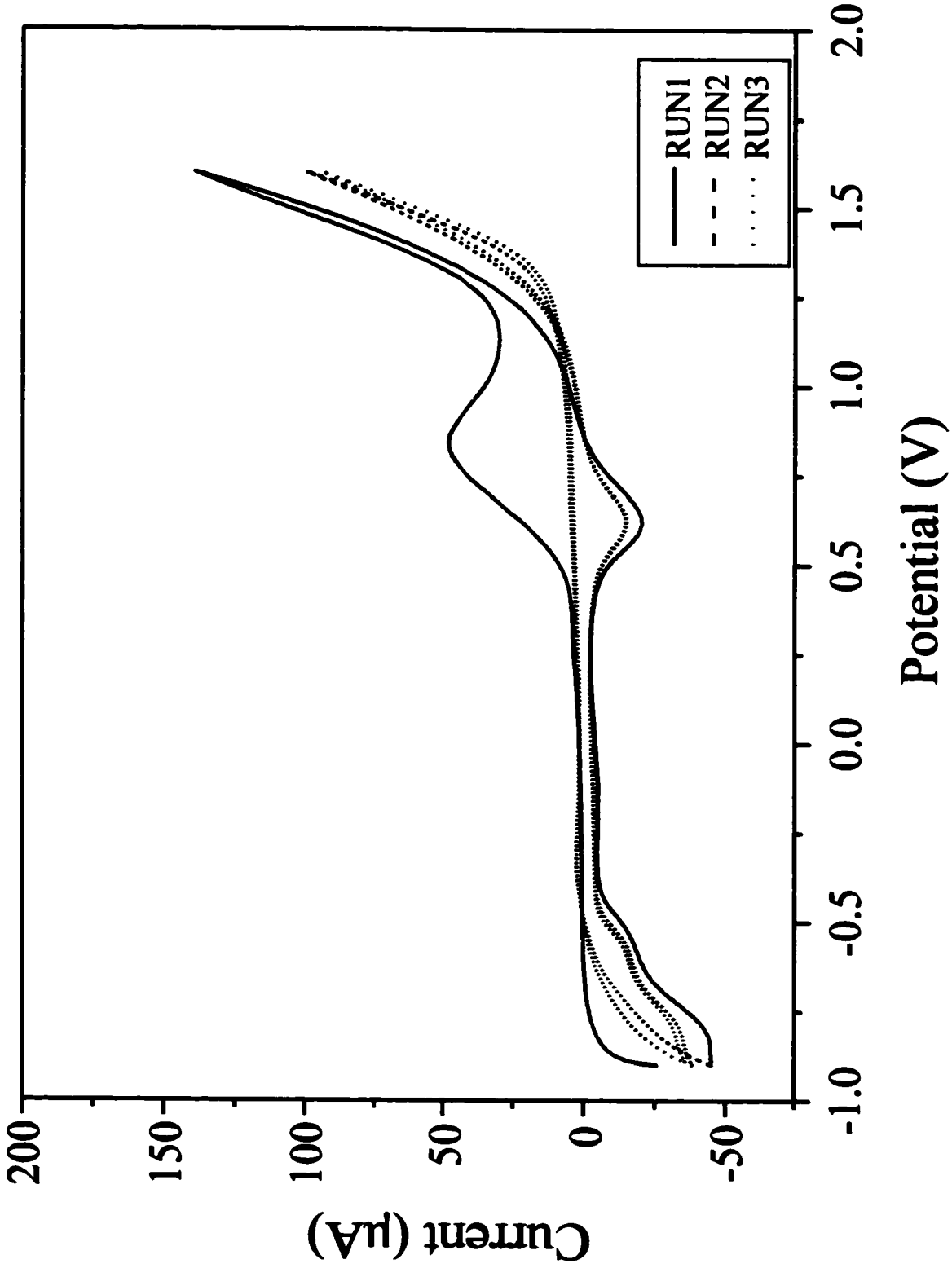

Figure 2.3. Cyclic voltammograms for a 10 mM solution of sodium *n*-hexadecylthiosulfate in THF from –0.9 to 1.2 V (0.1 M $LiClO_4$, 100 mV/s) using a gold working electrode and a $Ag/AgNO_3$ reference electrode (3 mM in CH_3CN).

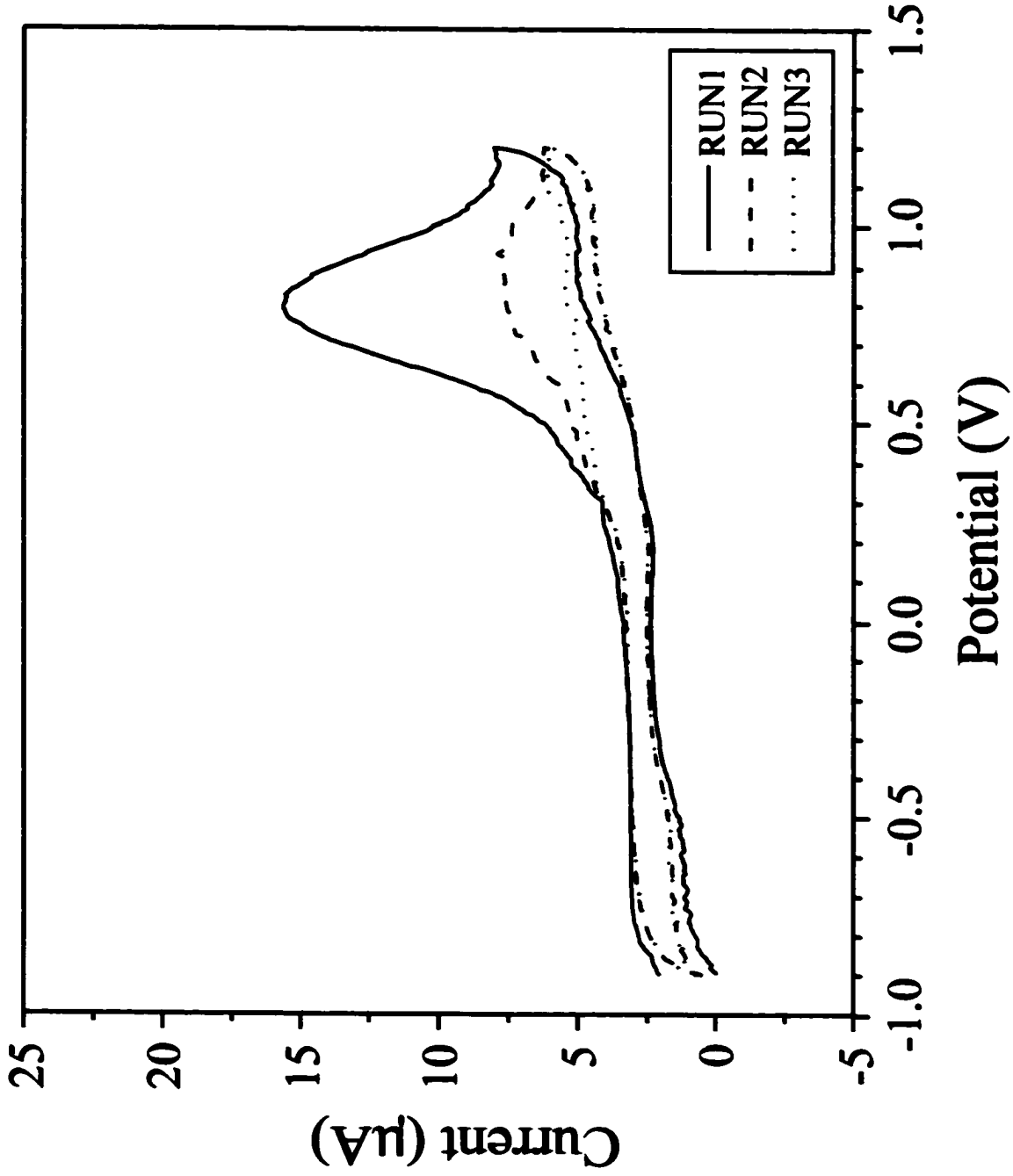

Figure 2.4. Cyclic voltammograms for a 10 mM solution of sodium *n*-hexadecylthiosulfate in THF (0.1 M Bu_4NBF_4, 100 mV/s) using a gold working electrode and a $Ag/AgNO_3$ reference electrode (3 mM in CH_3CN). The inset shows a cyclic voltammogram for a bare gold electrode in THF (0.1 M Bu_4NBF_4, 100 mV/s) using a $Ag/AgNO_3$ reference electrode.

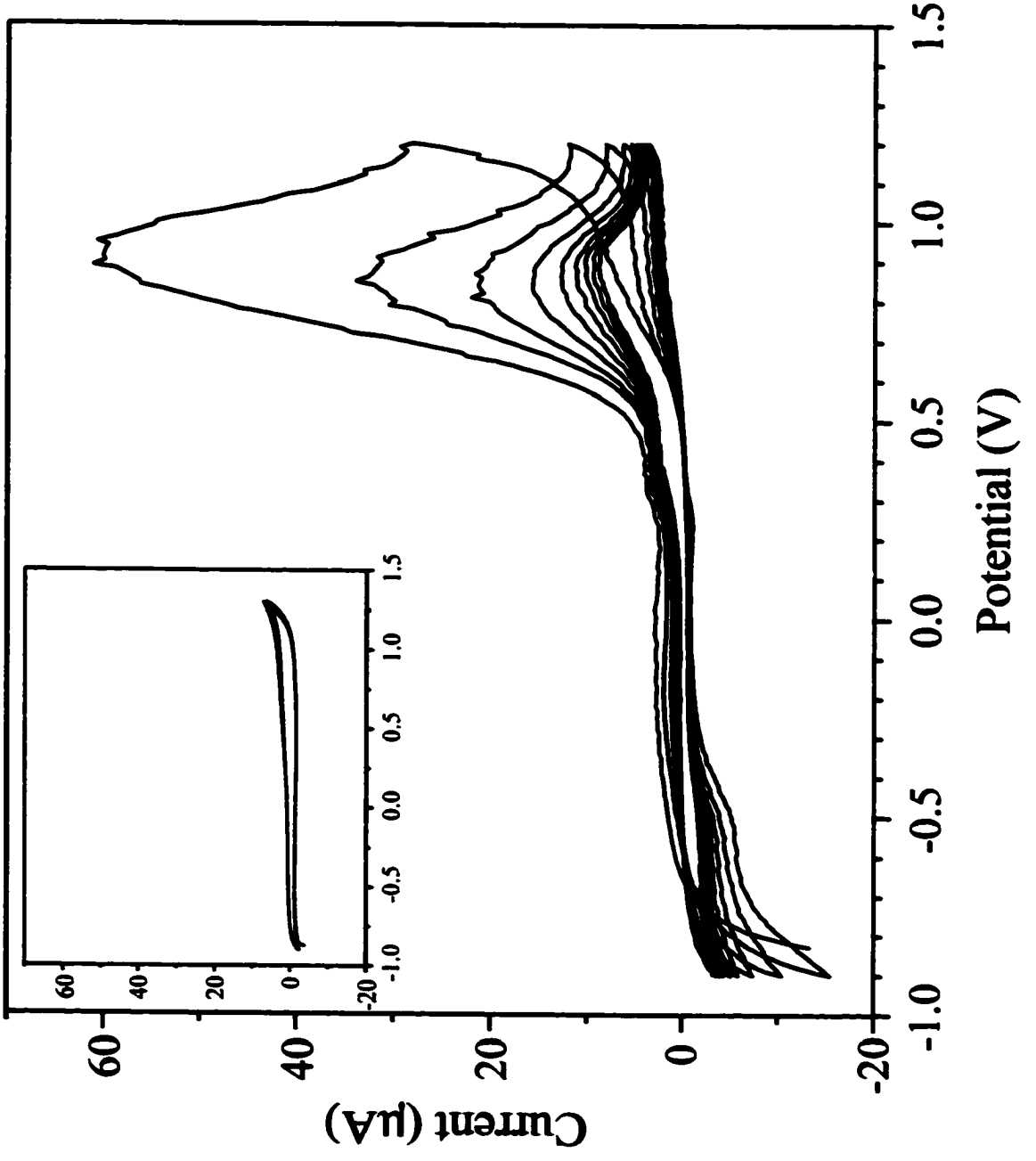

from chemisorption of the SAM.

Electrochemical Formation of Ordered Monolayers

As with $LiClO_4$, cycling to 1.6 V with Bu_4NBF_4 as the supporting electrolyte did *not* produce ordered SAMs. A monolayer formed in this way, using even 200 scans, had a contact angle of hexadecane of only 30°. For comparison, monolayers formed by chemisorption of hexadecanethiol gave contact angles of hexadecane of 44 to 46°. Cycling to lower potential (from –0.9 V to 1.2 V or –0.9 V to 1.3 V) for 8 scans, however, did produce ordered monolayers with contact angles of hexadecane of 45-46°. Figure 2.5a shows a cyclic voltammogram for a gold electrode immersed in a 10 mM solution of sodium *n*-hexadecylthiosulfate in THF, with 0.1 M Bu_4NBF_4 as a supporting electrolyte and an $Ag/AgNO_3$ (3 mM in CH_3CN) reference electrode. The figure inset magnifies this voltammogram in the range of potential from –0.80 to +0.50 V in the anodic scan and clearly displays the onset of current flow at about –0.60 V. The current rose to a small steady-state value at potentials between approximately –0.20 and +0.20 V, after which it rose sharply into the main voltametric peak ($E_{p,a}$ +0.85 V).

Because the return wave in cyclic voltammetry was not necessary to build SAMs, we used simpler potentiometric "pulses" to assess our ability to form SAMs electrochemically. We used potential pulses within the range of potential giving measurable anodic current to assess our ability to form SAMs electrochemically and to minimize any oxidative degradation or disordering of the resulting monolayer Figure 2.5b). In these experiments, a gold electrode was immersed into the sodium *n*-

Figure 2.5. Cyclic voltammogram (top) for a 10 mM solution of sodium *n*-hexadecylthiosulfate in THF (0.1 M Bu_4NBF_4) using a gold working electrode and a $Ag/AgNO_3$ (3 mM in CH_3CN) reference electrode. The inset figure shows the onset of current flow in the anodic scan. The bottom plot shows the advancing contact angles of hexadecane on SAMs formed by electrochemical oxidation of *n*-hexadecylthiosulfate using 1 (open circles), 3 (squares), and 5 (filled circles) voltametric pulses to different potentials.

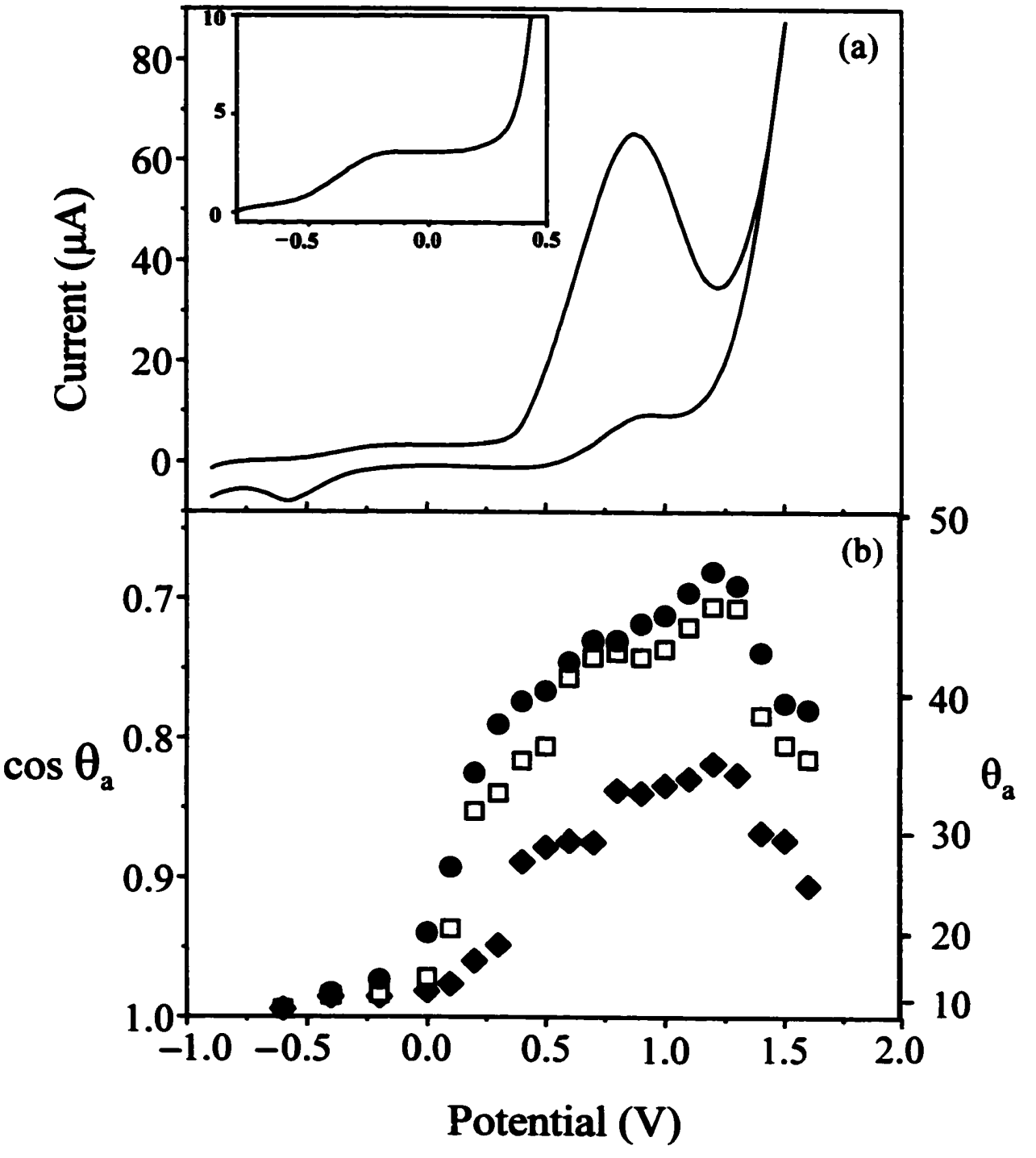

hexadecylthiosulfate solution (THF, 0.1 M Bu_4NBF_4), and its potential was then stepped from –0.90 V (again, vs. $Ag/AgNO_3$) to a particular value in the range producing anodic current in the cyclic voltammogram. It was held at this potential for 5 s and then stepped back to the –0.90 V resting potential. This process was repeated using a separate sample for each potential from –0.60 to +1.60 V, in 0.10-V increments. The advancing contact angle of hexadecane provided a convenient measure of the degree of completeness of the resulting monolayer films as a function of the applied potential used in their formation. Figure 2.5b shows these data for samples prepared using 1, 3, or 5 pulses to specific potentials. In all cases, the onset of anodic current at approximately –0.50 V corresponded closely to the appearance of a finite contact angle of hexadecane on the film produced. The contact angle increased with increasing applied potential, up to about 1.20 V, above which the contact angle began to decrease. The peak contact angles (45-47°) compared favorably with those reported for complete, well-ordered SAMs prepared by the self-assembly of hexadecanethiol.[2] The degradation in oleophobicity at high potential corresponded to a strong anodic current (Figure 2.5a), probably reflecting oxidation of the gold electrode or of THF and concomitant disordering of the films. These results were important because they defined the range of potential that would be useful for the synthesis of SAMs.

The monolayers in Figure 2.5b formed by 5 pulses gave slightly higher contact angles than those formed by 3 pulses; monolayers formed by a single pulse gave much lower contact angles, indicating less complete formation. We followed the growth of these films systematically, as a function of the number of potentiometric pulses, by

monitoring the thickness and wettability of monolayers formed by electrolysis of *n*-hexadecylthiosulfate at 1.20 V. These experiments utilized a single electrode, whose surface was characterized after each pulse or series of pulses. As the number of pulses was increased, the contact angles of both water and hexadecane rose as shown in Figure 2.6 (bottom), and reached limiting values consistent with a well-ordered monolayer (H_2O, 112-114°; hexadecane, 45-47°).[2] The ellipsometric thickness of the monolayer also increased as a function of the number of pulses to approximately 13 Å, consistent with the length of the alkyl chain of the adsorbate if some contamination was removed from the surface of the gold during the electro-chemisorption (Figure 2.6, top),[2] or with a small amount of free volume in the product film. For comparison, a monolayer formed at the same time by self-assembly of hexadecanethiol gave the same thickness.

We also prepared SAMs of tetradecanethiolate by oxidizing sodium *n*-tetradecylthiosulfate. In these experiments, a gold electrode was immersed into a solution (THF, 0.1 M Bu_4NBF_4) of sodium *n*-tetradecylthiosulfate, and the potential was stepped from a resting value of –0.90 V (*vs.* $Ag/AgNO_3$) to a particular value in the range producing anodic current in the cyclic voltammogram. The gold electrode was held at this potential for 5 s and then stepped back to the –0.90 V resting potential for 5 s. To optimize the procedure for synthesizing SAMs, this process was repeated 5 times using a separate sample for each potential from –0.50 to 1.60 V in 0.1-V increments. The degree of completeness of each resulting monolayer was assessed by measuring the advancing contact angles of hexadecane on its surface as shown in Figure 2.7. The contact angles increased with increasing applied potential, up to about 1.10 V, above which the contact

Figure 2.6. Ellipsometric thickness (top) and advancing contact angles of water and of hexadecane (bottom) on a gold electrode as a function of the number of potential pulses to 1.20 V (vs. $Ag/AgNO_3$) in a 10 mM solution of sodium *n*-hexadecylthiosulfate in THF (0.1M Bu_4NBF_4).

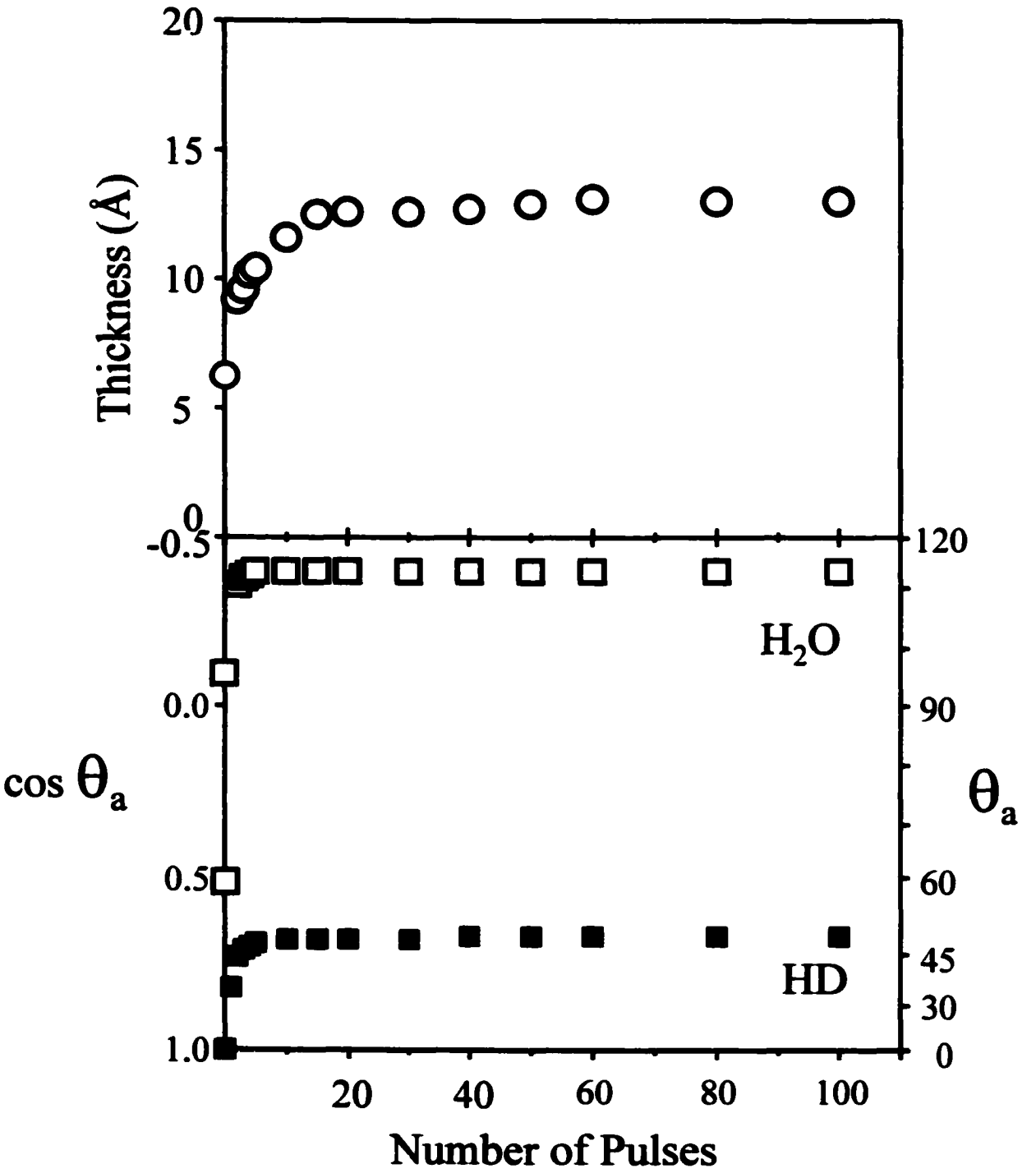

Figure 2.7. Advancing contact angles of hexadecane on SAMs formed by electrochemical oxidation of *n*-tetradecylthiosulfate using five voltametric pulses to various potentials.

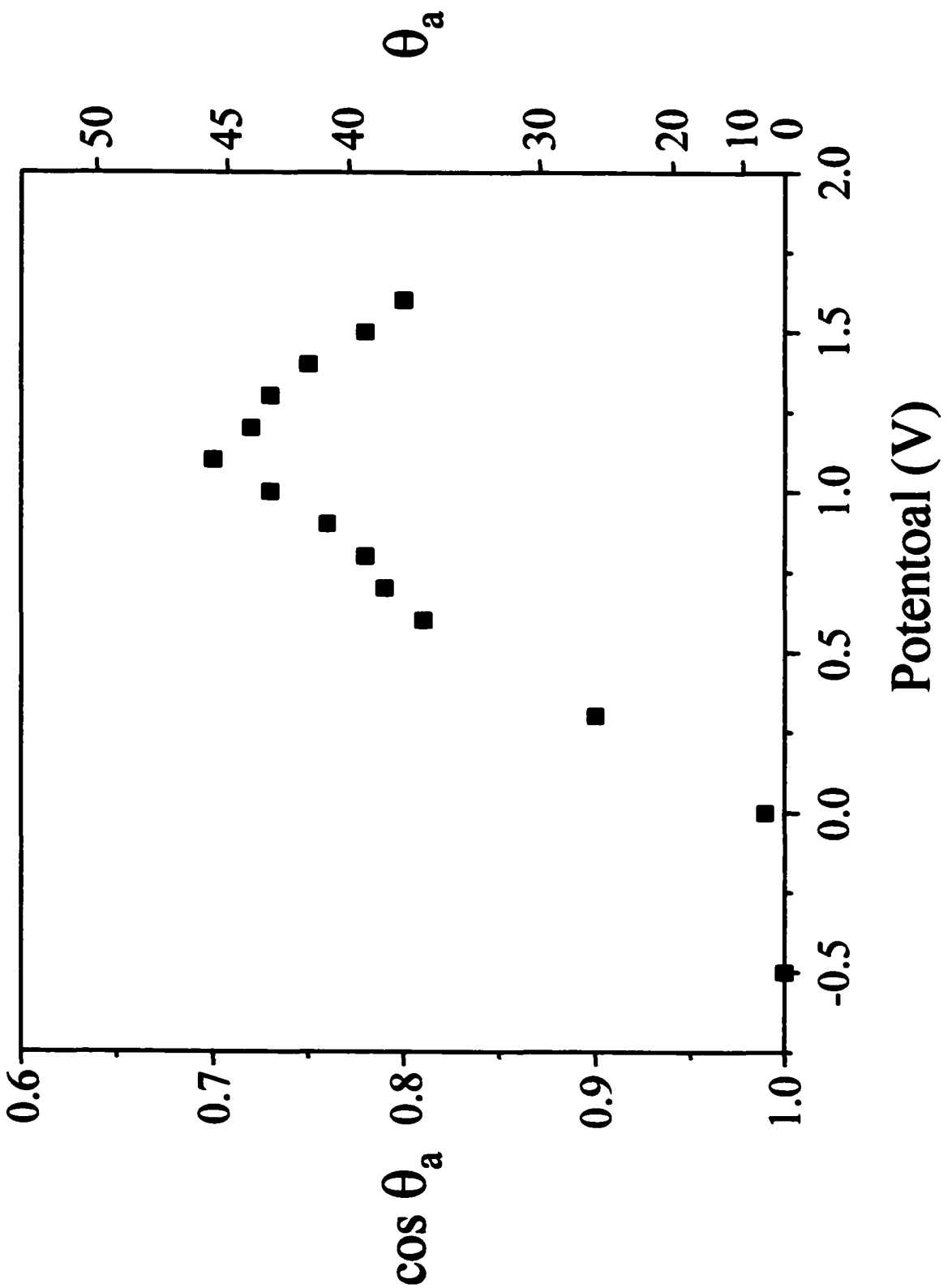

angles began to decrease. The maximum contact angles (45-46°) agreed with those reported for complete, well-ordered SAMs prepared by the chemisorption of *n*-tetradecanethiol (44-46°).[2]

We also followed the growth of these films systematically, as a function of the number of potentiometric pulses to a given potential by monitoring wettability by hexadecane on monolayers formed by electrolysis of *n*-tetradecylthiosulfate. Figure 2.8 shows these data for SAMs generated with from 1 to 100 pulses to 0.90, 1.00, 1.10, and 1.60 V. Using 0.90 V as the working potential, the contact angles of hexadecane on gold rose from 0 to 42° in the first ten pulses and then increased slowly to 45° after 100 cycles. With 1.00 V as the working potential, the contact angles of hexadecane reached 44° after 10 pulses and leveling off at 46° after 20 pulses. The optimum working potential for *n*-tetradecylthiosulfates, however, was 1.10 V, giving a SAM with a hexadecane contact angles of 44° after only 3 pulses, and quickly levelling off at 46° after only 5 cycles. Consistent with our results from cyclic voltammetry, using potentials higher than this optimum value gave incomplete monolayers. For example, pulses to 1.60 V gave lower contact angles of hexadecane in the first 20 pulses, and did not produce a monolayer with satisfactory contact angles (45-46°) after even 100 pulses.

The optimum potential to produce complete SAMs, judged by contact angles of hexadecane, varied as a function of the length of the alkyl chain of the alkylthiosulfates. We formed high quality SAMs from *n*-dodecylthiosulfates at 1.00 V, *n*-tetradecylthiosulfate at 1.10 V, and from *n*-hexadecylthiosulfate at 1.20 V. These data are consistent with ion migration and/or electron tunneling being important as these

Figure 2.8. Advancing contact angles of hexadecane on SAMs formed by electrochemical oxidation of *n*-tetradecylthiosulfate as a function of the number of voltametric pulses to 0.90 (●), 1.00 (◇), 1.10 (■) or 1.60 (□) V.

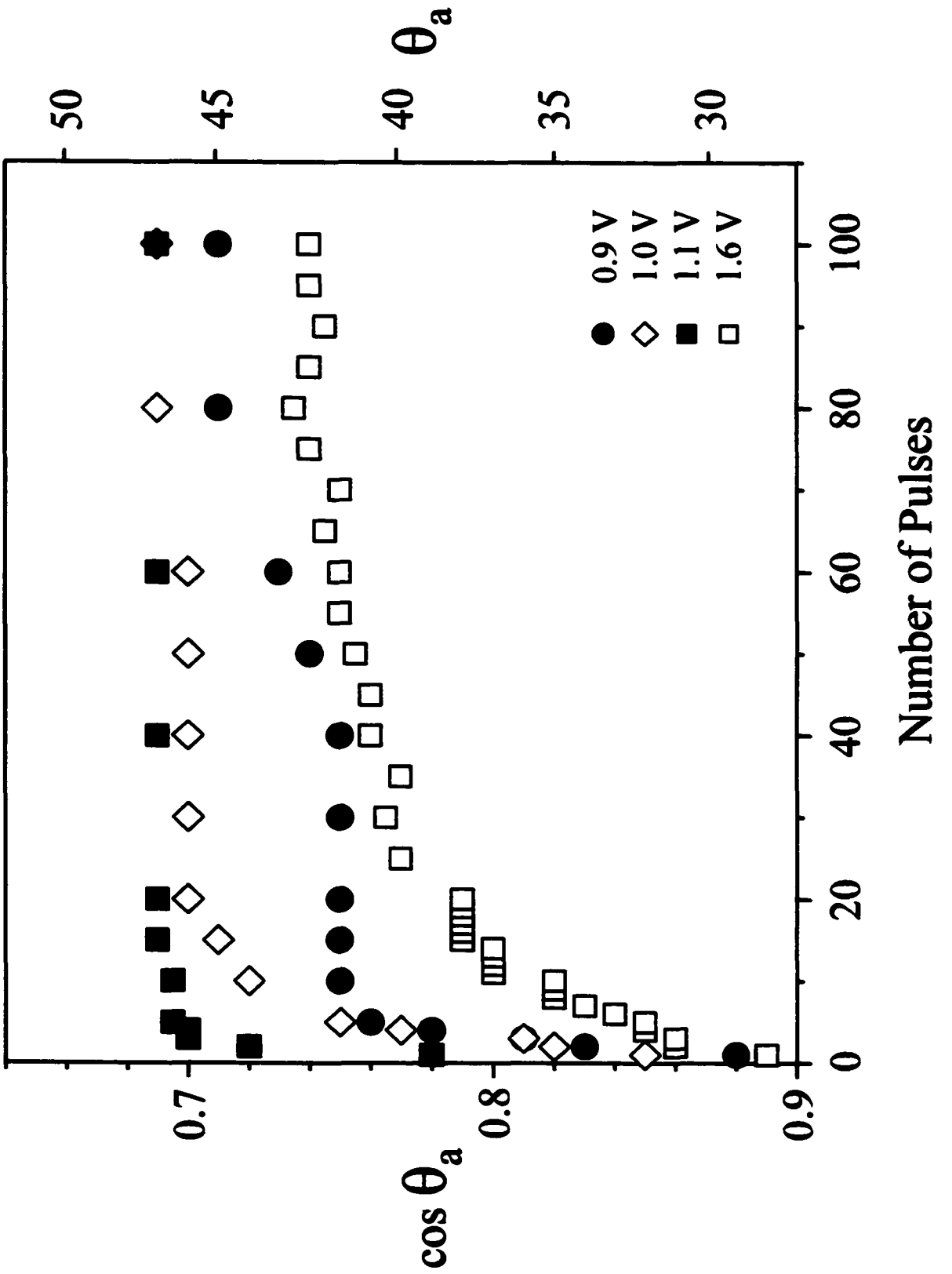

SAMs approach completion and explain why more complete SAMs are formed at higher potentials, up to the point were oxidation of the gold becomes a problem.[24] At a partially completed SAM, a potential slightly lower than the optimum potential, i.e. 1.00 V *vs.* 1.10 V, may not provide enough energy for an alkylthiosulfate ion to migrate, or for an electron to tunnel, through the film. Therefore, many more pluses were needed at 1.00 V than 1.10 V to get complete coverage. At even lower potential (e.g. 0.90 V), the monolayer only approached but did not reach completion. Potentials higher than 1.10 V resulted in oxidation of the gold, the SAM, or the solvent, with concomitant disordering of the monolayer.

Chemical analysis by x-ray photoelectron spectroscopy of SAMs formed electrochemically revealed the presence of only carbon and sulfur, as thiolate, on the gold surface (Figure 2.9). Survey spectra (20° take-off angle) of a monolayer formed by the electrolysis of *n*-hexadecylthiosulfate at 1.20 V (5 pulses) and of one formed by adsorption of *n*-hexadecanethiol from ethanol, shown in Figure 2.9, are nearly indistinguishable. Furthermore, high-resolution spectra (Figure 2.10, 20° take-off angle) of the same samples in the sulfur 2p region showed that both samples contained only thiolate sulfur, with no evidence of higher oxidation states due either to incomplete reduction of the thiosulfate or to oxidation of the thiolate by air (Figure 2.9, inset).[25] Likewise, the ratio of the integrated carbon (1s) to gold ($4f_{7/2}$) signals- a measure of the completeness of the monolayer- was very similar for the two types of monolayer (thiol, 3.0; thiosulfate, 2.8).[26]

Figure 2.9. X-ray photoelectron survey spectra of SAMs formed by adsorption of *n*-hexadecanethiol (a) and electro-chemisorption of *n*-hexadecylthiosulfate (b).

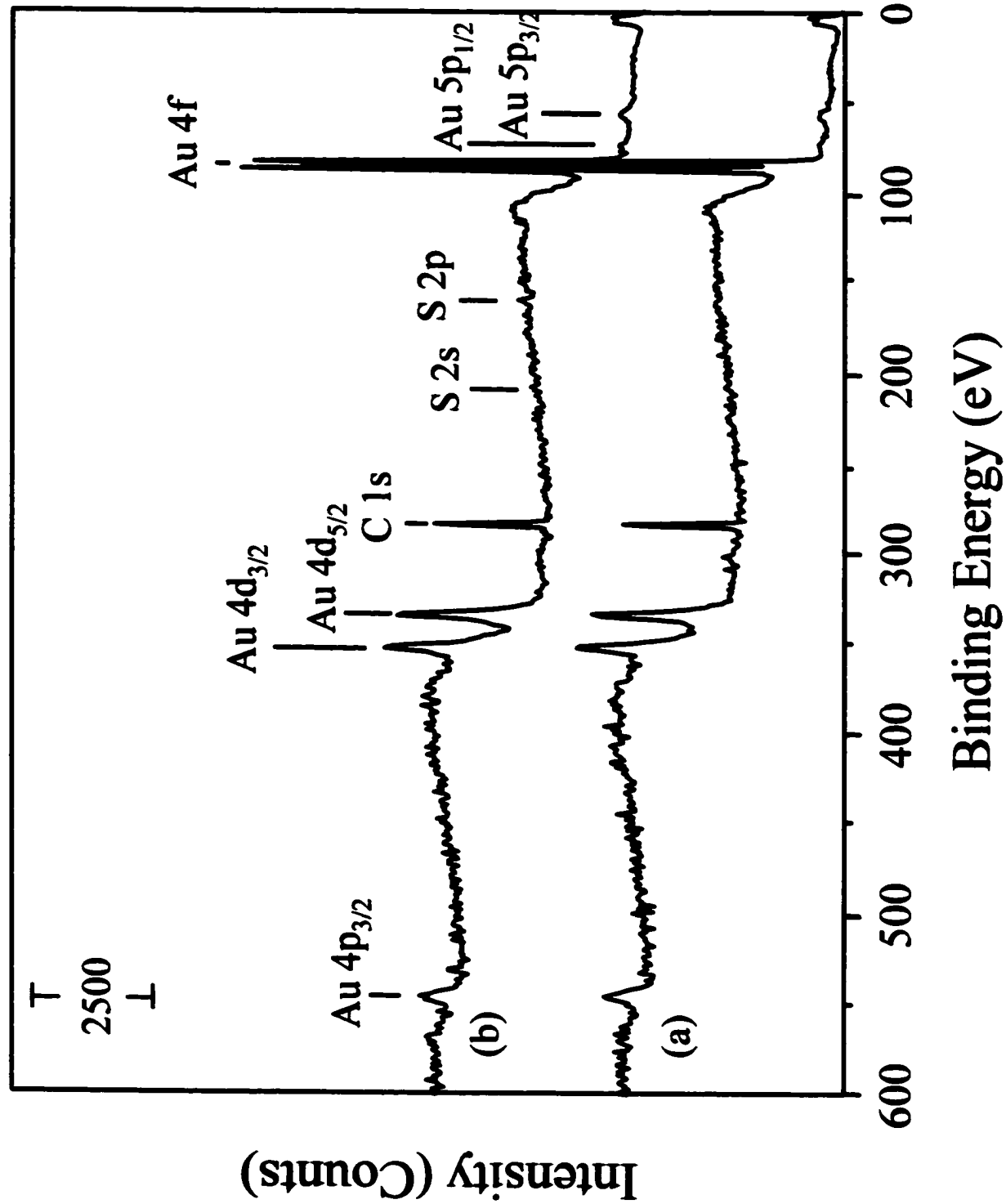

Figure 2.10. High-resolution X-ray photoelectron survey spectra in the sulfur 2p region of SAMs formed by (a) adsorption of *n*-hexadecanethiol and (b) by electro-chemisorption of *n*-hexadecylthiosulfate.

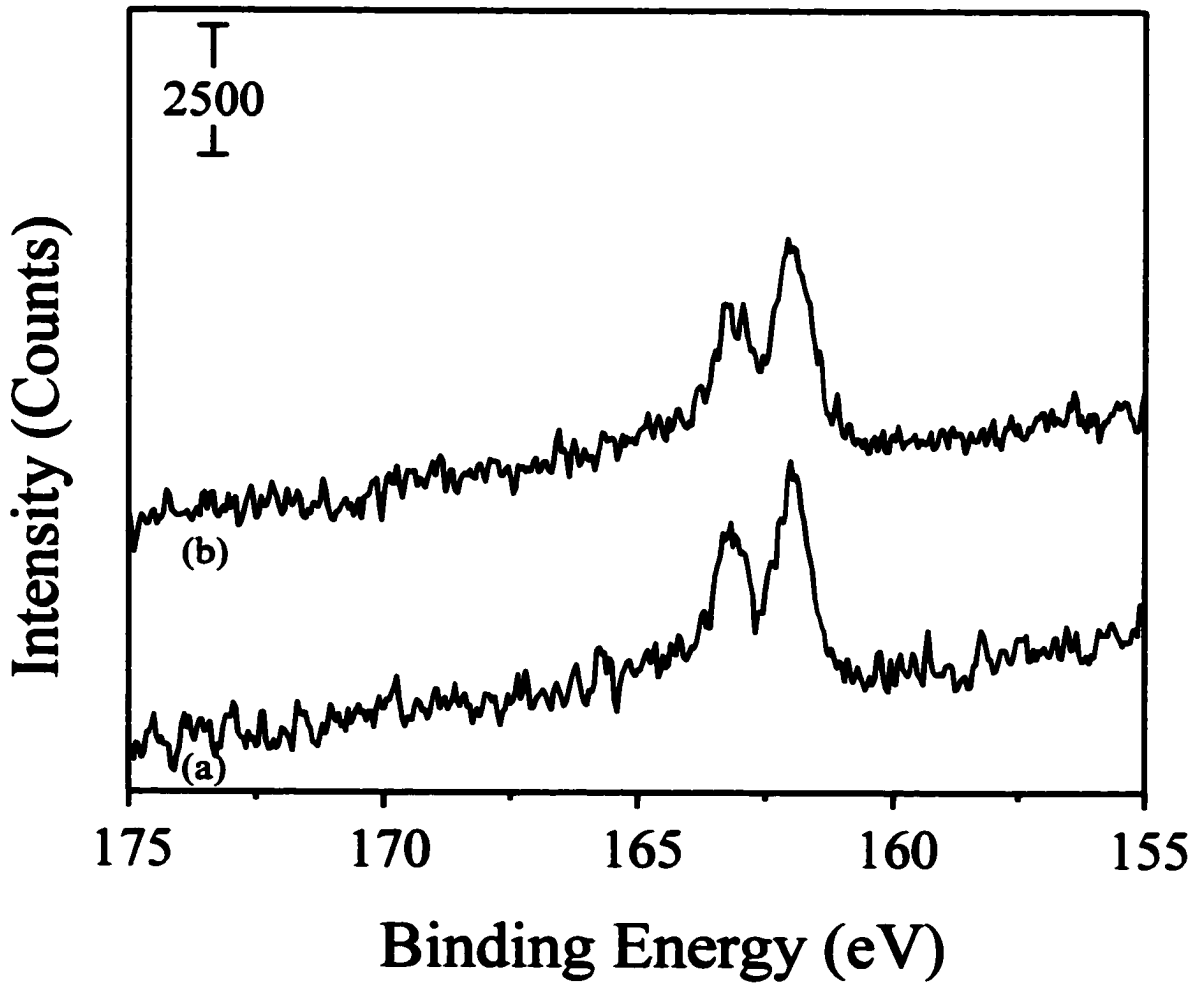

Spontaneous, Non-electrochemical Formation of SAMs from Bunte Salts.

In the absence of Bu_4NBF_4, a solution of *n*-hexadecylthiosulfate (10 mM in THF) formed complete a monolayer on gold spontaneously within 15 min, consistent with related observations by Lukkari and co-workers.[27] Thus, the selectivity of our approach depends on the ability of Bu_4NBF_4 to inhibit this spontaneous process in THF. In the presence of 0.1 M Bu_4NBF_4, it took 91 h to form an ordered monolayer by the spontaneous chemisorption of *n*-hexadecylthiosulfates in THF (Figure 2.11). Table 2.1 shows the contact angles of hexadecane on gold surfaces after treatment with THF solutions of *n*-hexadecylthiosulfate for 15 min in the presence of various amount of Bu_4NBF_4. As expected, low concentrations of Bu_4NBF_4 allowed monolayer formation to proceed to near completion within this time period, whereas higher concentrations significantly inhibited growth. Chemisorption was not inhibited, however, when tetrabutylammonium hexafluorophosphate (Bu_4NPF_6) or tetrabutylammonium perchlorate (Bu_4NClO_4) were used as the supporting electrolyte instead of Bu_4NBF_4, indicating that the tetrafluoroborate anion is responsible for inhibition of spontaneous chemisorption. One possible explanation may be the basicity of tetrafluoroborate in non-aqueous solvents such as THF, which could prevent acid hydrolysis of Bunte salt to produce thiol. In contrast, the presence of Bu_4NBF_4 (0.1 M in THF) did *not appear to* inhibit the formation of SAMs by chemisorption of *n*-hexadecanethiol (10 mM).

Electrolysis of Bunte salts at other Electrodes

When using platinum or graphite instead of gold as the working electrode (THF, 0.1 M Bu_4NBF_4), we did not observe oxidation attributable to the Bunte salt by cyclic

Figure 2.11. Advancing contact angles of hexadecane (θ_a) on a gold electrode as a function of the immersion time in a 10 mM solution of sodium *n*-hexadecylthiosulfate with (■) and without (○) 0.1 M Bu_4NBF_4. The inset shows the change in contact angles of hexadecane within the first 4 h.

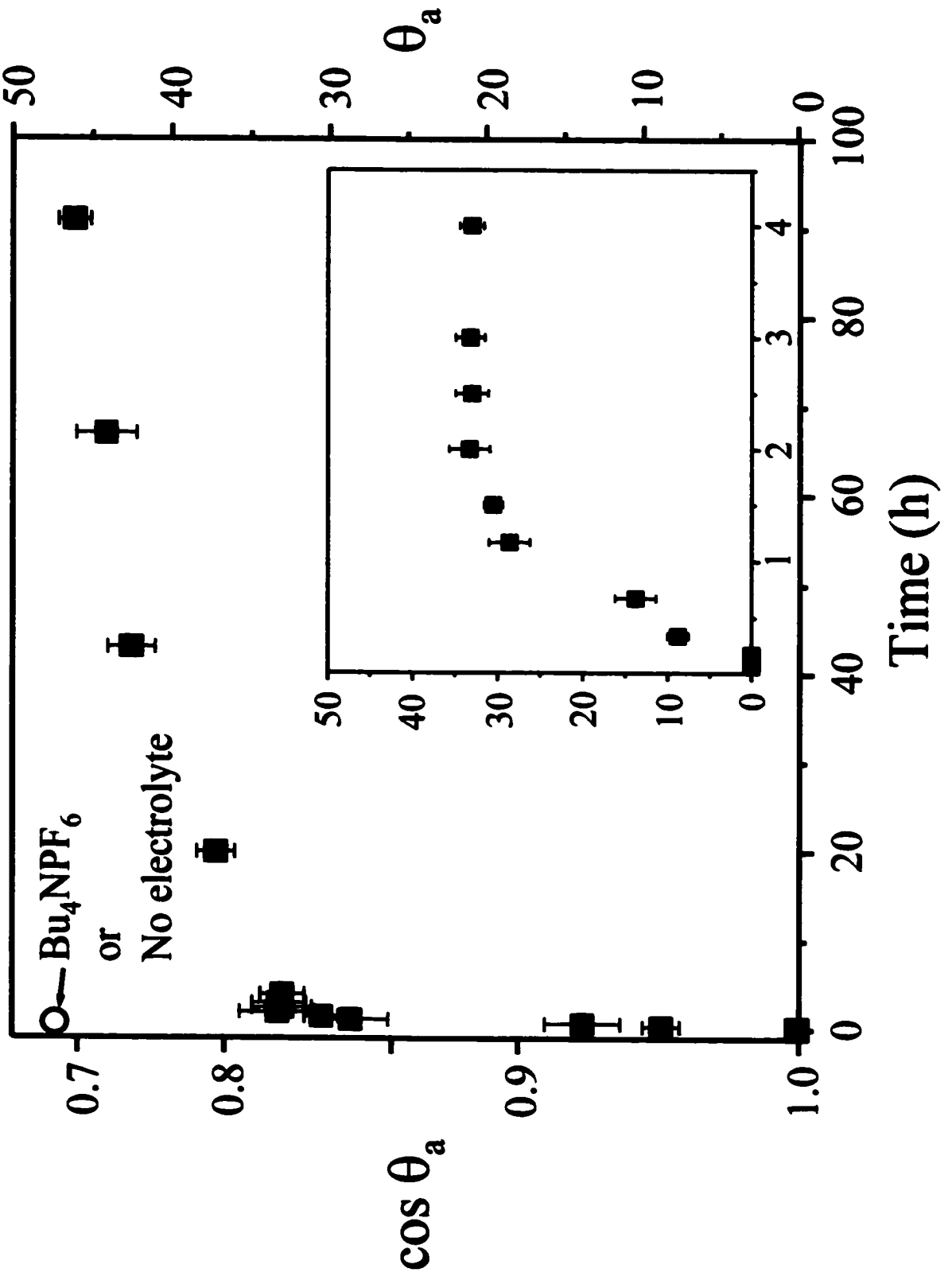

Table 2.1. Contact Angles of Hexadecane on SAMs Formed by Spontaneous Chemisorption of *n*-Hexadecylthiosulfate. After 15 min in the Presence/Absence of Tetrabutylammonium Tetrafluoroborate.

$[Bu_4NBF_4]/[C_{16}H_{33}S_2O_3Na]$	0	1	5	10
θ_a	46	42	16	<10°

Figure 2.12. (a) Cyclic voltammograms for a 10 mM solution of sodium *n*-hexadecylthiosulfate in THF (0.1 M Bu_4NBF_4, 100 mV/s) using a graphite working electrode and a $Ag/AgNO_3$ reference electrode (3 mM in CH_3CN). The inset shows a cyclic voltammogram for a graphite electrode in the solution of 10 mM ferrocene in THF (0.1 M Bu_4NBF_4, 100 mV/s) before and after being used ($Ag/AgNO_3$ reference electrode). (b) Cyclic voltammograms for a 10 mM solution of sodium *n*-hexadecylthiosulfate in THF (0.1 M Bu_4NBF_4, 100 mV/s) using a platinum working electrode and a $Ag/AgNO_3$ reference electrode (3 mM in CH_3CN). The inset shows a cyclic voltammogram for a platinum electrode in the solution of 10 mM ferrocene in THF (0.1 M Bu_4NBF_4, 100 mV/s) before and after being used ($Ag/AgNO_3$ reference electrode).

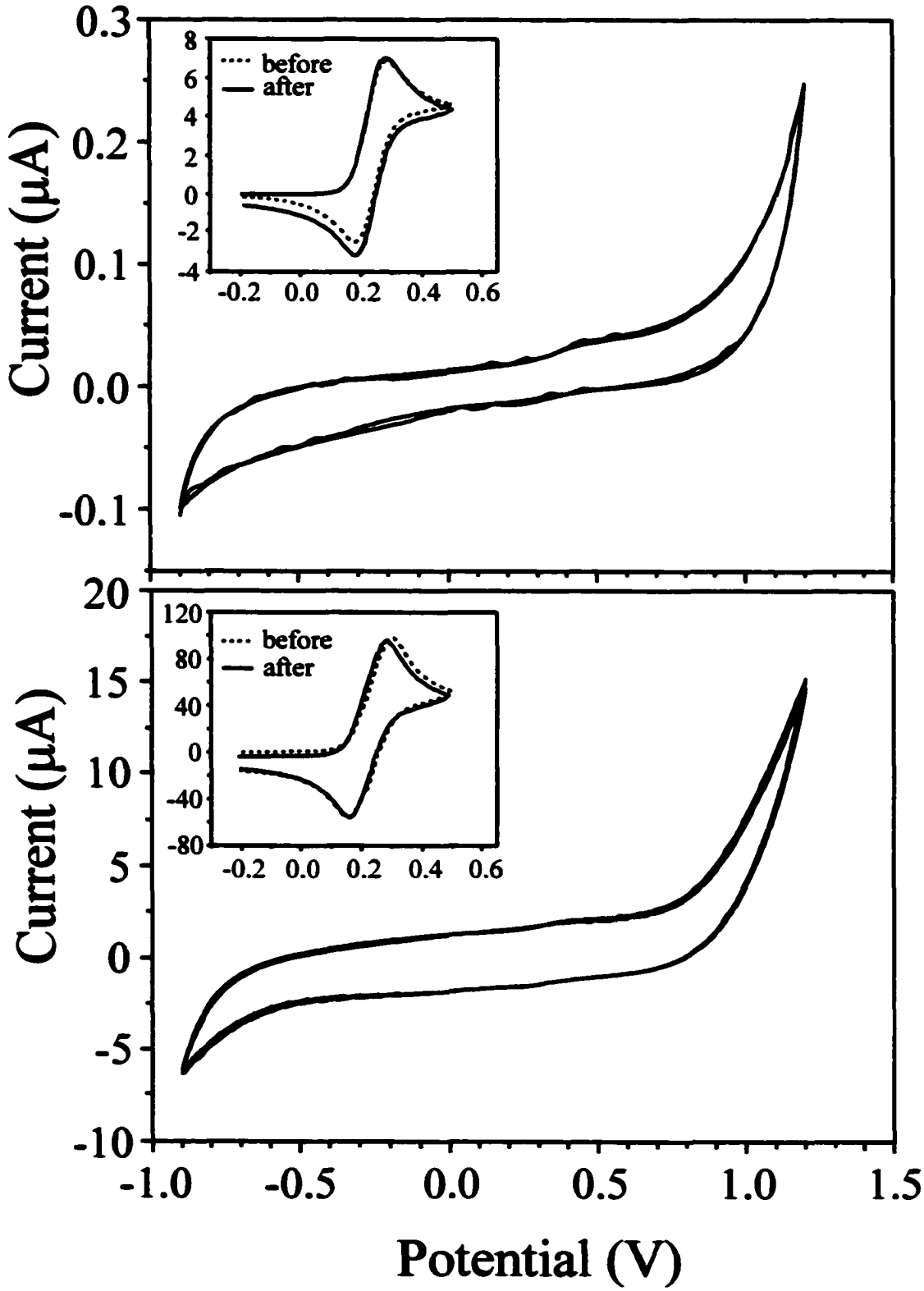

voltammetry. Figure 2.12 shows typical voltammograms for *n*-hexadecylthiosulfate (10 mM in THF, 0.1 M Bu_4NBF_4) using graphite and platinum as the working electrode, respectively. No oxidation peaks were observed at either electrode between –0.9 to 1.2 V. To rule out the possibility of electrode fouling during the cyclic scans, the electrodes were checked using ferrocene-ferricinium as a probe redox couple. Both electrodes showed normal electrochemical responses both before and after the Bunte-salt experiments (Figure 2.12, insets). Interestingly, the bulk electrolysis of Bunte salts at platinum electrodes in *acidic* water (0.1 M H_2SO_4 or 0.5 M $NaHSO_4$) has been reported previously.[17] Our results clearly indicate the involvement of gold surface chemistry in the electrochemically directed self-assembly of Bunte salts to form monolayers.

Mechanism of Monolayer Formation by Electrolysis at Gold Electrodes

Our mechanistic hypothesis, summarized in Figure 2.1, for the formation of SAMs in this way proposes the loss of SO_3 from the initially formed radical, followed by hydration to produce sulfuric acid. Because sulfate salts of sodium are only sparingly soluble in THF, one might expect precipitation at the electrode surface. To test this hypothesis, we analyzed the monolayer formed by oxidation of *n*-hexadecylthiosulfate both before and after rinsing with water, using x-ray photoelectron spectroscopy. The monolayers used in these studies were formed by electrolysis of *n*-hexadecylthiosulfate at 1.20 V using 5 pulses. After monolayer formation, one sample was rinsed with dry THF, and the other was rinsed with dry THF and then with water. The survey spectra (Figure 2.13) of these two samples were similar, expect for the photoemission due to Na (1s) at 1072.0 eV and O (1s) at 532.5 eV in the sample rinsed only with THF. The surface ratio

Figure 2.13. X-ray photoelectron survey spectra of SAMs formed by electrochemisorption of *n*-hexadecylthiosulfate, and that had been washed with only THF or washed with THF and water.

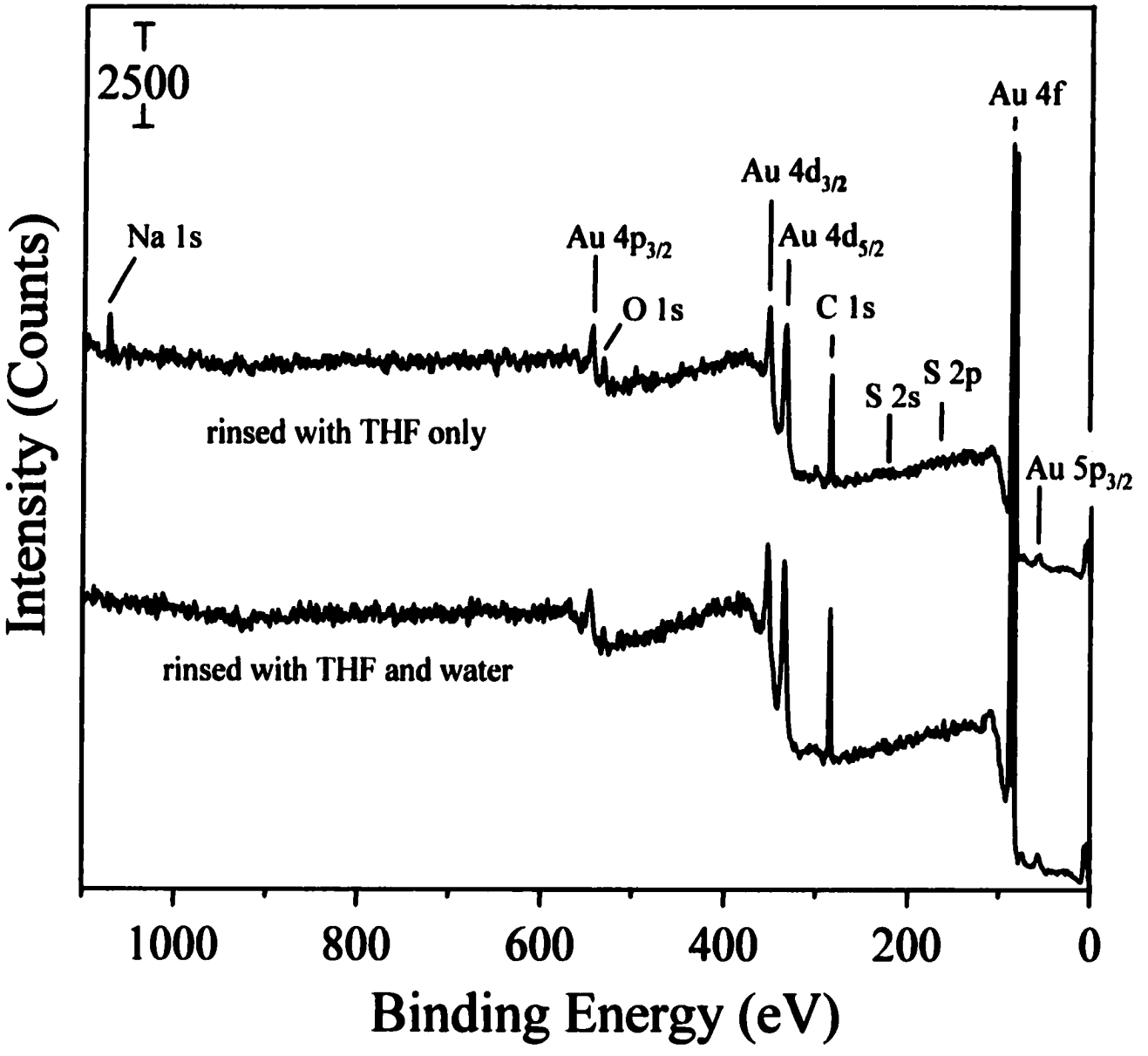

of sodium : sulfur (as sulfate): oxygen is 1.5 : 1 : 4 based on high-resolution spectra (Au $4f_{7/2}$, C 1s, O 1s, and Na 1s, and S 2p region) indicating a mixture of bisulfate and sulfate were produced during the electrolysis.[28] To minimize the influence of damage to the sample, these high-resolution spectra were collected from a different spot on the sample where the survey spectrum and the C, S, and Au regional scans were obtained. The sulfur spectrum was collected twice so that this ratio came from the same spot.

High-resolution scans of the sulfur 2p region (Figure 2.14) revealed an additional difference: the sample rinsed only with THF contained two types of sulfur, a spin-orbit doublet at 162.0 and 163.1 eV due to the thiolate and an additional doublet at higher binding energy (170.0 and 171.3 eV) assigned to sulfate.[28] In contrast, the monolayer washed with THF and water contained photoemission from sulfur only as thiolate (162.0 and 163.2 eV). The ratio of Na : S (as sulfate): O in the monolayers rinsed with only THF suggested the formation of mixture of sodium sulfate and sodium bisulfate. These data are consistent with the proposed conversion of alkylthiosulfate to thiolate and sulfate, as summarized in Figure 2.1.

Because sulfate is produced stoichiometrically in Figure 2.1, we expected bulk electrolysis of *n*-hexadecylthiosulfate to produce a large amount of it. Indeed, 72 h of continuous pulses to 1.20 V were applied in 20 mL of a 30 mM *n*-hexadecylthiosulfate solution (0.3 M Bu_4NBF_4) in THF at a gold electrode. A white solid precipitated onto the electrode during the electrolysis. The solution was centrifuged and the precipitate collected, and an infrared spectrum of the crude solid indicated the presence of a mixture of Bu_4NBF_4, Na_2SO_4, and $NaHSO_4$. After extraction of the Bu_4NBF_4 with THF, the

Figure 2.14. High-resolution sulfur 2p x-ray photoelectron spectra of SAMs formed by electro-chemisorption of *n*-hexadecylthiosulfate, and washed with only THF or washed with THF and water.

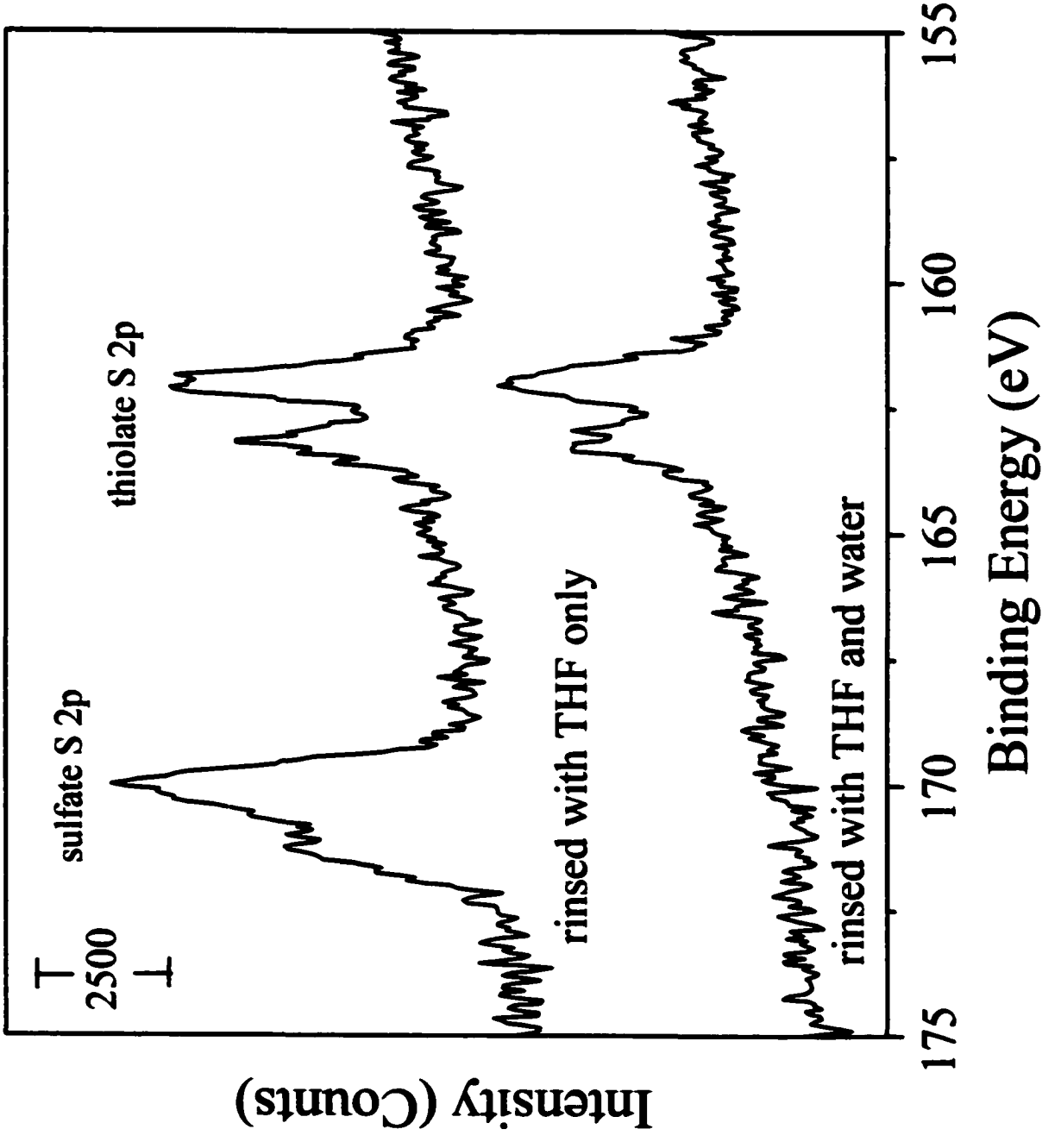

Figure 2.15. The infrared spectra of: (i) the aqueous extracts of product in bulk electrolysis of sodium *n*-hexadecylthiosulfate in THF; (ii) sodium sulfate; (iii) sodium bisulfate; and (iv) sodium *n*-decylthiosulfate.

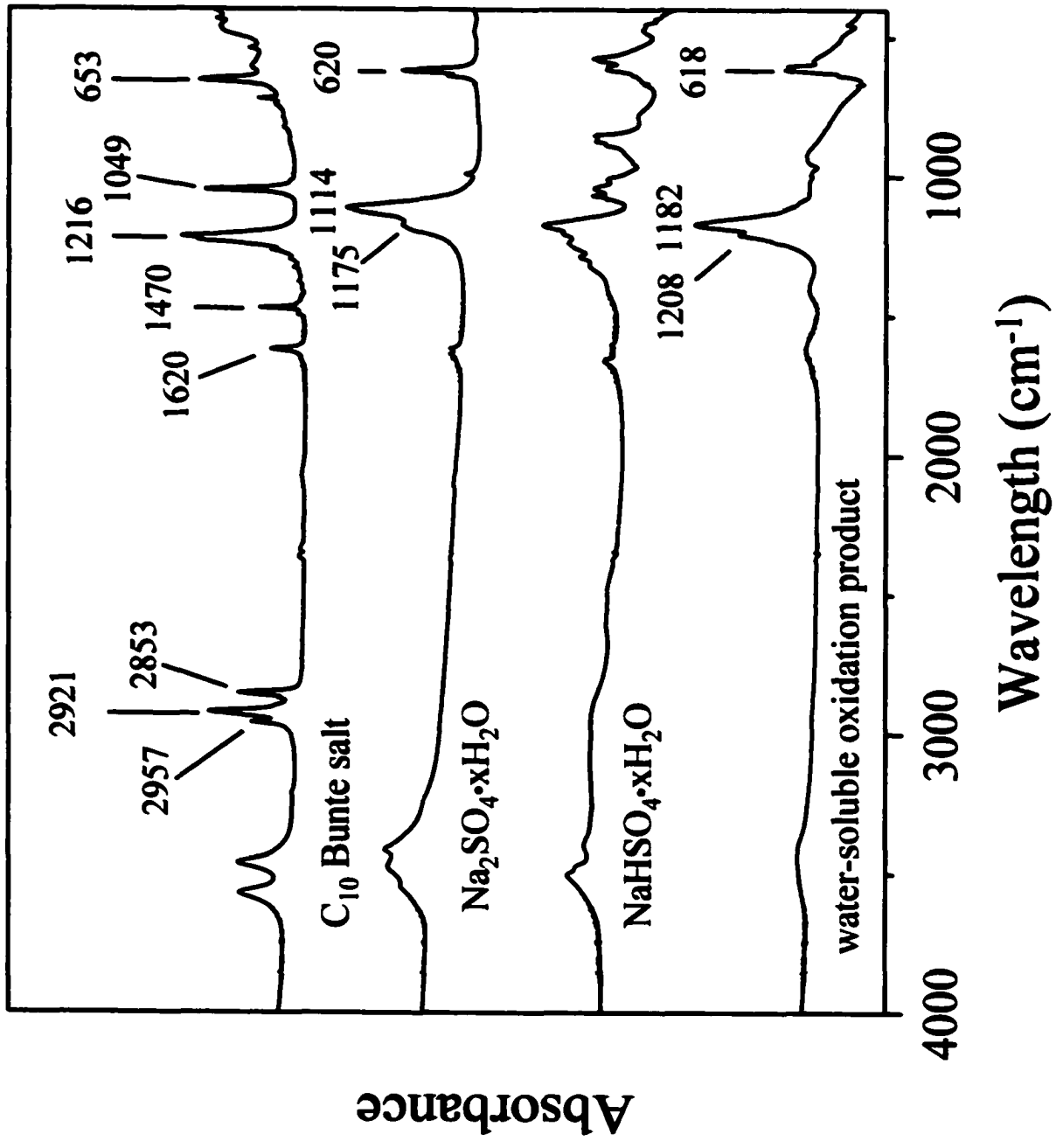

infrared spectrum of the purified solid (Figure 2.15) indicated that the product was mainly $NaHSO_4$.[29]

Advantages of this Electrochemical Synthesis of SAMs

One advantage of this electrochemical synthesis of SAMs is that clean gold is not required to form complete monolayers. To demonstrate this feature in dramatic way, two *dirty* gold electrodes were prepared by soaking in pump oil, followed by rinsing using hexanes and THF and drying with a stream of N_2. A good monolayer (θ_a = 44° for hexadecane) was obtained on one of these electrodes after 100 pulses to 1.10 V with *n*-tetradecylthiosulfate. In contrast, even 24 h of immersion in a 50-mM solution of hexadecanethiol in ethanol gave only an incomplete monolayer, with a 37° contact angle of hexadecane. These data suggest that the potential pulses either removed contamination from gold electrode or that the applied potential served to "drive" the alkylthiosulfate ion through the contamination and thereby displace it.

An even more important key advantage of this electrochemical synthesis over the conventional chemisorption of alkanethiols and -disulfides is that it provides *selectivity* in the placement of a SAM only on electrodes at potentials high enough to oxidize the thiosulfate precursor. We demonstrated this feature of the synthesis by selectively modifying one electrode in the close proximity of another. The samples used in these studies were triple-track testers,[30] comprising a serpentine pattern of three 76-μm-wide gold lines spaced 76 μm apart on an alumina substrate. The two outer lines were connected at one end and electronically isolated to differentiate an inner electrode.

In order to make the electrochemical modifications on the triple-track tester, we first covered its leads using epoxy to avoid the interference from the leads that were made of iron. We calculated the theoretical pulsing time that was short enough to avoid the diffusion of the alkyl thiolate radicals generated from the working gold track during modification. We estimated the thickness of a diffusion layer according the following equation:

$$\Delta^2 = 2\,Dt \qquad (2.1)$$

where Δ is the mean square displacement of the molecule, D is the diffusion coefficient (a typical value of D is 5×10^{-5} cm^2/sec in aqueous solution), and t is time.[31] In order to make the diffusion layer thickness smaller than the distance between each track, 76 μm, the pulse sequence must be less than about 1 s according to equation 2.1. This theoretical prediction was examined experimentally as follows: the triple track tester was immersed into a 1 mM solution of $K_3Fe(CN)_6$ in water. Two of the triple tracks were monitored simultaneously by using the bi-potential function of the potentiostat. At the beginning, both tracks were held at 0.5 V so that no $Fe(CN)_6^{3-}$ would be reduced to $Fe(CN)_6^{4-}$. The potential of one track was then changed to 0 volt so that $Fe(CN)_6^{3-}$ near this track began to be reduced to $Fe(CN)_6^{4-}$ and could diffuse away from the track. After 1.1 s, we observed a spike from the other track due to the oxidation of $Fe(CN)_6^{4-}$ that had diffused from the other track. From this experiment, we learned that the experimental value matched the theoretical value quite well and defined how short our pulses had to be to avoid the diffusion layer to reach the neighboring electrode. However, we also recognized that the diffusion layer could be built up if continuous pulses were applied

and the idle period was not short enough.

We started to modify our track by oxidizing *n*-dodecylthiosulfate salt with various pulse periods and checked the monolayer coverage by the blockage of redox of $Fe(CN)_6^{3-}$ /$Fe(CN)_6^{4-}$. Contact angle measurements could not be applied on such a small surface, 76μm in width, to provide information about the film quality. The literature contains reports that an ordered monolayer could effectively block the diffusion of $Fe(CN)_6^{3-}$ from the bulk solution by electron tunneling.[32] We saw very little blockage of the redox of $Fe(CN)_6^{3-}$/$Fe(CN)_6^{4-}$ on the track after even several hundred 0.01- and 0.05-s pulses. The monolayer gave only partial blockage on the track after 150 cycles of 0.1 s pulse sequences. Finally, 0.2-s pulses gave satisfactory results.

To demonstrate selectivity in this process, a triple-tracks-tester was then immersed into a 10 mM solution of sodium *n*-dodecylthiosulfate (THF, 0.1 M Bu_4NBF_4), and the potential of the central electrode was stepped from –0.90 V (vs. $Ag/AgNO_3$) to +0.90 V. It was held at this potential for 200 ms and then stepped back to the –0.90 V resting potential. This process was repeated through 150 pulses, with a 6-s interval between pulses; the outer electrode was electronically isolated throughout this process. The differences between this protocol and that used to form the SAMs of *n*-hexadecylthiosulfate reflect optimization to minimize cross-contamination of the nearby electrode in this experiment, as well as the difference in the chain lengths (C_{12} vs. C_{16}) of the precursors.

This process left the two electrodes on the device strongly differentiated, both in surface energy and electrochemical activity. Figure 2.16 shows a fluorescence

micrograph (100x magnification) of the device coated with a thin layer of a 1.06-mM aqueous solution of the fluorescent dye, rhodamine-6G.[33]

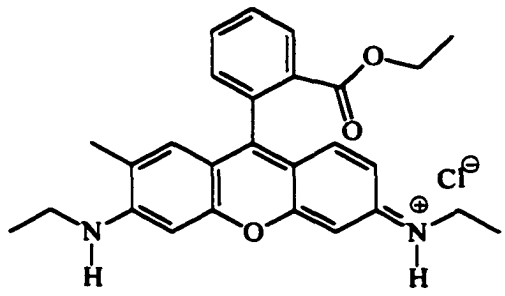

Blue excitation light B2A OM 510

450 ~ 490 nm main 480 nm

520 ~700 nm

Green excitation light G2A DM 580

510 ~ 560 nm main 546 nm

590 ~700 nm

The modified (central) electrode repels the solution and thus appears black due to the absence of the dye. The unmodified (outer) electrode is coated with the dye solution and thus appears greenish-yellow. Below the micrograph in Figure 2.16 are cyclic voltammograms for a second triple-track tester immersed in aqueous solution of ferricyanide, before and after electrode modification. The modified electrode B showed a normal response prior to modification but was electrochemically inactive after coating with a dodecanethiolate monolayer. In contrast, the response of the unmodified electrode A at this scan rate did not change significantly before and after treatment of electrode B.

2.4 Conclusions

In summary, we have developed an electrochemical method for the selective formation of self-assembled monolayers on a particular gold electrode in the presence of another nearby electrode. Self-assembled monolayers were prepared by electrolysis of alkylthiosulfates in THF in the presence of tetrabutylammonium tetrafluoroborate as the supporting electrolyte. The tetrafluoroborate ion was found to inhibit the spontaneous

Figure 2.16. A fluorescence micrograph (100x magnification) of a triple-track tester covered with a thin film of an aqueous solution of the fluorescent dye, rhodamine-6G (1.06-mM). The central electrode has been modified by 150 pulses to 0.90 V (vs. $Ag/AgNO_3$) in a 10 mM solution of sodium *n*-dodecylthiosulfate in THF (0.1 M Bu_4NBF_4) and is hydrophobic and dewetted by the dye solution. The outer electrode (two outer conducting lines) is unmodified and covered by the dye solution. Both the widths of the gold lines and the spacings between them were in the range of 70-80 μm. The cyclic voltammograms (1.0 mM $K_3Fe(CN)_6$, 0.1 M KCl, 100 mV/s) beneath the micrograph show the voltametric responses of both electrodes before (solid lines) and after (dashed lines) modification of the inner electrode.

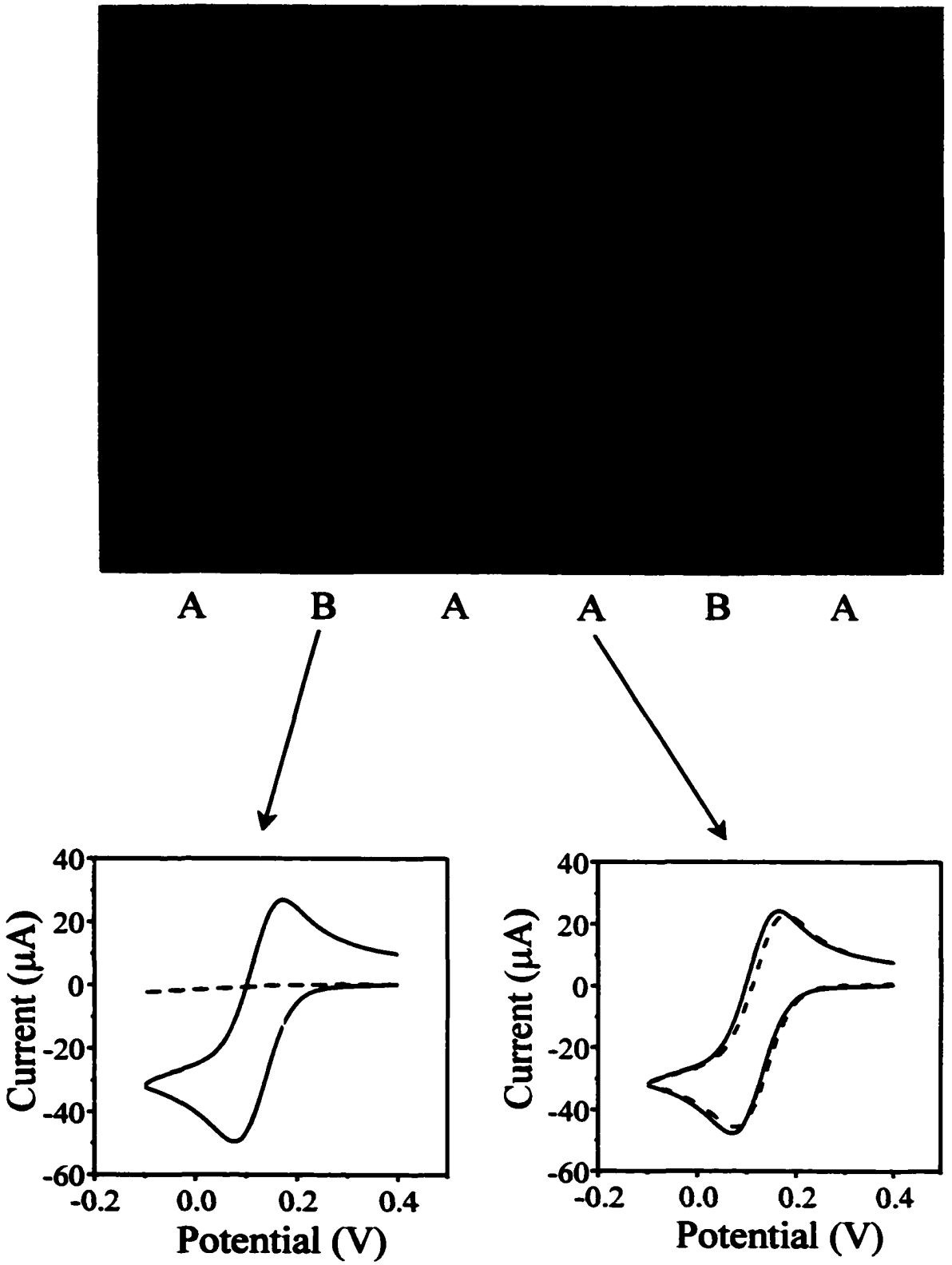

chemisorption of alkylthiosulfate onto gold, and thus SAMs only formed when a sufficiently anodic potential was applied. Cyclic voltammetry produced ordered monolayers, as long as the limiting upper voltage was not greater than 1.3 V. Likewise, potentiometric pulses could also be used to produce complete monolayers selectively in the presence of tetrafluoroborate ion. The degree of completeness of the resulting monolayers depended on the potential and number of pulses applied. A partial monolayer was formed when pulses to low potential were applied, and we attribute this result to an insufficient driving force for ion migration and/or electron tunneling through a partial film. At optimum potentials, however, a monolayer can be formed using only 5 pulses (less than 1 min). Use of a higher potential (e.g., 1.6 V) gave monolayers with low coverage due to oxidation of the gold, the SAM, or the solvent. The dependence of optimum potential upon alkyl chain length is consistent with the ion migration and/or electron tunneling hypothesis.

Spectroscopic evidence using both XPS and FT-IR indicated a byproduct of this process, that insoluble in THF, was a sulfate salt. Specifically, sulfur 2p photoemission in the XPS spectrum of SAMs that had been rinsed with only THF indicated the presence of both thiolate (monolayer) and sulfate (side-product) sulfur. An infrared spectrum of the product in a bulk electrolysis confirmed this assignment. These results are consistent with the mechanism in Figure 2.1.

The monolayers produced are very similar in thickness, wettability, blocking of heterogeneous electron transfer and elemental composition to analogous SAMs formed by the chemisorption of alkanethiols. The selectivity of this synthetic method should allow the preparation of microelectrode arrays having differentiated surface chemistry, a

goal of great importance in the fabrication of sophisticated sensor arrays.[34-35] Other attractive features of this electrosynthesis of SAMs are: i) the control it provides over the degree of coverage; ii) the short time necessary to form a SAM (less than a minute); iii) the ability to form SAMs easily on electrodes that are not clean; and iv) the use of precursors that lack an unpleasant odor (for alkyl groups containing more than about 10 carbons). Our use of alkylthiosulfates, rather than thiols or thiolates, as precursors avoids the risk of thiolate (solution)/thiolate (SAM) exchange that could prevent or complicate formation of a SAM on one electrode without contaminating a different SAM already in place on another.

2. 5 Experimental Methods

2.5.1 *Materials.* Hexadecanethiol (Aldrich, 92%) was purified by distillation under vacuum prior to use. Tetrabutylammonium hexafluorophosphate (98%), tetrabutylammonium perchlorate (99%), lithium perchlorate (95+%), sodium hydrogen sulfate (technical grade), 1-bromohexadecane (97%), 1-bromotetradecane (97%), 1-bromododecane (96%), 1-bromodecane (98%), 1-bromooctane (99%), potassium ferricyanide (99%), potassium ferrocyanide (99%), Rhodamine-6G (99%), and sodium thiosulfate pentahydrate (99.5%) were obtained from Aldrich and used as received. Ferrocene (dicyclopentadienyliron, 98%) was obtained from Alfa and used as received. Absolute ethanol (McCormick Distilling Co), sodium sulfate (EM Science, 99%), and silver nitrate (Kodak, 99.9%) were used as received. The hexadecane (Aldrich, 99%) used in the contact-angle measurements was purified by percolation twice through activated alumina. Tetrahydofuran (EM Science, 99.94%) was distilled from sodium-

benzophenone ketyl before use. Gold (99.99%) was obtained from Refining System Co and used as received. The epoxy, Epoxi-Patch, was from Dexter Corporation and used as received. Pump oil used in the "dirty gold" experiment was from VWR Scientific (vacuum pump oil No. 19) and used as received. All water used in this work was purified with a Milli-Pore Milli-Q system to a resistivity of at least 15 MΩ-cm.

2.5.2 *Preparation of Sodium Alkylthiosulfates, $CH_3(CH_2)_nS_2O_3Na$ (n= 7, 9, 11, 13, 15).* The Bunte salts were prepared following a literature procedure.[17] For example, 1-bromohexadecane (1.53 g, 5 mmol) dissolved in 20 mL of ethanol was added to a solution of sodium thiosulfate (1.24 g, 5 mmol) in 20 mL of water, and the mixture was brought to reflux until the solution became homogeneous. The solution was then cooled to room temperature, allowing the *n*-hexadecylthiosulfate to precipitate. The white solid was filtered and recrystallized using ethanol. ^{1}H NMR: $CH_3(CH_2)_{15}SSO_3Na$, 0.86, (t, 3H); $CH_3(CH_2)_{13}CH_2SSO_3Na$, 1.31-1.50, (m, 26H); $CH_3(CH_2)_{14}CH_2SSO_3Na$, 1.65, (doublet-triplet, 2H); $CH_3(CH_2)_{13}CH_2CH_2SSO_3Na$, 2.66, (t, 2H).

2.5.3 *Electrochemistry.* The electrochemistry experiments were carried out using Bioanalytical Systems BAS-100B or EG & G Potentiostat/Galvanostat Model 273 from Princeton Applied Research. A conventional three-electrode configuration is equipped. In all cases, the gold coated on glass was the working electrode, a platinum flag (7 mm x 20 mm) was the counter electrode, and a glass tube with a Vycor tip containing $Ag/AgNO_3$ (3 mM)[31] in acetonitrile plus 0.1 M $(Bu)_4NBF_4$ which freshly prepared prior to experiments was the reference electrode. This reference electrode was checked against the $Fe(CN)_6^{3-}/Fe(CN)_6^{2-}$ redox couple prior to these experiments. All the

cyclic voltammograms reported in this paper started with a scan in the anodic direction from –0.90 V and were collected at 100 mV/s in the presence of 0.1 M Bu_4NBF_4 as a supporting electrolyte.

2.5.4 *Sample Preparation.* Glass microscope slides were treated with (3-mercaptopropyl)trimethoxysilane according to a published procedure to act as an adhesion promoter for a gold overlayer.[36] Gold films were then deposited by thermal evaporation of the metal at ~ 0.5 Å/s at a background pressure of approximately $2x10^{-6}$ Torr, to a final thickness of about 1000 Å. The gold electrode was placed into 10 mM sodium alkylthiosulfate with 0.10 mM $(Bu)_4NBF_4$ in THF. The potential was stepped from –0.90 V to 1.20 V for 5 s and then stepped back to the –0.90 V resting potential for 5 times for sodium *n*-hexadecylthiosulfate. The working potentials for the tetradecyl and dodecyl analogues were set at 1.10 V and 1.00 V, respectively, while the resting potential was kept at –0.90 V. The substrate was then rinsed with THF and absolute ethanol and dried with a stream of N_2.

2.5.4 *X-ray Photoelectron Spectroscopy.* The XPS spectra in this paper were obtained using a Scienta ESCA-300 spectrometer, equipped with a rotating anode (Al Kα) source producing approximately 39.0 kW of X-ray power, a monochromator, and a 300-mm (diameter) hemispherical analyzer. All spectra were collected at a 20° take-off angle between the plane of the surface and the detector, a slit width of 11 mm, and were referenced to the Au $4f_{7/2}$ peak set at 84.0 eV. The background pressure in the sample chamber was $2x10^{-9}$ Torr. Survey scans were collected with a pass energy of 75 eV and a step energy of 1.0 eV, and took 5.5 min to complete. Sulfur 2p regional scans were

collected with a pass energy of 150 eV and a step energy of 0.05 eV, and took 10 min to complete (5 scans). Carbon 1s regional scans were collected with a pass energy of 150 eV and a step energy of 0.05 eV, and took 4.5 min to complete (2 scans). Gold $4f_{7/2}$ regional scans were collected with a pass energy of 75 eV and a step energy of 0.2 eV, and took 1 min to complete (single scan). Oxygen 1s regional scans were collected with a pass energy of 150 eV and a step energy of 0.05 eV, and took 6 min to complete (3 scans). Sodium 1s regional scans were collected with a pass energy of 150 eV and a step energy of 0.05 eV, and took 6.5 min to complete (5 scans).

For quantitative analysis, the sensitivity factors used to correct the number of counts under each peak (or envelope) were: Au $4f_{7/2}$, 9.58; C 1s, 1.000; O 1s, 2.8370; S 2p (both components), 2.1735; and Na 1s, 8.520. The sensitivity factors for oxygen, carbon, and sulfur, and sodium photoemission were determined by A. C. Miller with the Scienta ESCA-300 at Lehigh University. The value for gold is the Scofield value.[37] The curve fitting was performed using Scienta ESCA system software[38] following a published procedure:[39] Each peak is described as a sum of Gaussian and Lorentzian functions, assuming a linear baseline. For C 1s photoemission, all fits had reasonable mixing ($m \geq 0.85$) and asymmetry ($A \leq 0.12$) ratios, as well as acceptable line widths (1.00-1.25 eV, fwhm). For Au $4f_{5/2}$ photoemission, all fits had reasonable mixing ($m \geq 0.70$) and asymmetry ($A \leq 0.14$) ratios with line width between 0.65-0.68 eV (fwhm). For S 1s photoemission, all fits had mixing (≥ 0.60) and asymmetry (≤ 0.21) ratios, as well as acceptable line widths (0.60-0.860 eV, fwhm). For Na 1s photoemission, the fwhm was 1.79 eV, with an asymmetry ratio of 0.012, and mixing ratio of 1. For O 1s

photoemission, the fwhm was 1.39 eV, with an asymmetry ratio of 0.14, and mixing ratio of 1.

2.5.5 *Contact Angle and Ellipsometry Measurements.* Advancing contact angle measurements of hexadecane and water were measured using a Rame-Hart NRL Model 100 goniometer. A minimum of six measurements on three independent drops were made for each sample. Ellipsometric measurements were made using an automatic null ellipsometer (Rudolph Auto-EL III) equipped with helium-neon laser (λ = 632.8 nm) set at a 70° incident angle, employing the manufacturer's program. Measurements were collected from four arbitrarily chosen spots on the samples. Calculations of film thickness typically assumed a refractive index of monolayer is 1.5.

2.5.6 Infrared Spectroscopy. Infrared spectra were collected using a Perkin-Elmer FT-IR 1600 spectrometer, at a resolution of 2 cm^{-1}. In each case, 64 scans were averaged to achieve a satisfactory signal-to-noise ratio.

2.5.7 *GC-MS and NMR.* The masses of sufficiently volatile products were confirmed using a Hewlett Packard 5890 Series II Gas Chromatography, equipped with Hewlett Packard 5972 series Mass Selective detector. ^1H NMR spectra were acquired using a Bruker AMX 360 spectrometer, referenced to $CHCl_3$ at 7.24 ppm and are reported in unit of δ.

2.5.8 *Fluorescence Microscopy.* The fluorescence microscopy was done using Nikon Microflex UFX-II, Nikon Biological Microscope OPTIPHOT equipped with Nikon FX-35A camera. The magnification in this experiment was 100x. A red filter was

used when the pictures were taken. Rhodamine-6G (1.06 mM) in water was used as the dye solution.

2.6 Acknowledgements

We gratefully acknowledge partial funding from the Polymer Interfaces Center, an Industry/University Cooperative Research Center at Lehigh sponsored by the National Science Foundation, and from Lehigh University. We also want to thank Dr. Michael Freund and Dr. Chen-Chan Hsueh for their suggestions, discussions, and help during the collaborative work in this project. We thank AT&T Bell Laboratories (now Lucent, Inc.) for a gift of the triple-track testers. We also thank A. C. Miller for assistance with the XPS measurements and L. Lowe-Krentz for allowing the use of the fluorescence microscope.

2.7 References

1. Nuzzo, R. G.; Allara, D. L. *J. Am. Chem. Soc.* **1983**, *105*, 448.
2. Bain C. D.; Troughton, E. B.; Tao, Y.-T.; Evall, J.; Whitesides, G. M.; Nuzzo, R. G. *J. Am. Chem. Soc.* **1989**,*111*, 321-335.
3. Ulman, A. *Chem. Rev.* **1996**, *96*, 1533.
4. (a) Abe, K.; Takiguchi, H.; Tamada, K. *Langmuir* **2000**, *16*, 2394. (b) Abbott, S.; Ralston, J.; Reynolds, G.; Hayes, R. *Langmuir* **1999**, *15*, 8923. (c) Graupe, M.; Koini, T.; Kim, H. I.; Garg, N.; Miura, Y. F.; Takenaga, M.; Perry, S. S.; Lee, T. R. *Colloids Surf., A* **1999**, *154*, 239. (d) Miura, Y. F.; Takenaga, M.; Koini, T.; Graupe, M.; Garg, N.; Graham, R. L. Jr.; Lee, T. R. *Langmuir* **1998**, *14*, 5821. (e) Engquist, I.; Liedberg,

B. *J. Phys. Chem.* **1996**, *100*, 20089. (f) Ulman, A. *Thin Solid Films* **1996**, *273*, 48. (g) Drelich, J.; Miller, J. D.; Good, R. J. *J. Colloid Interface Sci.* **1996**, *179*, 37. (h) Lee, T. R.; Carey, R. I.; Biebuyck, H. A.; Whitesides, G. M. *Langmuir* **1994**, *10*, 741. (i) Laibinis, P. E.; Whitesides, G. M. *J. Am. Chem. Soc.* **1992**, *114*, 1990. (j) Laibinis, P. E.; Fox, M. A.; Folkers, J. P.; Whitesides, G. M. *Langmuir* **1991**, *7*, 3167. (k) Bain, C. D.; Whitesides, G. M. *J. Am. Chem. Soc.* **1989**, *111*, 7164.

5. (a) Quon, R. A.; Ulman, A.; Vanderlick, T. K. *Langmuir* **2000**, *16*, 8912. (b) Callow, M. E.; Callow, J. A.; Ista, L.K.; Coleman, S. E.; Nolasco, A. C.; Lopez, G. P. *Appl. Environ. Microbiol.* **2000**, *66*, 3249. (c) Clear, Susannah C.; Nealey, Paul F. *J. Colloid Interface Sci.* **1999**, *213*, 238. (d) Glodde, M.; Hartwig, A.; Hennemann, O.-D.; Stohrer, W.-D. *Int. J. Adhes. Adhes.* **1998**, *18*, 359. (e) Zhuk, A. V.; Evans, A. G.; Hutchinson, J. W.; Whitesides, G. M. *J. Mater. Res.* **1998**, *13*, 3555. (f) Opila, R. L.; Legrange, J. D.; Markham, J. L.; Heyer, G.; Schroeder, C. M. *J. Adhes. Sci. Technol.* **1997**, *11*, 1. (g) Silin, V.; Weetall, H. *Proc. Annu. Meet. Adhes. Soc.* **1996**, *19*, 211. (h) Wiencek, K. M.; Fletcher, M. *J. Bacteriol.* **1995**, *177*, 1959.

6. (a) Schoenfisch, M. H.; Ovadia, M.; Pemberton, J. E. *J. Biomed. Mater. Res.* **2000**, *51*, 209. (b) Bruening, M. L.; Zhou, Y.; Aguilar, G.; Agee, R.; Bergbreiter, D. E.; Crooks, R. M. *Langmuir* **1997**, *13*, 770. (c) Rudolph, A. S. *J. Cell Biochem.* **1994**, *56*, 183.

7. (a) Retna, R. C.; Ohsaka, T. *Bioelectrochem.* **2001**, *53*, 251. (b) Grunze, M. *Proc. Annu. Meet. Adhes. Soc.* **2000**, *23*, 4. (c) Wiencek, K. M.; Fletcher, M. *Biofouling* **1997**, *11*, 293. (d) Ista, L. K.; Fan, H.; Baca, O.; Lopez, G. P. *FEMS Microbiol. Lett.* **1996**, *142*, 59. (e) Lindner, E. *Biofouling* **1992**, *6*, 193. (f) Whitesides, G. M.;

Ferguson, G. S.; Allara, D.; Scherson, D.; Speaker, L.; Ulman, A. *Rev. Surf. Chem.* **1993**, *3*, 49.

8. (a) Emberly, E.; Kirczenow, G. *J. Appl. Phys.* **2000**, *88*, 5280. (b) Forzani, E. S.; Solis, V. M.; Calvo, E. J. *Anal. Chem.* **2000**, *72*, 5300. (c) Deng, W.; Fujita, D.; Yang, L.; Nejo, H.; Bai, C. *Jpn. J. Appl. Phys. Part 2*, **2000**, *39*, L751. (d) Berlin, A.; Zotti, G. *Macromol. Rapid Commun.* **2000**, *21*, 301. (e) Cheng, Y.; Corn, R. M. *J. Phys. Chem. B.* **1999**, *103*, 8726. (f) Nishimura, N.; Ooi, M.; Shimazu, K.; Fujii, H.; Uosaki, K. *J. Electroanal. Chem.* **1999**, *473*, 75. (g) Reinerth, W. A.; Jones, L., II; Burgin, T. P.; Zhou, C.-w.; Muller, C. J.; Deshpande, M. R.; Reed, M. A.; Tour, J. M. *Nanotechnology* **1998**, *9*, 246. (h) Nakanishi, T.; Ohtani, B.; Uosaki, K. *J. Phys. Chem. B* **1998**, *102*, 1571. (i) Kaifer, A. E. *Prog. Colloid Polym. Sci.* **1997**, *103*, 193. (j) Clark, S. L.; Montague, M.; Hammond, P. T. *Supramol. Sci.* **1997**, *4*, 141. (k) Lee, Y. J.; Jeon, I. C.; Paik, W.-k.; Kim, K. *Langmuir* **1996**, *12*, 5830. (l) Davis, F.; Stirling, C. J. M. *J. Am. Chem. Soc.* **1995**, *117*, 10385. (m) Tour, J. M.; Jones, L. II; Pearson, D. L.; Lamba, J. J. S.; Burgin, T. P.; Whitesides, G. M.; Allara, D. L.; Parikh, A. N.; Atre, S. *J. Am. Chem. Soc.* **1995**, *117*, 9529. (n) Bell, C. M.; Yang, H. C.; Mallouk, T. E. *Adv. Chem. Ser.* **1995**, *245*, 211. (o) Evans, S. D.; Freeman, T. L.; Flynn, T. M.; Batchelder, D. N.; Ulman, A. *Thin Solid Films* **1994**, *244*, 778. (p) Schneider, T. W.; Buttry, D. A. *J. Am. Chem. Soc.* **1993**, *115*, 12391. (q) Spinke, J.; Liley, M.; Guder, H. J.; Angermaier, L.; Knoll, W. *Langmuir* **1993**, *9*, 1821. (r) Thomas, R. C.; Sun, L.; Crooks, R. M.; Ricco, A. J. *Langmuir* **1991**, *7*, 620.

9. (a) Gaspar, S.; Zimmermann, H.; Gazaryan, I.; Csoregi, E.; Schuhmann, W.

Electroanalysis, **2001**, *13*, 284 (b) Ferretti, S.; Paynter, S.; Russell, D. A.; Sapsford, K. E.; Richardson, D. J. *Trends Anal. Chem.* **2000**, *19*, 530. (c) Yang, S.; Perez-Luna, V. H.; Lopez, G. P. *Proc. SPIE-Int. Soc. Opt. Eng.* **2000**, *3926*, 181. (d) Chen, C. S.; Ostuni, E.; Whitesides, G. M.; Ingber, D. E. *Methods Mol. Biol.* **2000**, *139*, 209. (e) Alexander, P. W.; Rechnitz, G. A. *Electroanalysis* **2000**, *12*, 343. (f) Nyquist, R. M.; Eberhardt, A. S.; Silks, L. A., III; Li, Z.; Yang, X.; Swanson, B. I. *Langmuir* **2000**, *16*, 1793. (g) Everhart, D. S. *Chemtech* **1999**, *29*, 30. (h) Liedberg, B; Cooper, J. M. in *Immobilized Biomolecules in Analysis*; Cass, T.; Ligler, F. S. Ed.; Oxford University Press. 1998, p55-78. (i) Cotton, C.; Glidle, A.; Beamson, G.; Cooper, J. M. *Langmuir* **1998**, *14*, 5139. (j) Gooding, J. J.; Praig, V.; Hall, E. A. H. *Anal. Chem.* **1998**, *70*, 2396. (k) Chen, C. S.; Mrksich, M.; Huang, S.; Whitesides, George M.; Ingber, D. E. *Biotechnol. Prog.* **1998**, *14*, 356. (l) Tender, L. M.; Opperman, K. A.; Hampton, P. D.; Lopez, G. P. *Adv. Mater.* **1998**, *10*, 73 (m) Sampath, S.; Lev, O. *Adv. Mater.* **1997**, *9*, 410-413, and references therein.

10. (a) Collinson, M.; Bowden, E. F.; Tarlov, M. J. *Langmuir* **1992**, *8*, 1247. (b) Willner, I.; Katz, E.; Riklin, R.; Kasher, R. *J. Am. Chem. Soc.* **1992**, *114*, 10967.
11. (a) Chan, K. C.; Kim, T.; Schoer, J. K.; Crooks, R. M. *J. Am. Chem. Soc.* **1995**, *117*, 5875. (b) Kumar, A.; Whitesides, G. M. *Appl. Phys. Letter* **1993**, *163*, 2002. (c) Wilber, J. L.; Kim, E.; Xia, Y.; Whitesides, G. M. *Adv. Mater.* **1995**, *7*, 649. (d) Tarlov, M. J.; Burgess, D. R. F., Jr.; Gillen, G. *J. Am. Chem. Soc.* **1993**, *115*, 5305. (e) Gorman, C. B.; Biebuyck, H. A.; Whitesides, G. M. *Chem. Mater.* **1995**, *7*, 526. (f) Gardner, T. J.; Frisbie, C. D.; Wrighton, M. S. *J. Am. Chem. Soc.* **1995**, *117*, 6927.

12. (g) Tao, Y.-T.; Kannaiyan, P.; Lee, W.-C. *Langmuir* **1998**, *14*, 6158. (h) Xia, Y.; Zhau, X.-M.; Whitesides, G. M. *Microelectronic Engineering* **1996**, *32*, 255. (i) Wilbur, J. L.; Biebuyck, H. A.; MacDonald, J. C.; Whitesides, G. M. *Langmuir* **1995**, *11*, 827. (j) Bar, G.; Rubin, S.; Parikh, A. N.; Swanson, B. I.; Zawodzinski, T. A.; Whangbo, M. H. *Langmuir* **1997**, *13*, 373. (k) Bar, G.; Rubin, S.; Taylor, T. N.; Swanson, B. I.; Zawodzinski, T. A.; Chow, J. T.; Ferraris, J. P. *J. Vac. Sci. Technol., A* **1996**, *14*, 1794. (l) Hayes, W. A.; Kim, H.; Yue, X.; Perry, S. S.; Shannon, C. *Langmuir* **1997**, *13*, 2511.

12. For examples, see: (a) Kumar, A.; Whitesides, G. M. *Appl. Phys. Lett.* **1993**, *63*, 2002. (b) Kumar, A.; Biebuyck, H.; Whitesides, G. M. *Langmuir* **1994**, *10*, 1498. (c) Xia, Y.; Kim, E.; Whitesides, G. M. *J. Electrochem. Soc.* **1996**, *143*, 1070. (d) Xia, Y.; Zhao, X.-M.; Whitesides G. M. *Microelectron. Eng.* **1996**, *32*, 255.

13. (a) Weisshaar, D. E.; Lamp, B. D.; Porter, M. D. *J. Am. Chem. Soc.* **1992**, *114*, 5860. (b) Tender, R. L.; Worley, H.; Fan, H.; Lopez, G. P. *Langmuir* **1996**, *12*, 5515. (c) Riepl, M.; Mirsky, V. M.; Wolfbeis, O. S. *Mikrochim. Acta* **1999**, *131*, 29.

14. (a) Widrig, C. A.; Chung, C.; Porter, M. D. *J. Electroanal. Chem.* **1991**, *310*, 335. (b) Walczak, M. M.; Popenoe, D. D.; Deihammer, R. S.; Lamp, B. D.; Chung, C.; Porter, M. D. *Langmuir* **1991**, *7*, 2687. (c) Walczak, C. A.; ALves, C. A.; Lamp, B. D. *J. Electroanal. Chem.* **1995**, *396*, 103 (d) Zhong, C.-J.; Porter, M. D.; *J. Am. Chem. Soc.* **1994**, *116*, 11616. (e) Hobara, D.; Ota, M.; Imabayashi, S.-i. Niki, K.; Kakiuchi, T. *J. Electroanal. Chem.* **1998**, *444*, 113. (f) Nishizawa, M.; Sunagawa, T.; Yoneyama, H.; Suita, Y.-o., *J. Electroanal. Chem.* **1997**, *436*, 213. (f) Wittstock, R.; Hesse, R.;

Schuhmann, W. *Electroanalysis* **1997**, *9*, 746. (g) Tender, L. M. Opperman, K. A.; Hampton, P. D.; Lopez, *Adv. Mater.* **1998**, *10*, 73. (h) Imabayashi, S.-i.; Hobara, D.; Kakiuchi, T. *Langmuir* **2001**, *17*, 2560. (i) Sawaguchi, T.; Sato, Y.; Mizutani, F. *J. Electroanal. Chem.* **2001**, *496*, 50. (j) Kakiuchi, T.; Iida, M.; Gon, N.; Hobara, D.; Imabayashi, S.-i.; Niki, K. *Langmuir* **2001**, *17*, 1599. (k) Esplandiu, M. J.; Hagenstroem, H.; Kolb, D. M. *Langmuir* **2001**, *17*, 828. (l) Kawaguchi, T.; Yasuda, H.; Shimazu, K.; Porter, Marc D. *Langmuir* **2000**, *16*, 9830. (m) Kakiuchi, T.; Sato, K.; Iida, M.; Hobara, D. Imabayashi, S.-i.; Niki, K. *Langmuir* **2000**, *16*, 7238. (n) Wong, Sze-Shun; Porter, M. D. *J. Electroanal. Chem.* **2000**, *485*, 135. (o) Hobara, D.; Ueda, K.; Imabayashi, S.-I.; Yamamoto, M.; Kakiuchi, T. *Electrochem.* **1999**, *67*, 1218. (p) Byloos, M.; Al-Maznai, H.; Morin, M. *J. Phys. Chem. B* **1999**, *103*, 6554. (q) Kondo, T.; Yanagida, M.; Shimazu, K.; Uosaki, K. *Langmuir* **1998**, *14*, 5656. (r) Aoki, K.; Kakiuchi, T. *J. Electroanal. Chem.* **1998**, *452*, 187. (s) Hobara, D.; Miyake, K.; Imabayashi, S.-i.; Niki, K.; Kakiuchi, T. *Langmuir* **1998**, *14*, 3590. (t) Szafranski, C. A.; Tanner, W.; Laibinis, P. E.; Garrell, R. L. *Langmuir* **1998**, *14*, 3570. (u) Yang, D.-F.; Morin, M. *J. Electroanal. Chem.* **1998**, *441*, 173. (v) Sato, Y.; Mizutani, F.; Tsukuba, H., *J. Electroanal. Chem.* **1997**, *438*, 99. (w) Arnold, S.; Feng, Z. Q.; Kakiuchi, T.; Knoll, W.; Niki, K. *J. Electroanal. Chem.* **1997**, *438*, 91. (x) Imabayashi, S.-i.; Hobara, D.; Kakiuchi, T.; Knoll, W. *Langmuir* **1997**, *13*, 4502. (y) Yang, D.-F.; Morin, M *J. Electroanal. Chem.* **1997**, *429*, 1. (z) Imabayashi, S.-i.; Iida, M.; Hobara, D.; Feng, Z. Q.; Niki, K.; Kakiuchi, T. *J. Electroanal. Chem.* **1997**, *428*, 33. (aa) Zhong, C.-J.; Zak, J.; Porter, M. D. *J. Electroanal. Chem.* **1997**, *421*, 9.

(bb) Yang, D.-F.; Al-Maznai, H.; Morin, M. *J. Phys. Chem. B* **1997**, *101*, 1158. (cc) Yang, D.-F.; Wilde, C. P.; Morin, M. *Langmuir* **1997**, *13*, 243. (dd) McCarley, T. D.; McCarley, R. L. *Anal. Chem.* **1997**, *69*, 130. (ee) Kwan, W. S. V.; Penneau, J. F.; Miller, L. L. *J. Electroanal. Chem. Interfacial Electrochem.* **1990**, *291*, 295. 15. (a) Affleck, J. G.; Doughatry, G. *J. Org. Chem.* **1950**, *15*, 865. (b) Milligan, B. L.; Swan, L. M. *J. Chem. Soc.* **1962**, 2172.

16. H. Bunte, *Chem. Ber*, **1874**, *7*, 646.

17. (a) Westlake, H. E. Jr., Dougherty, G. *J. Am. Chem. Soc.* **1941**, *63*, 658. (b) Weiss, U.; Sokol, A. *J. Am. Chem. Soc.* **1942**, *64*, 149. (c) Weiss, U.; Sokol, A. *J. Am. Chem. Soc.* **1950**, *72*, 1687. (d) Distler, H. *Angew. Chem. Internat. Eng.* **1967**, *6*, 544. (e) J. L. Kice, *J. Org. Chem.*, **1963**, *28*, 957.

18. (a) Alonso, M. E.; Aragona, H. *Org. Synth.* **1978**, *58*, 147. (b) Price, T. S.; Twiss, D. F., *J. Chem. Soc.* **1908**, 1395. (c) Price, T. S.; Twiss, D. F., *J. Chem. Soc.* **1908**, 1401.

19. Price, T. S.; Twiss, D. F., *J. Chem. Soc.* **1907**, 2021.

20. Czerwinski, A.; Orzeszko, A.; Kazimierczuk, Z.; Marassi, R.; Zamponi, S. *Anal. Lett.* **1997**, *30*, 2391.

21. (a) Orzeszko, A.; Czerwinski, A.; Kazimierczuk, Z. *J. Polym. Mater.* **1997**, *11*, 21. (b) Orzeszko, A. *J. Polym. Mater.* **1994**, *11*, 69.

22. Ulman, A. *An Introduction to Ultrathin Organic Films from Langmuir-Blodgett to Self-Assembly*, Academic Press, New York, 1991.

23. Lee, M.-T.; Hsueh, C.-C.; Freund, M. S.; Ferguson, G. S. *Angew. Chem. Int. Eng.* **2000**, *39*, 1228.

24. Miller, C.; Curndet, P.; Grätzel, M. *J. Phys. Chem.* **1991**, *95*, 877.

25. For recent examples, see: (a) Scott, J. R.; Baker, L. S.; Everett, W. R.; Wilkins, C. L.; Fritsch, I. *Anal. Chem.* **1997**, *69*, 2636. (b) Zhang, Y.; Terrill, R. H.; Tanzer, T. A.; Born, P. W. *J. Am. Chem. Soc.* **1998**, *120*, 2654. (c) Norrod K. L.; Rowlen, K. L. *J. Am. Chem. Soc.* **1998**, 120, 2656. (d) Schoenfisch M. H.; Pemberton, J. E. *J. Am. Chem. Soc.* **1998**, *120*, 4502. (e) Lee, M.-T.; Hsueh, C.-C.; Freund, M. S.; Ferguson, G. S. *Langmuir* **1998**, *22*, 6419.

26. These data were corrected for the different sensitivities of these elements and orbitals as well as for the number of scans. The take-off angles reported are between the detector and the plane of the surface.

27. Lukkari, J.; Meretoja, M.; Kartio, I.; Laajalehto, K.; Rajamaeki, M.; Lindstroem, M.; Kankare, J. *Langmuir* **1999**, *10*, 3529.

28. (a) Audi, A. A.; Sherwood, P. M. A. *Surf. Interface Anal.* **2000**, *29*, 265. (b) Olsson, C-O. A.; Agarwal, P.; Frey, M.; Landolt, D. *Corros. Sci.* **2000**, *42*, 1197. (c) Ardizzone, S.; Bianchi, C. L. *Appl. Surf. Sci.* **1999**, *152*, 63. (d) Engström, P.; Ambernstsson, A.; Skoglundh, M.; Fridell, E.; Smedler, G. *Appl. Catal., B* **1999**, *22*, 35.

29. For an infrared spectrum of $NaHSO_4$, see Baran, J.; Ilczyszyn, M. M.; Marchewka, M. K.; Ratajczak, H. *Spectrosc. Lett.* **1999**, *32*, 83. For an infrared of Na_2SO_4, see (a) Davies, J. E. D.; Sandford, W. F. *J. Chem. Soc., Dalton Trans.* **1975**, *19*, 1912. (b) Durie, R. A.; Milne, J. W. *Spectrochim. Acta, Part A*, **1978**, *34A*, 215.

30. (a) Mancke, R. G. *IEEE Trans. Comp. Hybr. Manuf. Techn.*, **1981**, *CHMT-4*, 492. (b) Fabianowski, W.; Jaccodine, R.; Kodnani, R.; Pearson, R.; Smektala, P. *Adv. Mater. Opt. Electron.* **1995**, *5*, 199.

31. Bard, A. J.; Faulkner, L. R. *Electrochemical Methods Fundamentals and Applications*, John Wiley & Son, New York, 1980.

32. Chailapakul, O.; Sun, L.; Xu, C.; Crooks, R. M. *J. Am. Chem. Soc.* **1993**, 115, 12459.

33. A few drops of the dye solution (1.06 mM) were spread evenly over all of the conducting tracks. Excess solution was then removed, causing the dewetting evident in the micrograph. The fluorescence micrographs were obtained using a Nikon Microflex UFX-II microscope, equipped with a Nikon FX35a camera, at a magnification of 100x.

34. (a) Freund M. S.; Lewis, N. S. *Proc. Natl. Acad. Sci.* **1995**, *92*, 2652. (b) Hseuh, C.-C.; Liu, Y.; Henry, M.; Freund, M. S. *Anal. Chim. Acta*, **1999**, *397*, 135.

35. (a) Ricco, A. J.; Crooks, R. M.; Osbourn, G. *Acc. Chem. Res.* **1998**, *31*, 289. (b) Crooks, R. M.; Ricco, A. J. *Acc. Chem. Res.* **1998**, *31*, 219.

36. Goss, C.A.; Charych, D. H.; Majda, M. *Anal. Chem.* **1991**, *63*, 85.

37. Scofield, J. H. *J. Electron. Spectrosc.* **1976**, *8*, 129.

38. Scienta ESCA300 Users' Manual; Scienta: Uppsala, Sweden, 1997.

39. Beamson, G.; Briggs, D. *High Resolution XPS of Organic Polymers;* The Scienta ESCA300 Database; Wiley: New York, **1992**.

Chapter 3

Stepwise Synthesis of a Well-Defined Silicon (Oxide)/Polyimide Interface

This chapter includes material that has been modified with permission from: Mong-Tung Lee and Gregory S. Ferguson *Langmuir*, **2001**, *17*, 762-767. Copyright 2001, American Chemical Society.

3.1 Abstract

Self-assembly of 1-bromo-16-(trichlorosilyl)hexadecane leads to highly ordered bromide-terminated monolayer films on silicon (oxide) substrates. The bromides were converted to azides by treatment with sodium azide and then reduced to corresponding amines using lithium aluminum hydride. Protonation of these amine surfaces was difficult to reverse and rendered them unreactive toward electrophiles. The unprotonated form, however, reacted with molten phthalic anhydride to form the corresponding imide. These chemical transformations were characterized by ellipsometry, attenuated total reflectance infrared spectroscopy (ATR-IR), contact angle goniometry, and X-ray photoelectron spectroscopy (XPS). Spin-coating of a polyamic acid, the precursor of poly-*N*',*N*'(4,4'-oxydiphenylene)pyromellitimide, onto the pure amine-terminated surface, followed by curing (up to 350 °C), resulted in covalent linkages between substrate and the polymeric coating. The success of this curing was confirmed by infrared spectroscopy. Adhesion test results showed that this amine-terminated monolayer enhanced the adhesion of polyimide films to these substrates.

3.2 Introduction

In studies focused on adhesion and delamination at silicon (oxide)/polymer interfaces, we have prepared a structurally well-defined system, modeled after the technologically important use of 3-aminopropyltrimethoxysilane (APS) as an adhesion promoter at these interfaces. Although APS has been used successfully in applications such as glass-fiber-reinforced composites,[1-3] polymer-metal adhesion,[4,5] and protection of microelectronics,[6] the mechanism by which it enhances adhesion has been a matter of debate due to the lack of well-defined structure in the siloxane networks derived from this difunctional reagent.[7,8] In principle, hydrolysis and condensation of the silyl group at one end of the molecule could form a quasi-two-dimensional network anchored to the surface of SiO_2 through siloxane linkages, and the amine group at the other end could provide covalent linkages to a polymeric coating. In addition to this mode of bonding, which has been demonstrated for polyimide and model compounds,[9,10] however, the basic amine group can also react with surface silanols by proton transfer and hydrogen bonding as well as participate in the condensation reactions that form the siloxane network and thereby lead to the formation of complex multilayers.[9] Mechanical interlocking, arising from diffusion of polymer chains from a coating into this three-dimensional siloxane network, has also been proposed as a mechanism for enhancing adhesion.[10-11]

Our approach to a well-defined model system involved first forming ordered self-assembled *mono*layers (SAMs) via the reaction of alkyltrichlorosilanes at the surface of a silicon wafer, followed by chemical derivatization of the outermost atoms of the

monolayers to produce amine groups. These amine groups were then used to form covalent attachments to a polyimide coating.[9,10] Stepwise chemical synthesis to form amine groups at the surface of such SAMs has been demonstrated by others,[12-15] though preliminary experiments in our laboratories indicated that the amines produced by these methods were curiously unreactive toward electrophiles. The lack of reactivity of these SAMs prevented their use as effective coupling agents, so we conducted the present study to solve this problem, as well as to provide a more detailed characterization of the surfaces involved than previously reported. Unlike coupling layers formed from APS, our system provides a system free of ambiguity regarding whether adhesion results from interfacial contact and bonding or from mechanical interlocking. This system should be also useful in understanding the fundamental of interface failure in polymeric coatings and silicon (oxides) substrates, thus perhaps allowing the semiconductor packaging industry to develop better adhesion promoters based on our model.

3.3 Results and Discussion

Synthesis of Bromide-Terminated Silane.

Bromohexadec-15-ene was synthesized following a literature procedure,[16] and the product was purified using flash chromatography (hexanes) to give an isolated yield of ~65%. Analyses by both nuclear magnetic resonance spectroscopy (NMR) and gas chromatography-mass spectrometry (GC-MS) confirmed the purity of the product. The desired bromide-terminated silane, 1-bromo-16-(trichlorosilyl)hexadecane, was then synthesized by hydrosilation of 1-bromo-15-hexadecene with trichlorosilane, catalyzed by

Figure 3.1. The synthesis of 1-bromo-16-(trichlorosilyl)hexadecane.

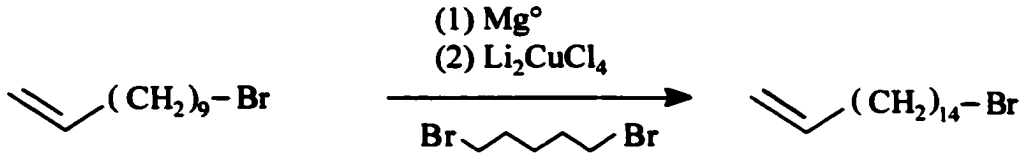

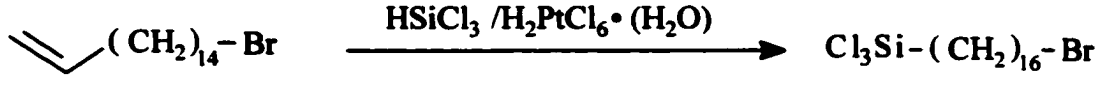

hydrogen hexachloroplatinate (IV) hydrate, according to a literature procedure.[17] The product was purified by Kugelrohr distillation at 150–165 °C and 0.1 Torr, and its purity was confirmed by NMR.

Synthesis and Characterization of Bromide-Terminated Monolayers.

Bromide-terminated siloxane monolayers were prepared on clean silicon wafers (Si/SiO_2) by immersion of the substrate in a (1%, w/w) solution of 1-bromo-16-(trichlorosilyl)hexadecane (**1**) in toluene. The average thickness, determined by ellipsometry, of these monolayers was ~26 Å, consistent with the anticipated length of a trans-extended conformation of this absorbate as well as with results reported by others.[18] Attenuated total reflectance (ATR) infrared spectra of a monolayer formed on a silicon ATR crystal revealed C-H stretching bands at 2920cm^{-1} (ν_a, CH_2) and 2851cm^{-1} (ν_s, CH_2), indicative of crystalline-like order in the SAM.[19] The advancing contact angles of water on these SAMs, 81-85°, were also consistent with values reported by others.[12-15,20,21] Hexadecane wet the bromo-terminated monolayer.

Atomic force microscopic (AFM) images (Figure 3.2) of a Br-terminated monolayer on silicon, as well as of a bare silicon wafer for comparison, were acquired with a NanoScope (Digital Instrument) using standard Si_3N_4 tips. The AFM was operated in contact mode, with a scan rate of 1 Hz and minimum contact forces. The AFM images of both surfaces were generally featureless. The surface that had been treated with 1-bromo-16-(trichlorosily)hexadecane had a root-mean-square roughness of 1.5 Å, in agreement with literature values for monolayers formed from *n*-octadecyltrichlorosilane[22]

Figure 3.2. Atomic Force Microscopic images of a: (a) bare silicon wafer (1μm x 1 μm); (b) bare silicon wafer (3.5 μm x 3.5 μm); (c) Br-terminated monolayer (1 μm x 1 μm); (d) Br-terminated monolayer (3.5 μm x 3.5 μm).

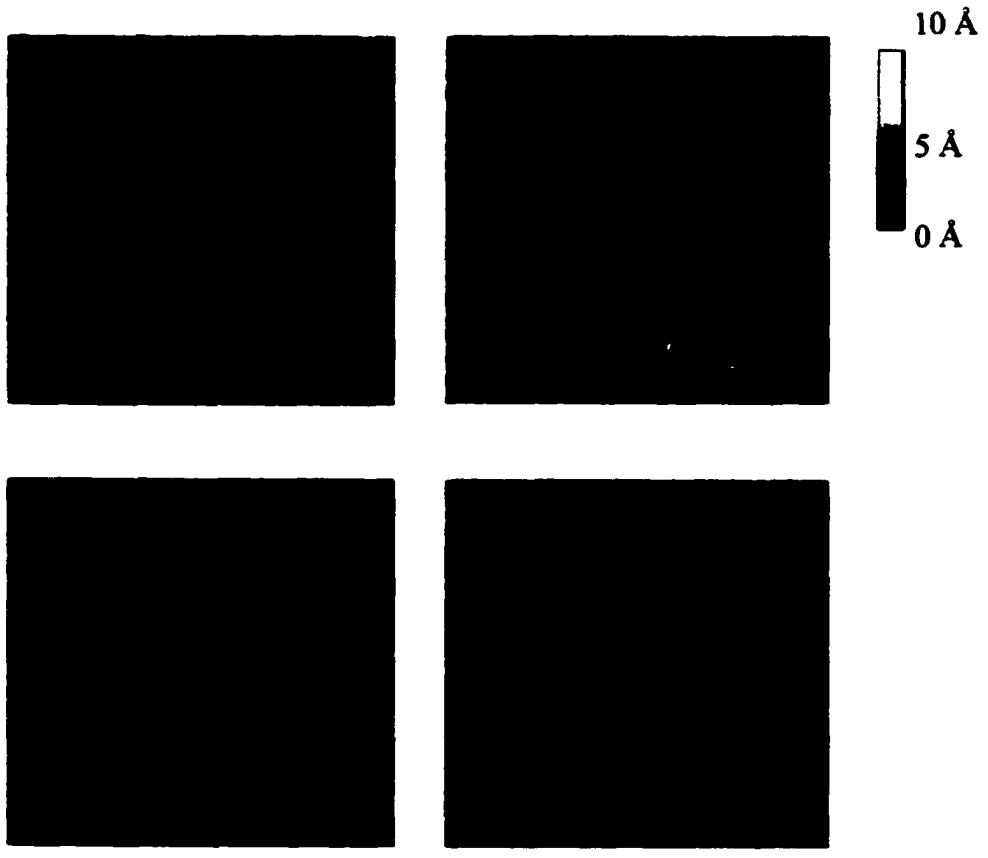

and thus consistent with monolayer formation.

X-ray photoelectron spectroscopy (XPS) was used to determine the composition of pure and mixed (brominated and unbrominated) monolayers, as well as to follow subsequent functional-group transformations. Figure 3.3, for example, shows a plot of terminated monolayers were very susceptible to X-ray-induced damage during these measurements.[20,24] For example, the intensity of the Br (3d) photoemission decreased by approximately 10%, and the N(1s) peaks of azide-terminated monolayer almost disappeared, after a single high-resolution scan. To maximize the reliability of XPS data from these surfaces, the survey and high-resolution scans were collected at different spots on the sample.

Infrared spectroscopy confirmed that the azidation reaction had occurred and that the azide-terminated monolayer was ordered. An ATR-IR spectrum of the product contained a band at 2097 cm^{-1}, assigned to the N_3 asymmetric stretching mode.[25] In the mole fraction of bromoalkylsiloxane in pure and mixed monolayers formed by adsorption from solutions containing the bromoalkylsilane (**1**) and the corresponding unbrominated compound, hexadecyltrichlorosilane (**2**). The linearity of these data confirmed that the composition of mixed monolayers mirrored the composition of the solutions from which they were adsorbed, as found by one other group,[20] but not by a second.[14] The wetting behavior of these mixed monolayers was roughly linearly related to the mole fractions of the two components on the surface, as predicted by the Cassie equation (equation 3.1.),[23]

$$\cos\theta = \sum[f_i \cos\theta_i] \qquad (3.1)$$

Figure 3.3. A plot of the mole fraction of brominated adsorbates in SAMs, preparedusing pure and mixed solution of 1-bromo-16-(trichlorosily)hexadecane [1] and hexadecyltrichlorosilane, *versus* the mole fraction of brominated precursor in the solutions from which they were adsorbed. The XPS spectra were collected using a take-off angle of 5°. The error bars indicate the estimated uncertainty in quantifying the Bromide 3d photoemission.

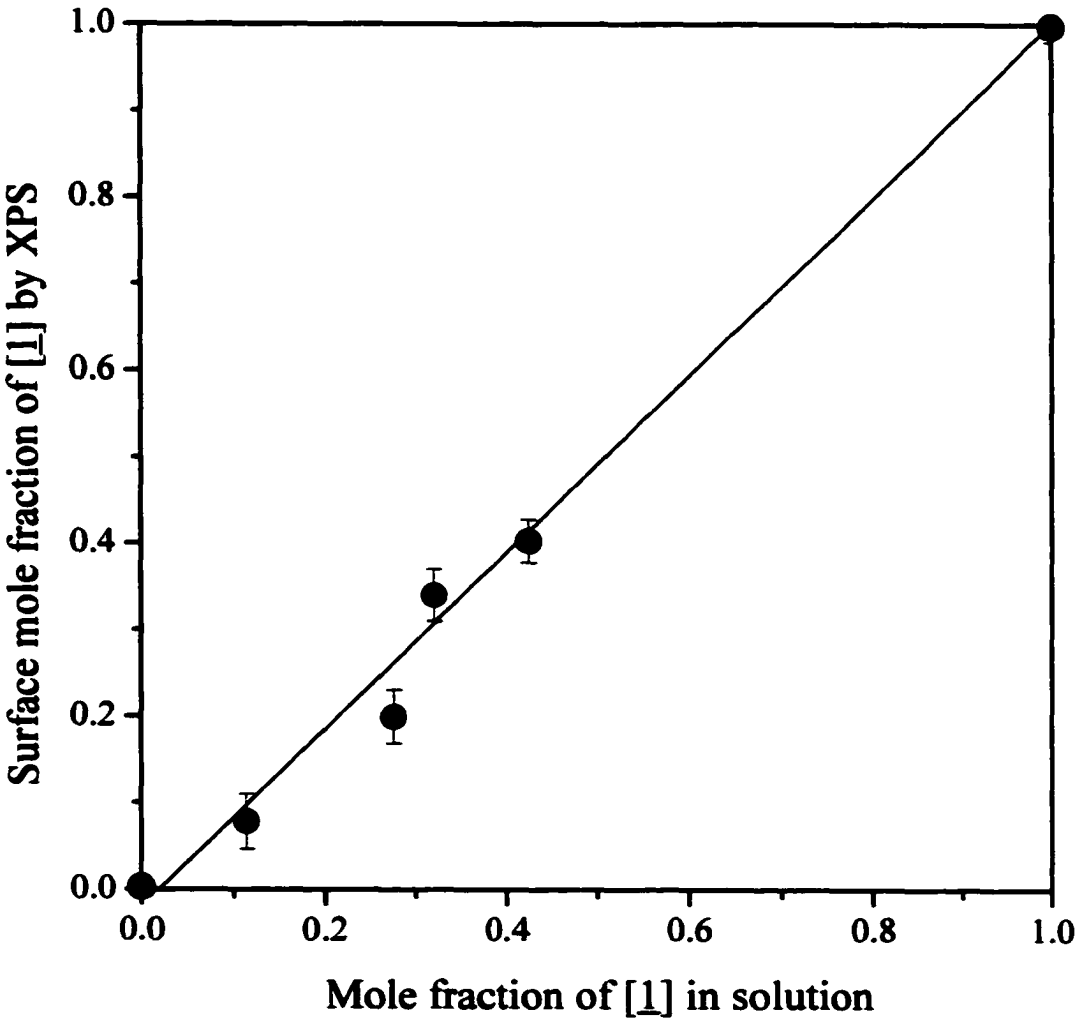

where θ is the contact angle on the composite surface, θ_i is that on a pure surface of the i^{th} component, and f_i is the mole fraction of i^{th} component in the composite surface. Figure 3.4 shows a plot of cos θ *versus* f_i for the pure and mixed monolayers.

Chemical Derivatization of These Monolayers.

A two-step synthetic approach, reported previously by others,[12] was used to convert these surface-bound bromides to the amine groups needed as coupling agents (Figure 3.5). Bromide-terminated monolayers were immersed in a stirred 0.12-M solution of sodium azide in DMF for different periods of time and checked by XPS (5° take-off angle) to assess the extent of conversion. Contact angles of water could not provide information about the degree of completion because the wettability of an azide-terminated monolayer is similar to that of a bromide-terminated surface, around 84-86°. Although this reaction was reported to be complete within 12 h,[12] we found by XPS that a longer time was required. A 40-h immersion resulted in quantitative conversion of the bromide to the corresponding azide by XPS (Figure 3.6).[15] The appearance of N (1s) photoemission at 402.1 and 405.0 eV, and the disappearance of the Br (3d) peak at 71.0 eV, confirmed the azidation. The fully azide- terminated monolayer had a contact angle of water of 75-79°. The bromide- and azide-addition, the positions and relative intensities of the peaks in the C-H stretching region were the same as those found for the starting monolayer, indicating that the chemical transformation did not disrupt the order of the SAM.

Figure 3.4. A plot of the cosine of the contact angle of water on mixed brominated and unbrominated monolayers *versus* the mole fraction of brominated silanol on surface determined by XPS. The error bars indicate the range of values within one standard deviation of the average.

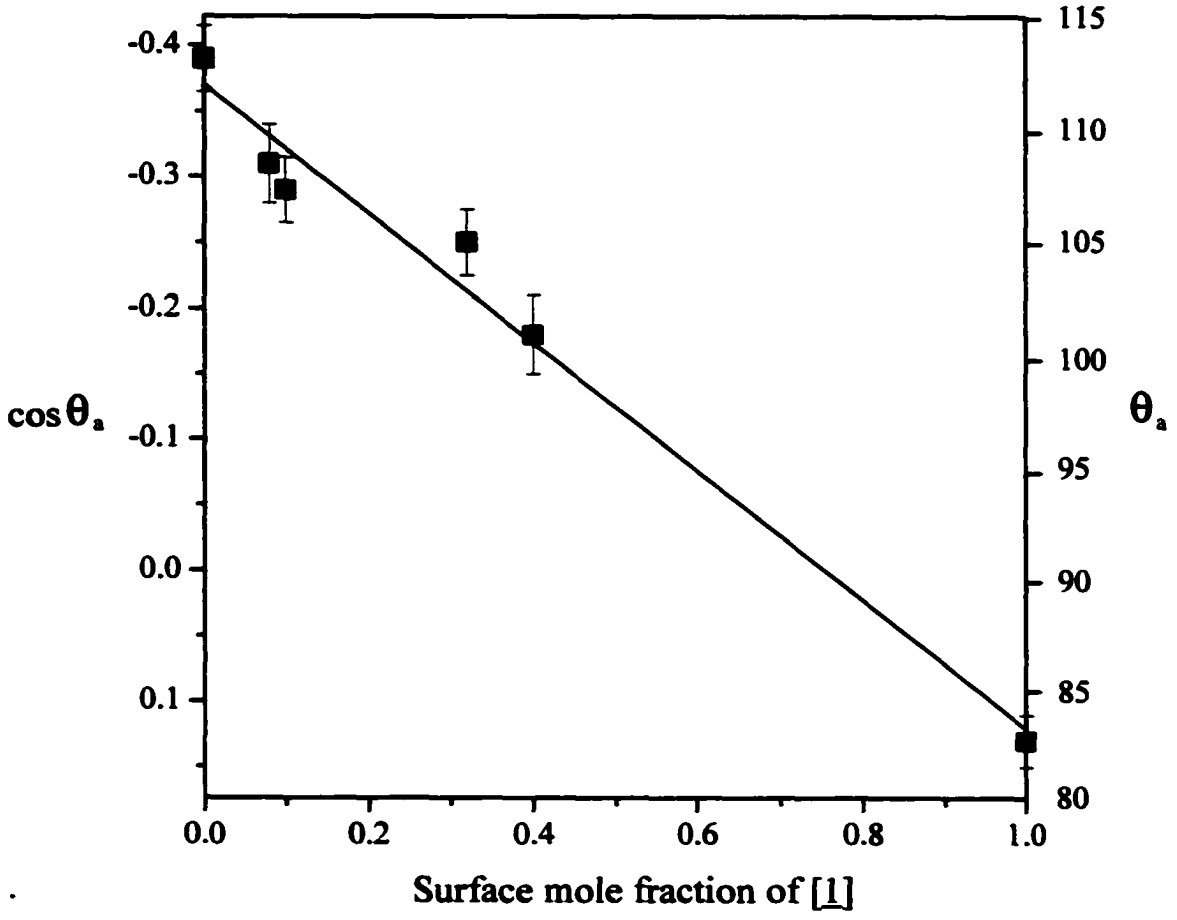

Figure 3.5. Scheme representing surface modification by *in-situ* chemistry on self-assembled monolayers.

R = phthalimide, trifluoroacetamide, or PMDA-ODA

Figure 3.6. X-ray photoelectron spectra (N 1s, left; Br 3d, right) of a mixed (brominated and unbrominated, 1:2) monolayer treated for 24 and 40 h with NaN_3. A spectrum of the unreacted, bromide-terminated monolayer is added for comparison.

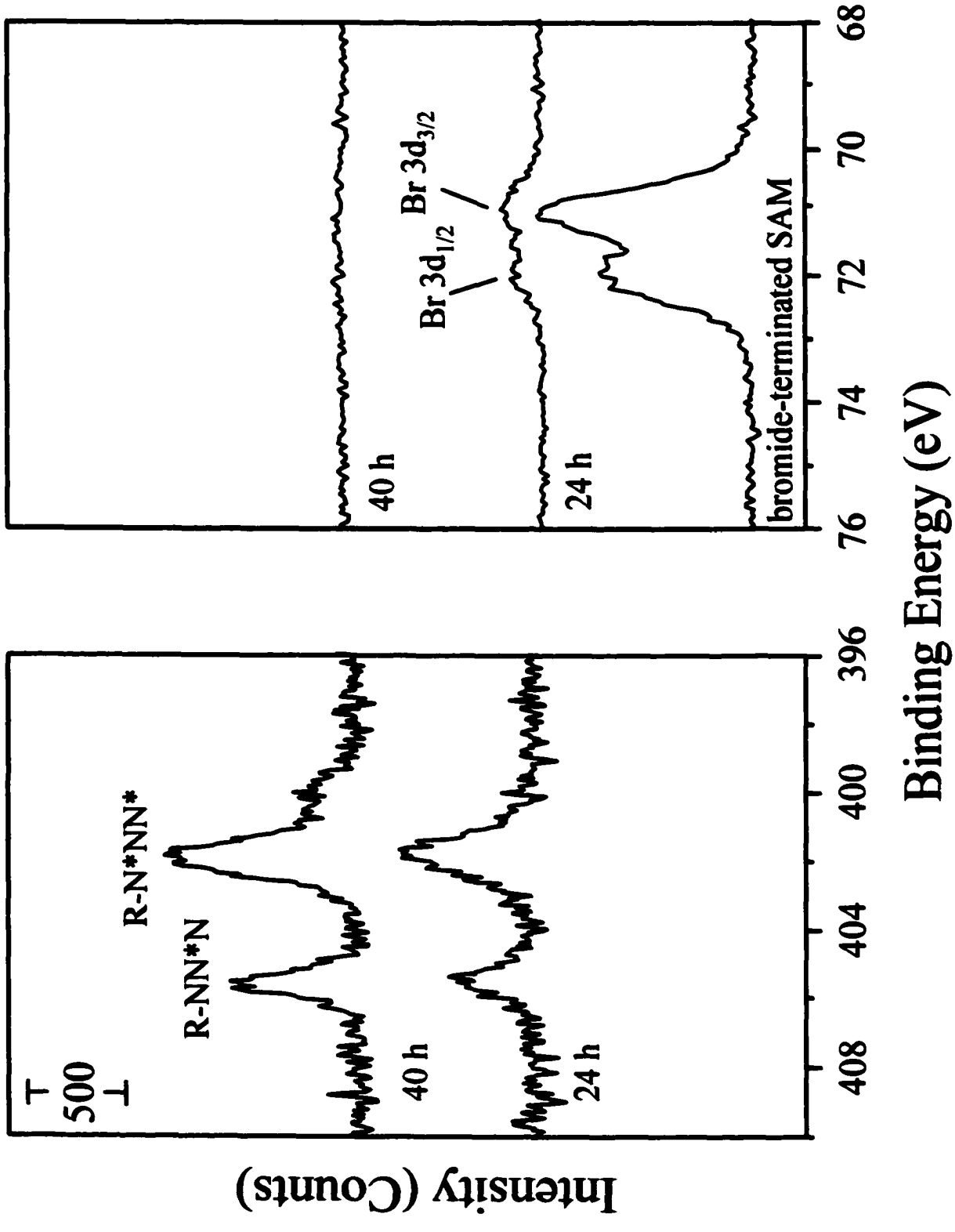

We used two methods previously reported to reduce azide-terminated monolayers to the corresponding amine-terminated monolayers.[12] In our laboratories, treatment with $SnCl_2$ in methanol at room temperature for 4 h gave only partial reduction, as indicated by the continued presence of an azide band in the infrared spectrum of the product. Immersion in $SnCl_2$/methanol for 24 h resulted in partial desorption of the siloxane monolayer, evidenced by decreased peak intensities due to methylene stretching modes and a shift of these peaks to higher frequency (2923 cm^{-1},ν_a; and 2853 cm^{-1}, ν_s), though a weak azide band was still present. An alternative method, [12] using lithium aluminum hydride ($LiAlH_4$) as the reductant, successfully produced the amine surface.

The azide-terminated monolayers were immersed in a slurry of $LiAlH_4$ (0.05 M) in dry THF overnight at room temperature, followed by an acidic work-up (1.2 M HCl). The substrate was then immersed in triethylamine for 5 h at room temperature in an attempt to deprotonate any ammonium groups at the surface. [12] The near disappearance of the N_3 stretching band in the infrared spectrum indicated that the reduction was successful, and X-ray photoelectron spectra of the product also confirmed the near-quantitative reduction.

The amine-terminated surface produced in this way, however, was surprisingly unreactive toward electrophiles: acetic anhydride, phthalic anhydride, and even trifluoroacetic anhydride.[9,26] For example, treatment of the amine-terminated monolayer with neat acetic anhydride at room temperature overnight, followed by rinsing with acetone and drying with a stream of N_2,[28] did not produce the corresponding acetamide-

terminated monolayer, as determined by ATR-IR. Likewise, treatment of the amine surface with a 0.1-M solution of trifluoroacetic anhydride in toluene for 12 h did not produce the corresponding trifluoroacetamide surface.[28]

X-ray photoelectron spectroscopy provided insight into the reason for the lack of reactivity of this surface. A high-resolution spectrum in the N (1s) region of the amine surface revealed an asymmetric envelope containing at least two peaks, at approximately 400.4 eV (assigned as free amine) and 402.2 eV (assigned as protonated amine) in a ratio of about 2:1 (Figure 3.7).[29] The breadth and position of this photoemission suggested that several different species, such as free amine, hydrogen-bonded amine, and various protonated species could exist on the surface. Protonation to give ammonium groups could explain the lack of reactivity of these surfaces toward electrophiles. The inability of triethylamine to deprotonate the surface indicates that the amine-terminated SAM behaves like a bi- or polydentate Brønsted base, with corresponding ammonium ions having pK_a values much higher than that of the triethylammonium ion. To avoid the problem of surface protonation, we quenched our $LiAlH_4$-reductions with 0.5 M aqueous NaOH (1 min) instead of 10% HCl. The resulting N (1S) peak in the XPS spectrum of the product was much narrower and at lower binding energy than the acid-treated surface, indicating a much higher concentration of free amine (~90%).

Consistent with the presence of unprotonated amine on surfaces prepared in this way, the infrared spectrum of a monolayer initially comprising approximately 30% terminal amine and 70% terminal methyl groups and treated with trifluoroacetic

Figure 3.7. X-ray photoelectron spectra of the N 1s region for mixed monolayers (azide and methyl, 1:2) that had been reduced with $LiAlH_4$, followed by an acidic work-up (10% HCl) or by a basic work-up (0.5 M NaOH).

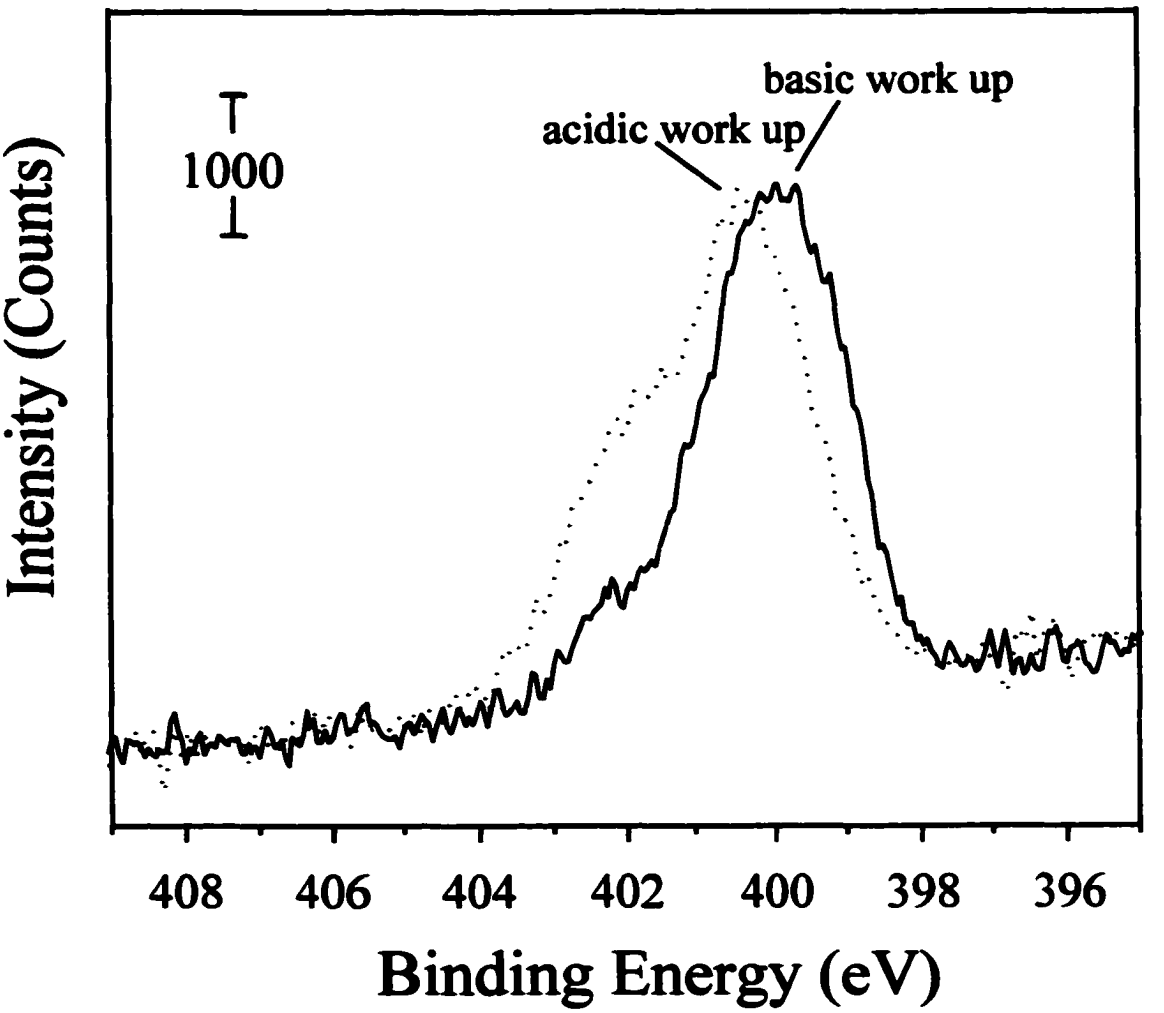

anhydride contained a peak at 1685 cm^{-1}, which we attribute to the conversion of the amines to trifluoroacetamide groups.[30] As a model for the type of imidation reaction to be used to attach polyimide chains to the surface, we also examined the reactivity of the surface amines toward phthalic anhydride. The amine-terminated (100% amine) SAM reacted with neat molten phthalic anhydride (170 °C) to form the corresponding imide, though it failed to react under less rigorous conditions (i.e., 0.1 M in acetone at room temperature for 30 min or at 60 °C for 18 h).[10] The conversion of phthalic anhydride to surface-bound phthalimide was confirmed by the appearance of new C=O stretching bands at 1718 cm^{-1} (ν(C=O) antisymmetric) and 1775 cm^{-1} (ν(C=O) symmetric) in the ATR-IR spectrum of the product (Figure 3.8).[9,10,31] The C-H stretching bands due to methylene groups (2922 cm^{-1},ν_a; and 2853 cm^{-1}, ν_s) shifted to slightly higher frequency relative to those of the amine precursor, and the intensities of these bands remained unchanged, indicating that though somewhat less ordered, the monolayer remained intact after having been subjected to molten phthalic anhydride (170 °C). The XPS data in Figure 3.9 also confirmed the success of this imidation reaction: the N (1s) photoemission shifted from 400.0 eV (amine) to 401.1 eV, which is in accordance with the literature value for an imide nitrogen,[32,33] and an additional C (1s) peak appeared at 289.4 eV, consistent with the presence of the carbonyl groups of the imide. [32,33] The yield of phthalimide was high, 85%, based on the ratio of carbonyl C (1s) to N (1s) photoemission.

Figure 3.8. Attenuated total reflectance infrared spectra of: (i) a monolayer formed by adsorption of $BrC_{16}H_{33}SiCl_3$; (ii) the same monolayer after azidation; (iii) the monolayer after $LiAlH_4$-reduction of the azide, followed by a basic work-up; (iv) a phthalimide-terminated monolayer formed by imidation of an amine-terminated monolayer with phthalic anhydride; and (v) a monolayer bearing a polyimide coating.

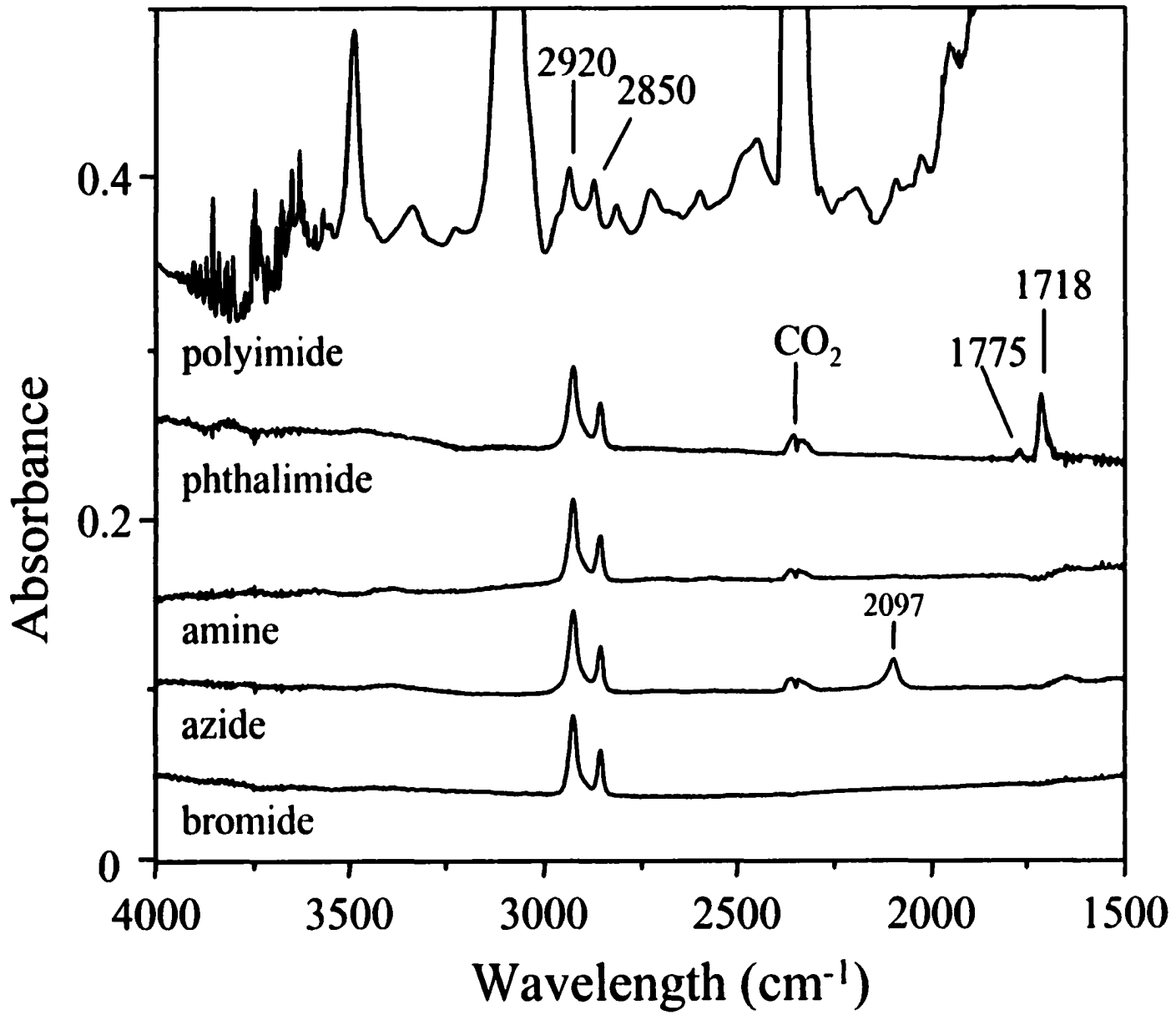

Figure 3.9. Survey XPS spectrum of a phthalimide-terminated monolayer on Si/SiO_2. The inset shows the high-resolution spectrum of this phthalimide-terminated monolayer in carbon 1s region.

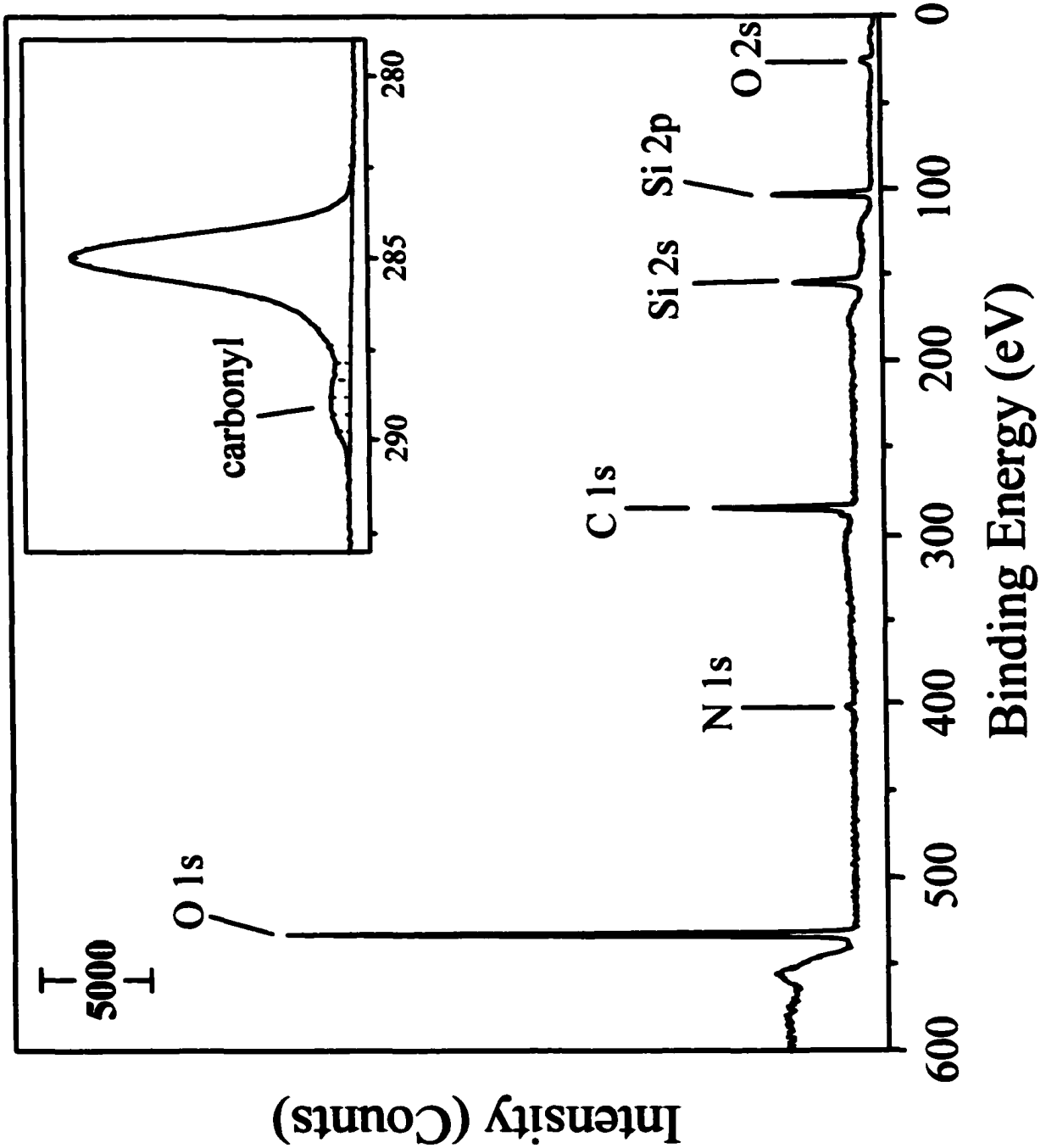

To extend these studies to adhesion of polyimide, we used spin-coating to treat a 30% amine-terminated (70% methyl-terminated) surface with a solution of a polyamic-acid (DuPont Pyralin resins PI-2545 in NMP, 11.1% w/w). The low surface energy of methyl groups on this surface, however, prevented the solution from wetting the monolayer. This solution did, however, wet the 100% amine-terminated surface when treated with the same way. The polyamic acid coating on this surface was cured (up to 350 °C) to produce a thin film of poly-*N*',*N*'(4,4'-oxydiphenylene)pyromellitimide. [32,33] Upon curing, a new absorption band at 1780 cm^{-1} appeared in the infrared spectrum, consistent with the presence of imide groups (Figure 3.10).[34] This spectrum also contained a band at 1720 cm^{-1}, consistent with imide groups, though this band is less informative because the polyamic-acid also absorbed in this region. Interestingly, this spectrum also contained methylene stretching bands at 2920 and 2850 cm^{-1} (Figures 3.8 and Figure 3.10), indicating that the monolayer remained intact and ordered.

As a preliminary test of the adhesion in this system, a cured polyimide film prepared in this way was placed into boiling water and monitored for delamination. A second cured polyimide film, supported on a bare silicon wafer, was treated in the same way for comparison. The polyimide film on bare Si/SiO_2 started to delaminate at one corner within 10 h of immersion and completely detached after 12 h. The polyimide film on the monolayer-coated surface remained unchanged after 3 d, and ~70% of the film still remained on the surface after 7 d. The imide linkages between the coating and the monolayer thus appeared to give rise to significantly enhanced adhesion under

Figure 3.10. Attenuated total reflectance infrared spectra of a monolayer bearing a polyimide coating.

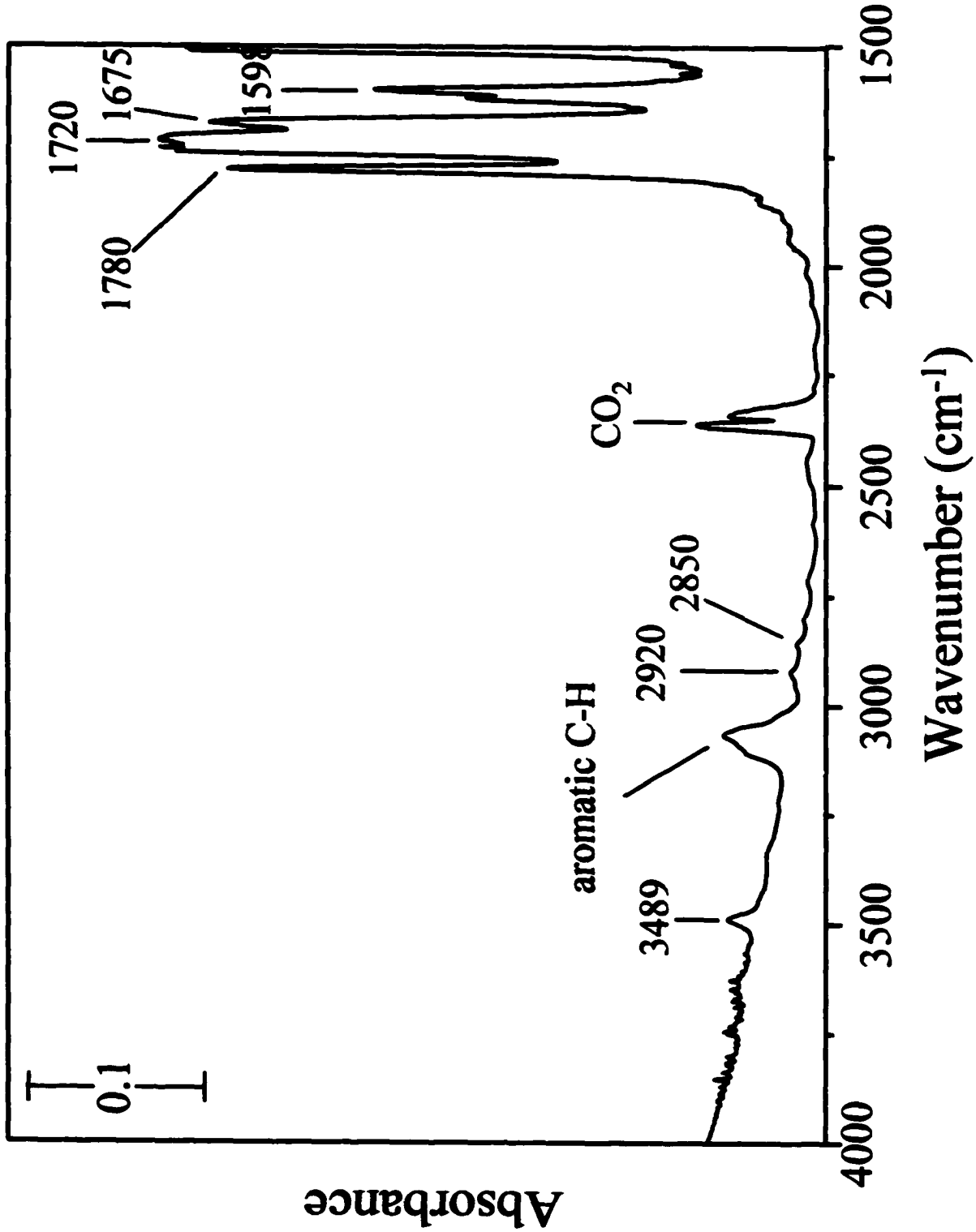

hydrothermal conditions. In a separate experiment, scotch® tape did not remove the polyimide from either type of sample and thus did not differentiate between them.

3.4 Conclusions

We have demonstrated a stepwise synthesis of a well-defined silicon (oxide)/polyimide interface that should prove useful in model studies of adhesion and de-adhesion in this technologically relevant system. A bromide-terminated siloxane monolayer on Si/SiO_2 was first prepared by treatment of the cleaned substrate with 1-bromo-16-(trichlorosilyl)hexadecane, or a mixture containing it, in toluene. Contact-angle measurements and X-ray photoelectron spectroscopy indicated that the surface composition of SAMs adsorbed from mixed solutions of brominated and unbrominated starting materials mirrored their solution compositions.

Bromide-terminated monolayers were converted to an azide-terminated SAMs by immersion in a solution of NaN_3 in DMF for 48 h. Reduction of these azides with $LiAlH_4$ produced the desired amine-terminated SAMs. The work-up of the reduction reaction was a critical step because protonation of amine groups was difficult to reverse and inhibited subsequent reactivity toward electrophiles. A basic work-up yielded a free-amine-terminated monolayer that was reactive toward amidation and imidation, however, vigorous conditions were required for imidation with phthalic anhydride. Nonetheless, imidation with molten phthalic anhydride formed the corresponding imide-terminated surface in high yield without destroying the SAM. The amine-terminated monolayer also allowed covalent attachment to polyimide, by reaction with a polyamic acid, followed by

curing. Preliminary adhesion testing confirmed the improved adhesion between the polymeric coating and the silicon substrate under aggressive hydrothermal conditions.

3.5 Experimental Methods

3.5.1 *Materials.* Hexadecane (Fisher Scientific, 99.4%) used in contact-angle measurements was purified by percolation twice through activated alumina. Chloroform (99.8%), *N,N*-dimethylformamide (99.94%), sulfuric acid, hydrogen peroxide (30% in water), and toluene (99.5%) were obtained from EM Science and used as received. Alumina (Fisher Scientific), hexanes (Pharmco, 98.5%), hydrochloric acid (J. T. Baker, 36.5%), and undec-10-enyl bromide (Lancaster, 98%) were used as received. 1,5-Dibromopentane (97%), dilithium tetrachlorocuprate (0.1 M solution in THF), hydrogen hexachloroplatinate (IV) hydrate (99.9%), lithium aluminum hydride, phthalic anhydride (99+%), silica gel (70-230 mesh, 60 Å), and $HSiCl_3$ (99%) were obtained from Aldrich and used as received. Diethyl ether (99+%) and tetrahydofuran (99.98%) were obtained from EM Science and were distilled from sodium-benzophenone ketyl before use. A syringe filter with a PTFE membrane, 0.25 μm, was obtained from VWR Scientific. Deuterated chloroform was obtained from Cambridge Isotope Laboratories and used as received. Pyralin PI-2545, 13.5% polyamic acid, pyromellitic dianhydride 4,4'-oxydianiline (PMDA-ODA) in *N*-methyl-2-pyrrolidone (NMP), and the thinner T9093 (NMP) were obtained from DuPont. Silicon wafers were manufactured by Wacker Siltronic and provided by WaferNet, Inc. These wafers were (100)-oriented, p-doped (boron), and 0.50-0.55 mm in thickness. Attenuated total reflectance IR crystals (50 mm

x 20 mm x 1 mm, 45° silicon prism) were obtained from Spectra-Tech, Inc. All water used in this work was purified with a Milli-Pore Milli-Q system to a resistivity of at least 15 MΩ-cm.

3.5.2 *Contact Angle and Ellipsometry Measurements.* Advancing contact angles of water were measured using a Rame-Hart NRL Model 100 goniometer. A minimum of six measurements on three independent drops were made for each sample. Ellipsometric measurements were made using an automatic null ellipsometer (Rudolph Auto-EL III) with a helium-neon laser (λ = 632.8 nm) set at an incident angle of 70°. Measurements were collected from at least four spots on the samples. Data were analyzed using the manufacturer's program, and calculations of film thickness assumed a refractive index of the monolayer of 1.5.

3.5.3 *Infrared Spectroscopy.* Infrared spectra were collected using a Perkin Elmer FT-IR 1600 spectrometer, at a resolution of 2 cm^{-1}. In each case, 1024 scans were averaged to achieve a satisfactory signal-to-noise ratio.

3.5.4 *X-ray Photoelectron Spectroscopy (XPS).* The XPS spectra in this paper were obtained using a Scienta ESCA-300 spectrometer, equipped with a rotating anode (Al Kα) source producing approximately 6.0 kW of X-ray power, a monochromator, and a 300-mm (diameter) hemispherical analyzer. Spectra were collected at various take-off angles between the plane of the surface and the detector (as noted), a slit width of 0.8 mm, and were referenced to the main C 1s peak set at 285.0 eV. The background pressure in the sample chamber was $2x10^{-9}$ Torr. Survey scans were collected with a pass

energy of 75 eV and a step energy of 1.0 eV and took 19 min to complete. High-resolution spectra were collected with a pass energy of 150 eV and a step energy of 0.1 eV. For quantitative analysis, the sensitivity factors used to correct the number of counts under each peak (or envelope) were: C 1s, 1.000; N 1s, 1.620; and Br 3d, 2.840. The sensitivity factors for carbon and nitrogen were determined by A. C. Miller with the Scienta ESCA-300 at Lehigh University; that for Br 3d photoemission is the Scofield value.[35]

3.5.5 *GC-MS and NMR.* The masses of sufficiently volatile (and hydrolytically stable) products were confirmed using a Hewlett Packard 5890 Series II Gas Chromatography, equipped with Hewlett Packard 5972 series Mass Selective detector. ^{1}H NMR spectra were acquired using a Bruker AMX 360 spectrometer, referenced to $CHCl_3$ at 7.24 ppm, and are reported in units of δ.

3.5.6 *Atomic Force Microscopy (AFM).* AFM images of a Br-terminated monolayer on silicon, as well as of a bare silicon wafer for comparison, were acquired with a NanoScope (Digital Instrument) using standard Si_3N_4 tips. The AFM was operated in contact mode, with a scan rate of 1 Hz and minimum contact forces.

3.5.7 *Bromohexadec-15-ene.* This compound was synthesized following a literature procedure,[16] and was purified using flash chromatography (hexanes). ^{1}H NMR: $BrCH_2CH_2(CH_2)_{11}$, 1.24~1.57, (m, 22H); $BrCH_2CH_2$, 1.83, (m, 2H); CH_2=CH-(CH_2), 2.00, (q, 2H); $BrCH_2$, 3.40, (t, J = 7 Hz, 2H); CH=CH_2, 4.88~5.02, (m, 2H); CH=CH_2, 5.79~5.92, (m, 1H). GC-MS: MW = 302.1 and 304.2 g/mol.

3.5.8 *1-Bromo-16-(trichlorosilyl)hexadecane*, [1]. This silane was synthesized by hydrosilation of 1-bromo-15-hexadecene with trichlorosilane, catalyzed by hydrogen hexachloroplatinate (IV) hydrate, according to a literature procedure,[17] and was purified by Kugelrohr distillation at 150–165 °C and 0.1 Torr. ^{1}H NMR: $Cl_3Si(CH_2)_{14}$, 1.24~1.57, (m, 28H); $BrCH_2CH_2$ 1.83, (m, 2H); $BrCH_2$ 3.40 (t, J = 7 Hz, 2H).

3.5.9 *Monolayer Preparation.* Samples were cut from silicon wafers to an appropriate size (3 cm x 1 cm) and cleaned by heating in a solution of concentrated H_2SO_4 and 30% H_2O_2 (70:30 v/v) at 90 °C for 0.5 h. (*Caution: this "piranha" solution reacts violently with many organic materials and should be handled with extreme care.*) The substrates were then rinsed with deionized water and dried with a stream of N_2. Within 15 min of cleaning a wafer, monolayers were formed by immersion into a solution of 1-bromo-16-(trichlorosilyl)hexadecane and/or hexadecyltrichlorosilane in toluene (1% by weight) for 0.5 h at room temperature.[36] After this treatment, the substrates were rinsed with chloroform to remove any residual silane and dried with a stream of N_2.

3.5.10 *Azide-Terminated Monolayer.* A silicon substrate bearing a bromide-terminated monolayer was immersed in 10 mL of a stirred 0.12-M solution of sodium azide in DMF at room temperature for 48 h. The substrate was then rinsed with deionized water and chloroform and dried with a stream of N_2.

3.5.11 *Amine-Terminated Monolayer.* Two methods were used for the reduction of azide-terminated SAMs to give amines:[12]

1. A sample bearing an azide-terminated monolayer was placed into 15 mL of a stirred solution of 0.02 M $SnCl_2$ in methanol at room temperature for 4 h, after which it was dipped into 20 mL of 1.2 M aqueous HCl and then rinsed with deionized water and dried with a stream of N_2.
2. A sample bearing an azide-terminated monolayer was immersed in a stirred slurry of $LiAlH_4$ (0.05 M) in dry THF at room temperature for 5 hours, followed by immersion in 15 mL of 0.5 M aqueous NaOH for 1 min, rinsing with deionized water, and drying with a stream of N_2.

3.5.12 *Amidation of Amine-Terminated Monolayer.* A silicon substrate bearing a 30-%-amine-terminated monolayer (70 % methyl-terminated) was immersed in 30 mL of a 0.1-M solution of trifluoroacetic anhydride in toluene at room temperature for 16 h and then rinsed with acetone and dried with a stream of N_2.

3.5.13 *Phthalimide-Terminated Monolayer.* A sample bearing an amine-terminated monolayer was immersed in neat molten phthalic anhydride at 175 °C for 1 h. After cooling slightly (to 160 °C), the sample was removed from the still-molten phthalic anhydride, cooled to near room temperature, rinsed with acetone to remove any residual phthalic anhydride, and dried with a stream of N_2.

3.5.14 *Spin-Coating of Polyamic Acid on Amine-Terminated Surfaces.* A solution of polyamic acid (DuPont Pyralin PI-2545) in NMP was formed by diluting the original PI-2545 according to guidelines provided by the manufacturer with the thinner TI-9039 (PI-2545:TI-9039 = 8:1, v/v). The solution was filtered using 0.25-μm syringe filters to

ensure that the solution was free of dust and microgel particles. The diluted PI-2545 was then spun onto an amine-terminated (100%) monolayer for 60 s at 5000 rpm. The coating was cured in a nitrogen atmosphere for the following sequence of temperatures and times: 100 °C/30 min; 150 °C/30 min; 200 °C/1 h; 300 °C/1 h; and 350 °C/15 min.[32] The rate of increase in temperature in each step was about 4-5 °C/min.

3.6 Acknowledgements

We gratefully acknowledge the National Science Foundation and industrial partners for support of this research through the Polymer Interfaces Center, an Industry/University Cooperative Research Center at Lehigh University. In addition, we thank Lehigh University for support of the Scienta ESCA facility, and Gary W. Simmons and A. C. Miller for technical assistance and helpful discussions. We also thank WaferNet for a gift of silicon wafers.

3.7 Reference

1. (a) Plueddemann, E. P. *Silane Coupling Agents*; Plenum: New York, 1982. (b) Ishida, H.; Kumar, G. *Molecular Characterization of Composite Interfaces*; Plenum Press: New York, 1985. (c) Ahlstrom, C.; Gerard, J. F. *Polym. Compos.* **1995**, *16*, 305-313. (d) Page, P. G.; Plueddemann, E. P. *J. Adhes. Sci. Technol.* **1991**, *5*, 831-842.
2. Mittal, K. L. *Silanes and Other Coupling Agents*; VSP: Utrecht, The Netherlands, 1992; pp 3-105, pp 401-541.
3. Tesoro, G.; Wu, Y. *J. Adhes. Sci. Technol.* **1991**, *5*, 771-784.

4. (a) Sung, N. H.; Kaul, A.; Chin, I.; Sung, C. S. P. *Polym. Eng. Sci.* **1982**, *22*, 637-644. (b) Kaul, A.; Sung, N. H.; Chin, I. J.; Sung, C. S. P. *Polym. Eng. Sci.* **1986**, *26*, 768-775.

5. (a) Kaul, A.; Sung, N. H. *Polym. Eng. Sci.* **1985**, *25*, 1171-1178. (b) Cave, N. G.; Kinloch, A. J. *J. Adhesion* **1991**, *34*, 175-187.

6. Soane, D. S.; Martyneko, Z. *Polymers in Microelectronics Fundamentals and Applications*; Elsevier: New York, 1989; Chapter 4.

7. (a) Moses, P. R.; Wier, L. M.; Lennox, J. C.; Finklea, H. O.; Lenhard, J. R.; Murray, R. W. *Anal. Chem.* **1978**, *50*, 576-585. (b) Chiang, C.-H.; Ishida, H.; Koenig, J. *J. Colloid Interface Sci.* **1980**, *74*, 396-404. (c) Child, M. J.; Heywood, M. J.; Pulton, S. K.; Vicary, L. A.; Yong, G. H.; Rochester, C. H. *J. Colloid Interface Sci.* **1982**, *89*, 202-208. (d) Caravajal, G. S.; Leyden, D. E.; Maciel, G. E.; In *Silane, Surfaces, and Interfaces*; Leyden, D. E., Ed.; Gordon and Breach: New York, 1986; p 283. (e) Zhdanov, S. P.; Koshleva, L. S.; Titova, T. I. *Langmuir* **1987**, *3*, 960-967. (f) Fowkes, F. M.; Dwight, D. W.; Cole, D. A.; Huang, T. C. *J. Non-Cryst. Solids* **1990**, *120*, 47-60. (g) Kang, H.-J.; Blum, F. D. *J. Phys. Chem.* **1991**, *95*, 9391-9396. (h) Wang, D.; Jones, F. R. *J. Mater. Sci.* **1993**, *28*, 1396-1408. (i) Hamada, H.; Ikuta, N.; Nishida, N.; Maekawa, Z. *Compos.* **1994**, *25*, 512-515. (j) Kallury, K. M. R.; Macdonald, P. M.; Thompson, M. *Langmuir* **1994**, *10*, 492-499. (k) Wang, D.; Jones, F. R. *J. Mater. Sci.* **1993**, *28*, 2481-2488. (l) Domingue, A.; Piyakis, K.; Sacher, E. *J. Adhesion* **1993**, *40*, 151-162. (m) Chu, C. W.; Kirby, D. P.; Murphy, P. D. *J. Adhes. Sci. Technol.*

1993, *7*, 417-433. (n) Piers, A. S.; Rochester, C. H. *J. Colloid Interface Sci.* **1995**, *174*, 97-103. (o) Vrancken, K. C.; De Coster, L.; Van Der Voort, P.; Grobet, P. J.; Vansant, E. F., *J. Colloid Interface Sci.* **1995**, *170*, 71-77. (p) Piers, A. S.; Rochester, C. H. *J. Chem. Soc., Faraday Trans.* **1995**, *91*, 105-112. (q) Piers, A. S.; Rochester, C. H. *J. Chem. Soc., Faraday Trans.* **1995**, *91*, 359-365. (r) Piers, A. S.; Rochester, C. H. *J. Chem. Soc., Faraday Trans.* **1995**, *91*, 1253-1260. (s) Trens, P.; Denoyel, R.; Rouquerol, J. *Langmuir* **1995**, *11*, 551-554. (t) Kurth, D. G.; Bein, T. *Langmuir* **1995**, *11*, 3061-3067. (u) Moon J. H.; Kim, J. H.; Kim, K.-j.; Kang, T.-H.; Kim, B.; Kim C.-H.; Hahn, J. H.; Park, J. W. *Langmuir* **1997**, *13*, 4305-4310. (v) Salmon, L.; Thominette, F.; Pays, M. F.; Verdu, J. *Composites Sci. Technol.* **1997**, *57*, 1119-1127. (w) Horr, T. J.; Arora, P. S. *Colloids Surf., A* **1997**, *126*, 113-121.

8. (a) Child, M. J.; Heywood, M. J.; Pulton, S. K.; Vicary, G. A.; Yong, G. H. *J. Colloid Interface Sci.* **1982**, *89*, 203-208. (b) Zhdanov, S. P.; Koshleva, L. S.; Titova, T. I. *Langmuir* **1987**, *3*, 960-967. (c) Kallury, K. M. R.; Macdonald, P. M.; Thompson, M. *Langmuir* **1994**, *10*, 492-499.
9. Lind, H. G. *J. Polym. Sci., Polym. Chem. Ed.* **1982**, *20*, 1031-1041.
10. Lind, H. G.; Gleason, R. T. *J. Polym. Sci., Polym. Chem. Ed.* **1984**, *22*, 3043-3062.
11. Chaudhury, M. K.; Gentle, T. M.; Plueddemann, E. P. *J. Adhes. Sci. Technol.* **1987**, *1*, 29-38.
12. Balachander, N.; Sukenik, C. N. *Langmuir* **1990**, *6*, 1621-1627.

13. (a) Liebmann-Vinson, A.; Lander, L. M.; Foster, M. D.; Brittain, W. J.; Vogler, E. A.; Majkrzak, C. F.; Satija, S. *Langmuir* **1996**, *12*, 2256-2262.

14. Heise, A.; Menzel, H.; Yim, H.; Foster, M. D.; Wieringa, R. H.; Schouten, A. J.; Erb, V.; Stamm, M. *Langmuir* **1997**, *13*, 723-728.

15. Fryxell, G. E.; Rieke, P. C.; Wood, L. L.; Engelhard, M. H.; Williford, R. E.; Graff, G. L.; Campbell, A. A.; Wiacek, R. J.; Lee, R.; Halverson, A. *Langmuir* **1996**, *12*, 5064-5075.

16. (a) Tamura, M.; Kochi, J. *Synthesis* **1971**, 303-305. (b) Friedman, L.; Shani, A. *J. Am. Chem. Soc.* **1974**, *96*, 7101-7104.

17. Wasserman, S. R.; Tao, Y.-T.; Whitesides, G. M. *Langmuir* **1989**, *5*, 1074-1087.

18. (a) Banga, R.; Yarwood, J.; Morgan, A. M. *Langmuir* **1995**, *11*, 618-622. (b) Tillman, N.; Ulman, A.; Schildkraut, J. S.; Penner, T. L. *J. Am. Chem. Soc.* **1988**, *110*, 6136-6144. (c) Bierbaum, K.; Grunze, M.; Baski, A. A.; Chi, L. F.; Schrepp, W.; Fuchs, H. *Langmuir* **1995**, *11*, 2143-2150. (d) Le Grange, J. D.; Markham, J. L.; Kurkjian, C. R. *Langmuir* **1993**, *9*, 1749-1753.

19. (a) Ulman, A. *An Introduction to Ultrathin Organic Films: From Langmuir-Blodgett to Self-Assembly*; Academic Press: New York, 1991. (b) Netzer, L.; Iscovici, R.; Sagiv, J. *Thin Solid Films* **1983**, *100*, 67-76. (c) Porter, M. D.; Bright, T. B.; Allara, D. L.; Chidsey, C. E. D. *J. Am. Chem. Soc.* **1987**, *109*, 3559-3568. (d) Gun, J.; Sagiv, J. *J. Colloid Interface Sci.* **1986**, *112*, 457-472. (e) Gun, J.; Iscovici, R.; Sagiv, J. *J. Colloid Interface Sci.* **1984**, *101*, 201-213. (f) Allara, D. L.; Parikh, A. N.; Rondelez,

F. *Langmuir* **1995**, *11*, 2357-2360. (g) Brunner, H.; Vallant, T.; Mayer, U.; Hoffmann, H. *Surf. Sci.* **1996**, *368*, 279-291.

20. Heise, A.; Stamm, M.; Rauscher, M.; Duschner, H.; Menzel, H. *Thin Solid Films* **1998**, *329*, 199-203.

21. (a) Lee, Y. W.; Reed-Mundell, J.; Sukenik, C. N.; Zull, J. E. *Langmuir* **1993**, *9*, 3009-3014. (b) Baker, M. V.; Walting, J. D. *Tetrahedron. Lett.* **1995**, *36*, 4623-4624.

22. (a) Bierbaum, K.; Grunze, M.; Baski, A. A.; Chi., L. F.; Schrepp, W.; Fuchs, H. *Langmuir* **1995**, *11*, 2143-2150. (b) Calistri-Yeh, M.; Kramer, E. J.; Sharma, R.; Zhao, W.; Rafailovich, M. H.; Sokolov, J.; Brock, J. D. *Langmuir* **1996**, *12*, 2747-2755. (c) Appelhans, D.; Ferse, D.; Adler, H.-J. P.; Plieth, W.; Fikus, A.; Grundke, K.; Schmitt, F.-J.; Bayer, T.; Adolphi, B. *Colloids Surf., A*: **2000**, *161*, 203-212. (d) Du, Y.-Z.; Wood, L. L.; Saavedra, S. S. *Mater. Sci. Eng., C* **2000**, *7*, 161-169.

23. Cassie, A. B. D. *Discuss. Faraday Soc.* **1948**, *3*, 11-16.

24. For damage to SAMs due to reduction by secondary electrons, see: (a) Tidswell, I. M.; Ocko, B. M.; Pershan, P. S.; Wasserman, S. R.; Whitesides, G. M.; Axe, J. D. *Phys. Rev. B: Condens. Matter* **1990**, *41*, 1111-1128. (b) Laibinis, P. E.; Graham, R. L.; Biebuyck, H. A.; Whitesides, G. M. *Science* **1991**, *254*, 981-983. (c) Tidswell, I. M.; Rabedeau, T. A.; Pershan, P. S.; Kosowsky, S. D.; Folkers, J. P.; Whitesides, G. M. *J. Phys. Chem.* **1991**, *95*, 2854-2861. (d) Graham, R. L.; Bain, C. D.; Biebuyck, H. A.; Laibinis, P. E.; Whitesides, G. M. *J. Phys. Chem.* **1993**, *97*, 9456-9464. (e) Rieke, P. C.; Baer, D. R.; Fryxell, G. E.; Engelhard, M. H.; Porter, M. S. J. *Vac. Sci.*

Technol., A. **1993**, *11*, 2292-2297. (f) Frydman, E.; Cohen, H.; Maoz, R.; Sagiv, J. *Langmuir* **1997**, *13*, 5089-5106.

25. Bellamy, L. J. *The Infra-Red Spectra of Complex Molecules*, John Wiley & Son: New York, 1958.

26. Buchwalter, L. P.; Greenblatt, J. *J. Adhesion* **1986**, *19*, 257-265.

27. Herbst, R. M.; Shemin, D. In *Organic Syntheses*, Blatt, A. H., Ed.; Wiley, New York, 1941, Vol. 2; pp 10-12.

28. Howard, J. C. In *Organic Syntheses*, Rabjohn, N., Ed.; Wiley, New York, 1955, Vol. 5; pp 42-45.

29. (a) Moses, P. R.; Wier, L. M.; Lennox, J. C.; Finklea, H. O.; Lenhard, J. R.; Murray, R. C. *Anal. Chem.* **1978**, *50*, 576-585. (b) Kallury, K. M. R.; Thompson, M.; Tripp. C. P.; Hair, M. L. *Langmuir* **1992**, *8*, 947-954. (c) Wang, D.; Jones, F. R. *J. Mater. Sci.* **1993**, *28*, 2481-2488. (d) Kallury, K. M. R.; Debono, R. F.; Krull, U. J.; Thompson, M. *J. Adhes. Sci. Technol.* **1991**, *5*, 801-814.

30. (a) Harland, P. A.; Hodge, P. Maughan, W.; Wildsmith, E. *Synthesis* **1984**, *14*, 941-943. (b) King, A. P.; Krespan, C. G. *J. Org. Chem.* **1974**, *39*, 1315-1316.

31. (a) Vanclef, A.; Bouché, R. *Spctrosc. Lett.* **1979**, *12*, 371-385. (b) Ishida, H.; Wellinghoff, S. T.; Baer, E.; Koenig, J. L. *Macromolecules* **1980**, *13*, 826-834. (c) Boese, D.; Lee, H.; Yoon, D. Y.; Swalen, J. D.; Rabolt, J. F. *J. Polym. Sci. Part B: Polym. Phys.* **1992**, *30*, 1321-1327. (d) Hasegawa, M.; Matano, T.; Shindo, Y.; Sugimura, T. *Macromolecules* **1996**, *29*, 7897-7909. (e) Siesler, H. W.; Holland-

Moritz, K. *Infrared and Raman Spectroscopy of Polymers*; Marcel Dekker: New York, 1980. (f) Jou, J. -H.; Huang, P.-T. *Macromolecules* **1991**, *24*, 3796-3803. (g) Echigo, Y.; Iwaya, Y.; Tomioka, I.; Yamada, H. *Macromolecules* **1995**, *28*, 4861-4865. (h) Li, W. S.; Shen, Z. X.; Zheng, J. Z.; Tang, S. H. *Appl. Spectrosc.* **1998**, *52*, 985-989.

32. Lee, K.-W. *J. Adhes. Sci. Technol.* **1994**, *8*, 1077-1092.
33. (a) Beamson, G.; Briggs, D. High resolution XPS of Organic Polymers, The Scienta *ESCA 300 Database*; John Wiley and Sons: New York, 1992. (b) Buchwalter, P. L.; Baise, A. L. In *Polyimides: Synthesis, Characterization, and Applications, 1*; Mittal, K. L. Ed.; Plenum: New York, 1984, pp 537-545. (c) Flament, O.; Russat, J.; Druet, E. *J. Adhes. Sci. Technol.* **1990**, *4*, 109-117. (d) Wöll, Ch.; Gölzhäuser, A.; Panov, S.; Schertel, A.; Grunze, M.; Mast, M; *Surf. Sci.* **1995**, *334*, 235-247.
34. (a) Vanclef, A.; Bouché, R. *Spctrosc. Lett.* **1979**, *12*, 371-385. (b) Ishida, H.; Wellinghoff, S. T.; Baer, E.; Koenig, J. L. *Macromolecules* **1980**, *13*, 826-834. (c) Boese, D.; Lee, H.; Yoon, D. Y.; Swalen, J. D.; Rabolt, J. F. *J. Polym. Sci. Part B: Polym. Phys.* **1992**, *30*, 1321-1327. (d) Hasegawa, M.; Matano, T.; Shindo, Y.; Sugimura, T. *Macromolecules* **1996**, *29*, 7897-7909. (e) Siesler, H. W.; Holland-Moritz, K. *Infrared and Raman Spectroscopy of Polymers*; Marcel Dekker: New York, 1980. (f) Jou, J.-H.; Huang, P.-T. *Macromolecules* **1991**, *24*, 3796-3803. (g) Echigo, Y.; Iwaya, Y.; Tomioka, I.; Yamada, H. *Macromolecules* **1995**, *28*, 4861-

4865. (h) Li, W. S.; Shen, Z. X.; Zheng, J. Z.; Tang, S. H. *Appl. Spectrosc.* **1998**, *52*, 985-989.

35. Scofield, J. H. *J. Electron. Spectrosc.* **1976**, *8*, 129.

36. McGoven, M. E.; Kallury, K. M. R.; Thompson, M. *Langmuir* **1994**, *10*, 3607-3614.

Chapter 4

Synthesis of a Branched, Semifluorinated Alkanethiol for Self-Assembly of Monolayer Films on Gold

We plan to publish this work in a scientific journal and copyright assigned to the publisher.

4.1 Abstract

A branched alkanethiol having one hydrocarbon chain and one fluorocarbon chain was synthesized as part of a collaborative study on 2-D phase behavior in self-assembled monolayers on gold. Tetradecanal was obtained by sequential conversion of tetradecanoic acid using $LiAlH_4$, and then PCC (pyridinium chlorochromate). This aldehyde condensed with 1,3-propanediol to give the cyclic trimethylene acetal, 2-tridecyl-1,3-dioxane, which in turn underwent ring-opening with allyltrimethylsilane to give the allyl-substituted alcohol, 3-[(1-propeneyltridecyl)oxy-propanol. Perfluoroalkylation of this olefin with perfluorodecyl iodide produced 3-hydroxypropyl, [14-(1,1,1,2,2,3,3,4,4,5,5,6,6,7,7,8,8,9,9,10,10-heneicosylfluoro-12-iodo-heptacosyl)ether. The iodide was then reduced to the corresponding alcohol, and the alcohol converted to the bromide. The bromide was converted to the desired thiol by reaction with potassium thioacetate followed by an acidic hydrolysis. After completion of the synthesis, a sample of the branched thiol was sent to our collaborator for characterization of its monolayer behavior.

4.2 Introduction

A branched alkanethiol having a long hydrocarbon and a long fluorocarbon chain was synthesized as part of a collaborative study of two-dimensional phase behavior in self-assembled monolayers (SAMs). The eventual goal of this research is to gain control over the size and features of grafted polymers films. Our collaborators in this study are Professor A. Balazs (theory, University of Pittsburgh) and Professor J. Rabolt (monolayer characterization, University of Delaware). Balazs's computational results, based on scaling arguments, suggested that this "Y-shaped" molecule could form well-defined structures at both dense and sparse grafting,[1] with the mixed state of hydrocarbon and fluorocarbon more stable at sparse grafting than at high grafting densities.

The specific branched molecule being used to test these hypotheses is 3-[14-(1,1,1,2,2,3,3,4,4,5,5,6,6,7,7,8,8,9,9,10,10-heneicosylfluorotridecyl) tetradecoxy]propanethiol (**9**). Self-assembled monolayers of this compound and its two-dimensional phase behavior are currently being studied using contact angle measurements and surface-enhanced Raman spectroscopy and infrared spectroscopy (Delaware).

The structure of branched alkanethiol has one hydrocarbon chain and one fluorocarbon chain of the same length, 13 carbon units ($C_{10}F_{21}(CH_2)_3$ *vs.* $C_{13}H_{27}$) and a thiol group to provide covalent bonding to gold in the SAM. An ether linkage was introduced into the branched alkanethiol because of two specific reasons. First, its introduction made the synthesis much easier. Many of our attempts to synthesize the

similar branched alkanethiols without an ether link were unsuccessful due to facile elimination of $R_FCH_2CH_2I$ species when used as electrophiles in substitution reactions.[2] Second, the ether group is similar in size and shape to a methylene group. The incorporation of an oxygen atom into the SAMs was known to promote local disordering within the film, however, the reflection absorption infrared spectroscopy (RAIRS) data revealed that this perturbation in the SAMs was relatively weak.[3-5] The vibrational bandwidth in IR indicate that the packing in these monolayers still retain crystalline.[4] Placement of an ether oxygen near the chain ends affect the structure more significantly than it does when the substitution is in the interior. Sum-frequency spectroscopy also confirmed that as the oxygen atom is further buried by the terminal outer groups, its influence becomes less significant, and it does not have an observable effect on the spectra of butyl ether.[5] An ellipsometric study on SAMs of various ω-alkoxy-alkanethiols also suggested that the ether oxygen did not dramatically disorder the structure of its SAMs.[3] A wettability study also indicated that the presence of ether was increasingly screened as bulkier terminal groups were used.[3,4] Because the alkoxy group we wanted to introduce into our branched alkanethiol was very bulky, we expected the ether group would have a minimum influence in the structural order of its SAMs. Therefore, we decided to incorporate this ether group into this branched alkanethiol for synthetic convenience.

4.3 Results and Discussion

Several synthetic routes to branched thiol using derivatives of 1-

(perfluoroalkyl)ethyl iodide as the starting material were initially tried without success. In many of these studies, facile elimination prevented the use of $R_FCH_2CH_2I$ species as electrophiles in substitution reactions.[2] To avoid this problem, we explored alternative approaches that did not rely on this troublesome functionality.

A successful strategy to provide compound (**9**) is shown in Figure 4.1. We began the synthesis of the branched alkanethiol by sequential conversion of tetradecanoic acid to tetradecanal. As shown in Figure 4.1, tetradecanol (**1**) was first obtained (95%) by reduction of tetradecanoic acid using $LiAlH_4$. Both thin layer chromatography (TLC) and nuclear magnetic resonance results indicated that the acid was completely reduced to the corresponding alcohol. The tetradecanol was oxidized to tetradecanal without further purification. We first used pyridinium dichromate (PDC) to oxidize the tetradecanol to tetradecanal,[6] however, the product of this reaction was difficult to extract from the resulting taffy-like mixture. As a result, the yield was unsatisfactorily low, ~ 65%, compared with a reported yield around 92%.[6] Using PCC (pyridinium chlorochromate)[7] as the oxidizing agent, however, gave the aldehyde (**2**) in 85% isolated yield after purification by column chromatography. Condensation of tetradecanal (**2**) with 1,3-propanediol, catalyzed by toluenesulfonic acid, gave the cyclic trimethylene acetal, 2-tridecyl-1,3-dioxane (**3**).[8] This condensation reaction was driven to completion by continuous removal of water using a Dean-Stark trap. The yield of the isolated acetal was 83%. The Lewis acid-catalyzed reaction of acetals with allylsilanes has been studied for the formation of new carbon-carbon bonds under mild conditions.[9] The acetal

Figure 4.1. Schematic representation of the synthesis of Y-shaped alkanethiol. Neclear magnetic resonance for all of the intermediates are provided in the Experimental Section.

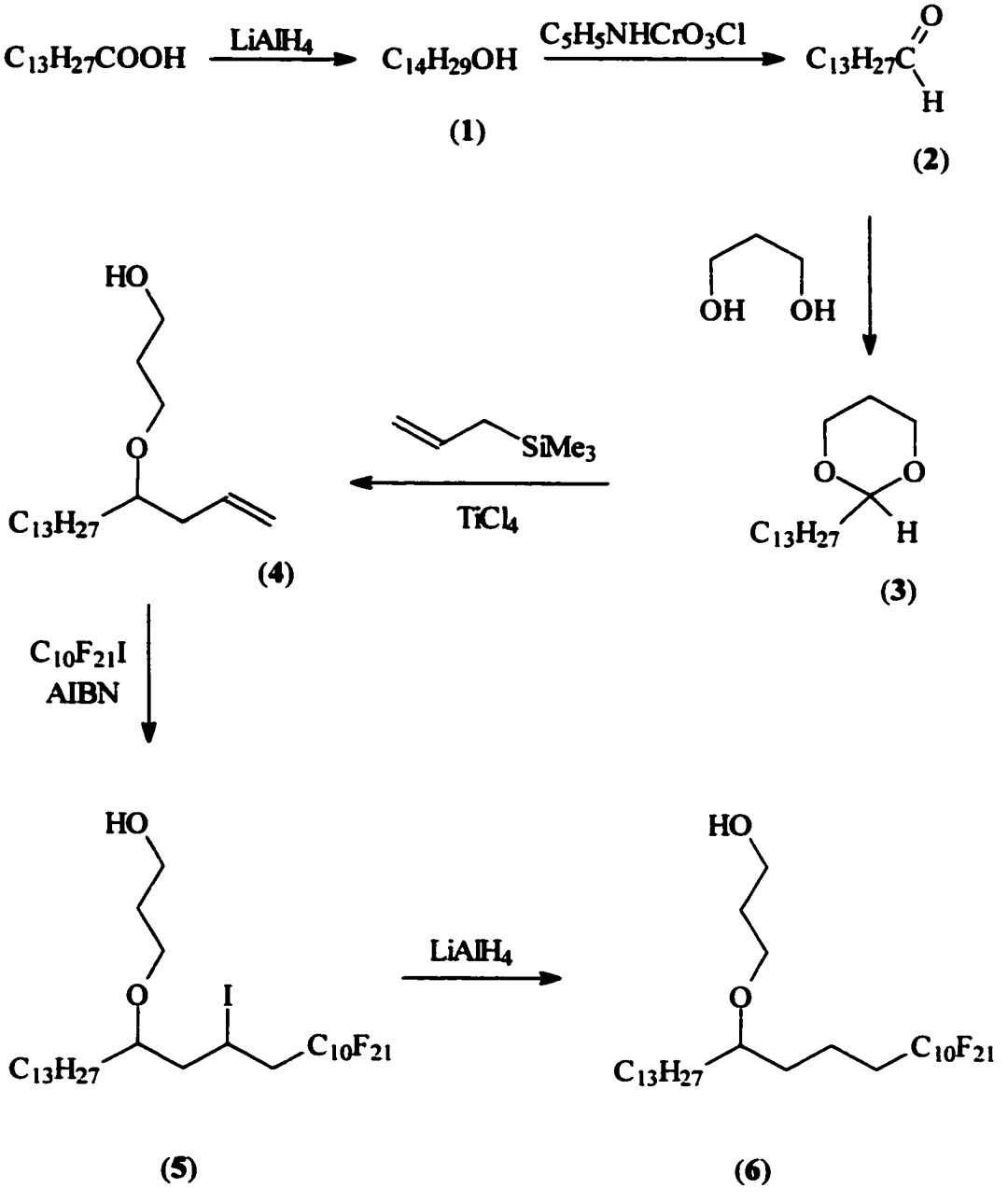

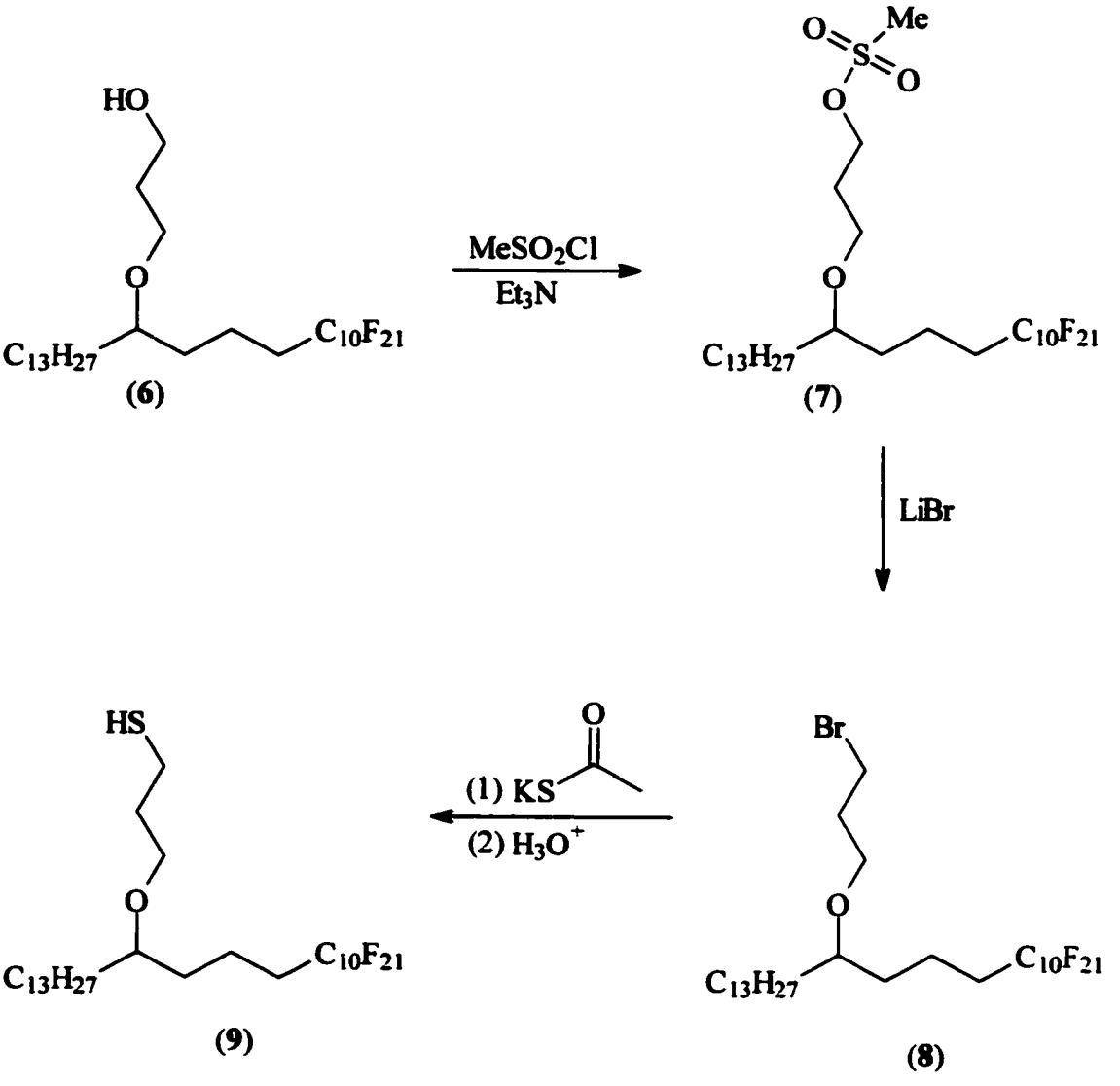

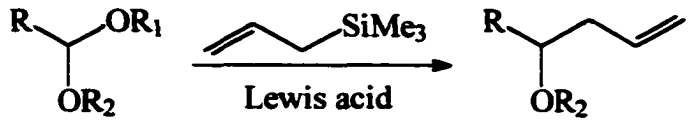

reacted with allyltrimethylsilane in presence of titanium chloride ($TiCl_4$) to give the isolated alcohol (**4**), 3-[(1-propeneyltridecyl)oxy-propanol in 75% yield.[9]

The reaction of perfluoroalkyl iodides with alkenes to give 1-(perfluoroalkyl)-2-iodoalkane in the presence of a catalytic amount of tetrakis(triphenylphosphine)palladium (0) in hexanes has been reported.[10] However, the addition of perfluorodecyl iodide to compound (**4**) using this method was unsuccessful.[10] It seems that the ether group was incompatible with the conditions used in this reaction. An alternative approach, reported by Greiner and coworkers,[11] radical addition of perfluoroalkyl iodides to alkenes, successfully produced the branched, semifluorinated alcohol. The addition was initiated by 2,2'-azobisisobutyronitrile benzene (AIBN) at 95 °C and produced 3-hydroxypropyl-[14-(1,1,1,2,2,3,3,4,4,5,5,6,6,7,7,8,8,9,9,10,10-heneicosylfluoro-12-iodo-heptacosyl)ether (**5**) in 28% yield.[11] Use of a different initiator for the radial addition, sodium dithionite, failed to produce the desired product.[12] This iodoalcohol was then reduced using $LiAlH_4$, and the resulting alcohol (**6**) was purified to give a yield of 50%.[13] An alternative procedure using $Zn/NiCl_2$ as the reductant failed to improve the yield of this product.[14]

To make the hydroxyl group of this alcohol a better leaving group, it was first converted to the corresponding mesylate (**7**) by reaction with methanesulfonyl chloride in the presence of triethylamine. Reaction of the crude mesylate with potassium thioacetate directly, in methanol/THF following a literature procedure,[15] produced a mixture from

which we were unable to separate the pure desired product (**9**). The crude mesylate was refluxed in an acetone solution of lithium bromide to give the corresponding bromide (**8**) in 90% yield. Upon refluxing in methanol/THF with potassium thioacetate under argon for 5 h, followed by acidic hydrolysis, the bromide was converted to the desired thiol (**9**).[15] Data from NMR and elemental analysis confirmed the purity of the product. This step completed the synthesis. The branched thiol and its monolayer behavior are currently being characterized in Professor J. Rabolt's laboratories at the University of Delaware.

4.4 Conclusion

We have completed a stepwise synthesis of a branched alkanethiol containing one long hydrocarbon chain and one long fluorocarbon chain, using tetradecanoic acid as the starting material. The key steps in the synthesis involved installing an alkyl group to form the highly functionalized hydroxypropylalkenyl ether (**4**) and then attachment of the fluorocarbon chain by radical addition of perfluorodecyl iodide to alkenyl function of (**4**). This reaction produced intermediate (**5**), which had the basic framework of the product intact. A series of straightforward functional-group transformations gave the desired branched alkanethiol.

4.5 Experimental Methods

4.5.1 *Materials.* Allyltrimethylsilane (99%), 2,2'-azobisisobutyronitrile benzene (AIBN, 99%), benzophenone (99%), chromium (VI) oxide (99.9%), Florisil (an activated

magnesium silicate, 200-300 mesh), lithium aluminum hydride (95%), lithium bromide (99%), potassium thioacetate (98%), methylsulfonyl chloride (99.5%), 1,3-propanediol (98%), pyridine (99%), silica gel (70-230 mesh, 60 Å), sodium (lump in kerosene, 99%), tetradecanoic acid (99.5%), tetrakis(triphenylphosphine) palladium (0) (99%), titanium (IV) chloride ($TiCl_4$) (1.0 M in dichloromethane), *p*-toluenesulfonic acid monohydrate (99+%), and triethylamine (99.5%), were obtained from Aldrich and used as received. Acetone (99.5%), chloroform (99.9%), dichloromethane (99.8%), ethyl acetate (99.8%), hydrochloric acid (36.5%), sodium bicarbonate (99.7%), sodium chloride (99%), sodium hydroxide (97%), sodium sulfate (anhydrous, 99%), were obtained from EM Science and used as received. Diethyl ether (99+%) and tetrahydofuran (99.9%) were obtained from EM Science and were distilled from sodium-benzophenone ketyl before use. Anhydrous dichloromethane (99.8%) was obtained from EM Science and distilled over calcium hydride prior to use. Absolute ethanol (McCormick Distilling Co.), hexanes (Fisher, 99.9+%), methanol (99.9%, Pharmca), perfluorodecyl iodide (97%, Lancaster) were used as received. Deuterated chloroform (99.8%), deuterium oxide (99.9%), and tetramethylsilane (99.9%) used as a reference in NMR were obtained from Cambridge Isotope Laboratories. All water used in this work was purified with a Milli-Pore Milli-Q system to a resistivity of at least 15 MΩ-cm. Thin layer chromatography (TLC) plates, pre-coated glass-backed TLC plates with Silica Gel 60 F_{254}, were also obtained from EM Science and used as received.

4.5.2. *Nuclear Magnetic Resonance Spectroscopy (NMR).* ^{1}H NMR spectra were acquired using a Bruker AMX 360 spectrometer, referenced to $CHCl_3$ at 7.24 ppm, and are reported in units of δ.

4.5.3. *Elemental Analysis.* Elemental analysis was done by Quantitative Technologies, Inc. (Whitehouse, NJ).

4.5.4 *1-Tetradecanol*, **(1).** The tetradecanoic acid (5.00 g, 21.7 mmol) was dissolved in 100 mL of dry THF and was slowly added to a slurry of $LiAlH_4$ (1.9 g, 50 mmol) in 20 mL of THF at 0 °C. The mixture was allowed to reflux for 16 h, then cooled to 0 °C and quenched by adding 1.9 mL of H_2O, 1.9 mL of 3.75 M NaOH in water, and then another of 5.7 mL of H_2O separately. The solution was filtered, dried with Na_2SO_4, and concentrated to give tetradecanol as a white solid in 95% yield. ^{1}H NMR: $CH_3(CH_2)_{11}$, 0.86, (t, 3H); $CH_3(CH_2)_{11}CH_2$, 1.20~1.35, (m, 22H); CH_2CH_2OH, 1.54, (m, 2H); CH_2OH, 3.62, (t, 2H), (see Figure 4.2).

4.5.5 *1-Tetradecal*, **(2).** The oxidizing agent, pyridinium chlorochromate (PCC), was prepared according to a literature procedure:[7] To 18.4 mL of a stirred aqueous solution of 6.0 M HCl (0.11 mol) was added 10.0 g (0.10 mol) of CrO_3. After 5 min, the homogeneous solution was cooled to 0 °C and 7.9 g (0.10 mol) of pyridine was carefully added to give a yellow-orange solid that was collected on a sintered-glass funnel and dried for 1 hr at ~ 100 Torr.

In a 250-mL round-bottomed flask fitted with a reflux condenser was suspended PCC (6.70 g, 31.2 mmol) in 40 mL of anhydrous dichloromethane. 1-Tetradecanol (4.50

Figure 4.2. The nuclear magnetic resonance spectrum of *n*-tetradecanol, (1).

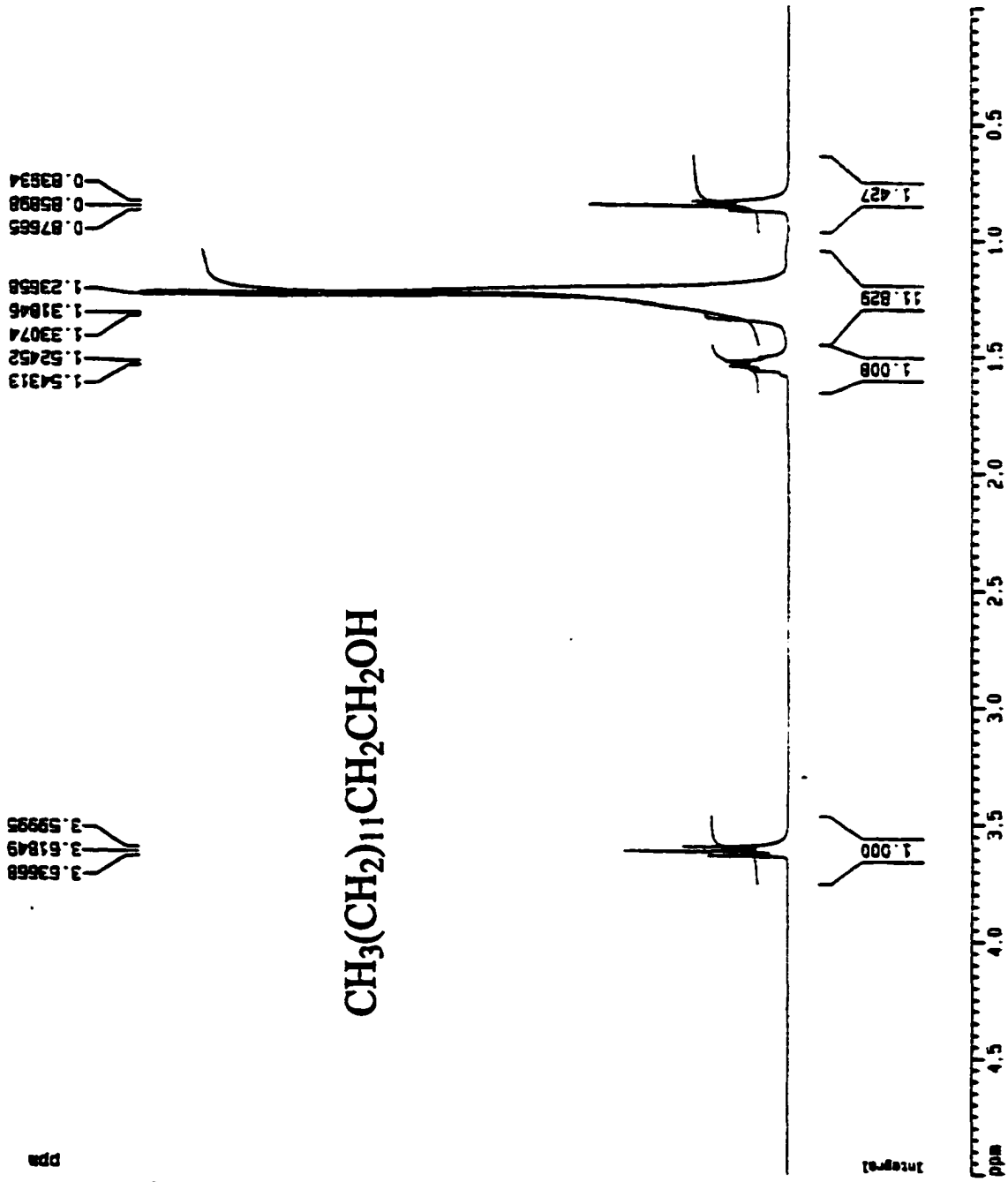

g, 20.8 mmol) in 30 mL of dichloromethane was added to this stirred PCC solution. After 2 h, 100 mL of dried ether was added and the supernatant decanted from the black gum. The insoluble residue was washed thoroughly 3 times with 50-mL portions of ether. The combined organic solution was passed through a Florisil (an activated magnesium silicate) on a sintered-glass funnel, and the solvents were removed by rotary evaporation. Purification by column chromatography (silica) using hexanes/ethyl acetate (20:1) to give tetradecanal as a colorless liquid in 85% yield. ^{1}H NMR: CH_3(CH$_2$)$_{12}$, 0.86, (t, 3H); CH$_3$(CH_2)$_{10}$, 1.20~1.35, (m, 20H); CH_2CH$_2$CHO, 1.60, (m, 2H); CH_2CHO, 2.40, (t, 2H); CH$_2$C*H*O, 9.75, (s, 1H), see Figure 4.3.

4.5.6 *2-Tridecyl-1,3-dioxane.* (**3**). Tetradecanal (1.15 g, 5.40 mmol), 1,3-propanediol (0.41 g, 5.4 mmol), and *p*-toluenesulfonic acid monohydrate (0.10 g, 0.54 mmol) were dissolved in 50 mL of benzene, and this mixture was brought to reflux (90 °C). Water was continuously removed using a Dean-Stark trap.[8] After 4 h, the solution was cooled to room temperature and then extracted with diethyl ether and the ethereal phase was washed with saturated NaHCO$_3$, saturated NaCl, and dried with Na$_2$SO$_4$. The solvents were then removed by rotary evaporation, and the resulting liquid was purified by column chromatography (silica) using hexanes/ethyl acetate (20:1) as an eluent to give compound (**3**) a colorless liquid in 83% yield. ^{1}H NMR: CH_3(CH$_2$)$_{11}$, 0.86, (t, 3H); CH$_3$(CH_2)$_{11}$, 1.20~1.40, (m, 22H); CH$_3$(CH$_2$)$_{11}$CH_2CHO$_2$, 1.55, (m, 2H); CH$_3$(CH$_2$)$_{11}$CHOCH$_2$CH_{ax}, 1.54, (m, 1H); CH$_3$(CH$_2$)$_{11}$CH$_2$OCH$_2$CH_{eq}, 2.05, (m, 1H); CH$_3$(CH$_2$)$_{11}$CHOCH_{ax}, 3.74, (dt, 2H); CH$_3$(CH$_2$)$_{11}$CHOCH_{eq}, 4.01, (dd, 2H); CH$_3$(CH$_2$)$_{11}$CH$_2$C*H*O$_2$, 4.48, (t, 1H), see Figure 4.4.

Figure 4.3. The nuclear magnetic resonance spectrum of *n*-tetradecal, (2).

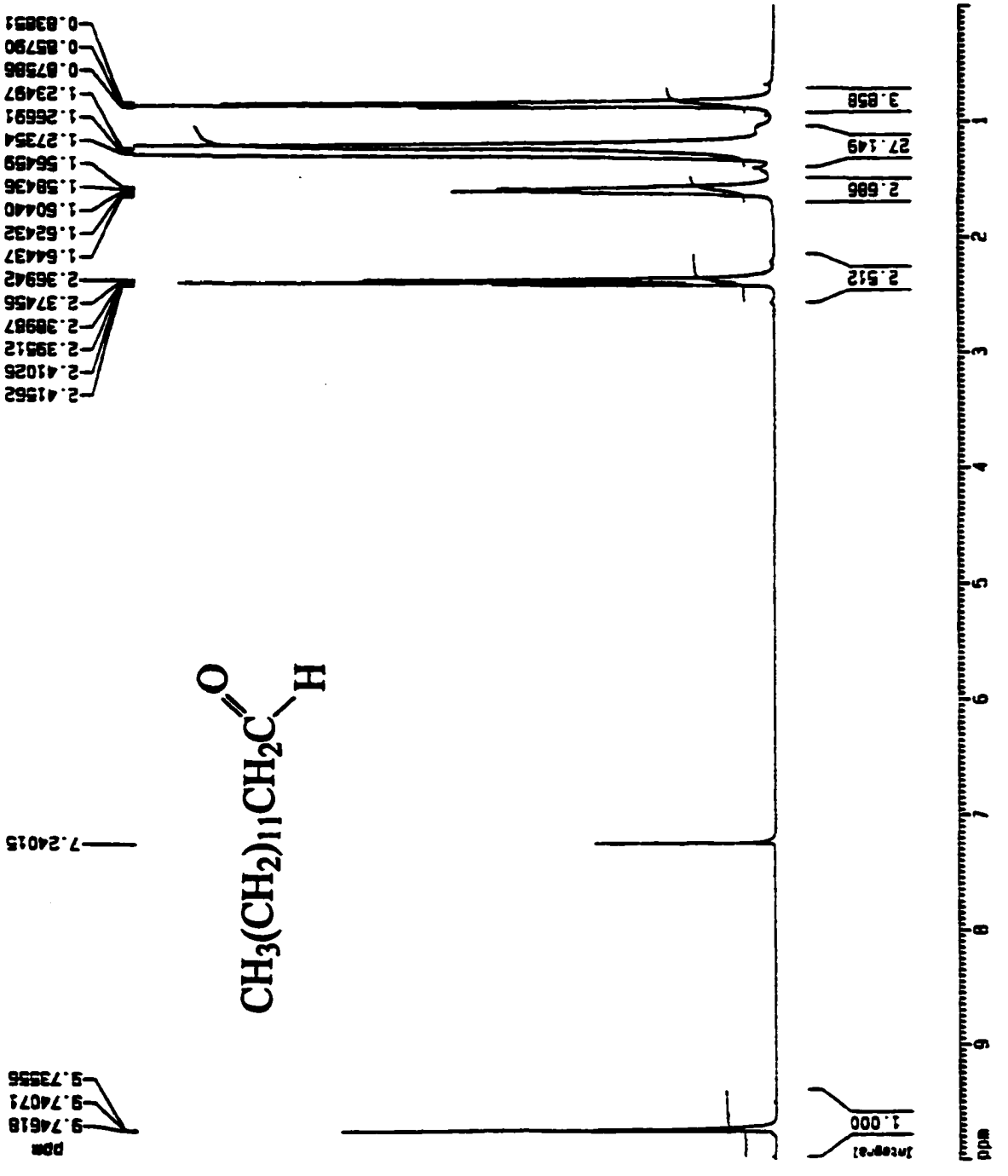

Figure 4.4. The nuclear magnetic resonance spectrum of *2*-tridecyl-*1,3*-dioxane, (3).

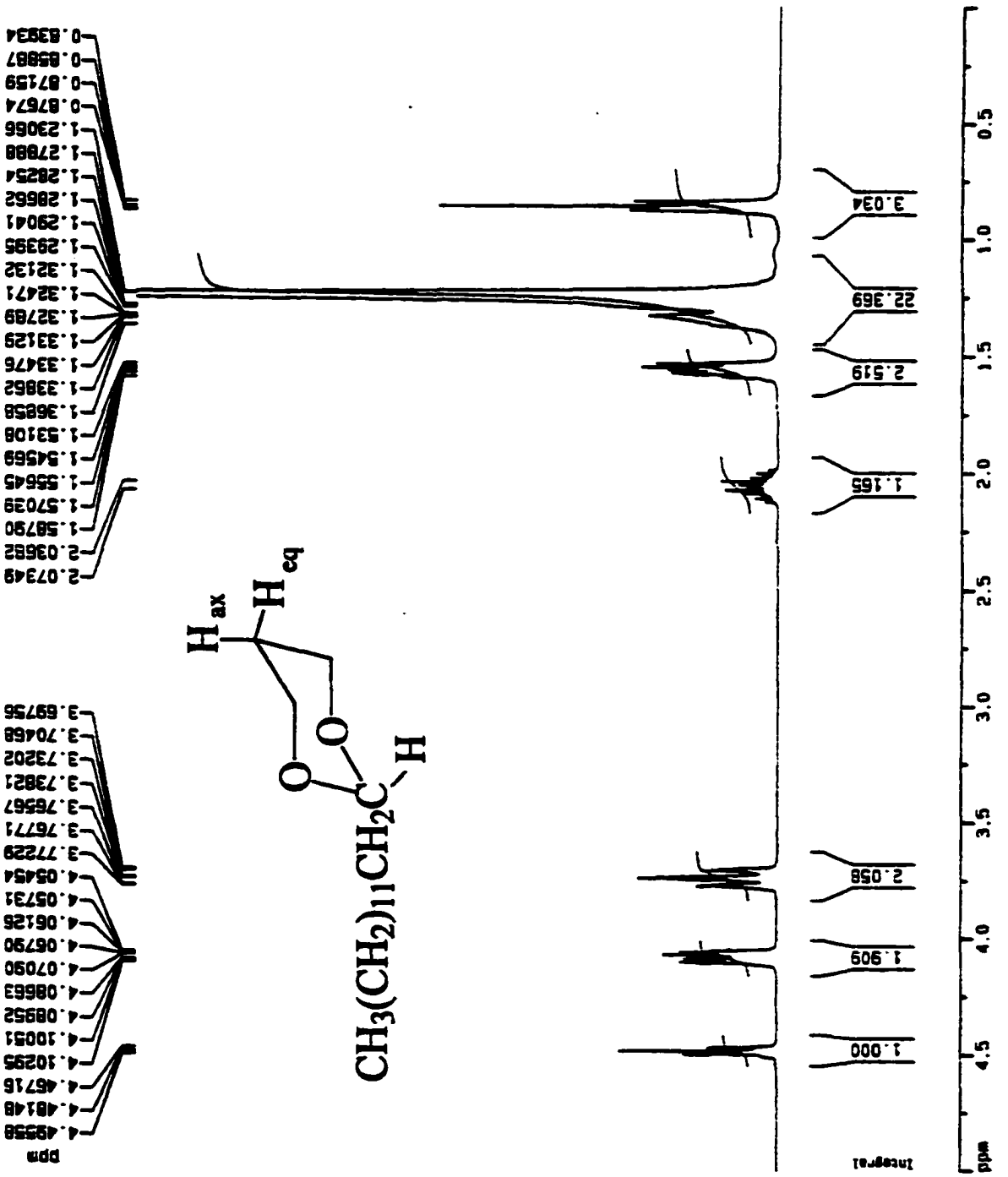

4.5.7 *3-[(1-propeneyltridecyl)oxy]propanol*, (**4**). A dichloromethane solution (15 mL) of the acetal **3** (270 mg, 1.00 mmol) was cooled to –78 °C under a nitrogen atmosphere. Allyltrimethylsilane (0.32 mL, 2.0 mmol) was added to the acetal solution at –78 °C, followed by the addition of $TiCl_4$ in dichloromethane (1.0 M, 1.0 mL, 1.0mmol), and the mixture was then stirred for 40 min at –78 °C.[9] This reaction was quenched by addition of 0.50 N NaOH in methanol (2.0 mL, 1.0 mmol), and the solution was allowed to warm to room temperature. The reaction mixture was poured into water and extracted with ether. The ethereal phase was washed with saturated aqueous $NaHCO_3$, dried with Na_2SO_4, and concentrated by rotary evaporation. The product was purified by column chromatography (silica) using hexanes/ethyl acetate (20:1) as an eluent to give (**4**) in 75% yield. ^{1}H NMR: $CH_3(CH_2)_{12}$, 0.86, (t, 3H); $CH_3(CH_2)_{12}$, 1.10~1.67, (m, 24H); $HOCH_2CH_2$, 1.79, (m, 2H); CH_2=$CHCH_2$, 2.24, (t, 2H); CH_2OH, 2.54, (s, 1H); $CH_3(CH_2)_{12}CHO$, 3.28, (m, 1H); $HOCH_2CH_2CH_2O$, 3.61, (m, 2H); CH_2OH, 3.75, (t, 2H); CH=CH_2, 4.88~5.05, (m, 2H); CH=CH_2, 5.75~5.82, (m, 1H), see Figure 4.5.

4.5.8 *(1,1,1,2,2,3,3,4,4,5,5,6,6,7,7,8,8,9,9,10,10-Heneicosylfluoro)-12-iodo-14-(3-hydroxylpropoxy)heptacosane*, (**5**). Compound (**4**) (0.20 g, 0.64 mmol), 1-iodoperfluorodecane (0.62 g, 0.96 mmol), and AIBN (3.0 mg, 0.02 mmol) were added into a pressure tube under nitrogen, and this mixture was heated to 95 °C for 1 h.[11] The mixture was then separated by column chromatography (silica) using hexanes/ethyl acetate (20:1) to give white (**5**) as a solid in 28% yield. ^{1}H NMR: $CH_3(CH_2)_{12}$, 0.86, (t, 3H); $CH_3(CH_2)_{12}$, 1.20~1.57, (m, 24H); $HOCH_2CH_2$, 1.82, (m, 2H); $OCHCH_2CHI$, 1.90,

Figure 4.5. The nuclear magnetic resonance spectrum of *3*-[(*1*-propeneyltridecyl)oxy] propanol, (4).

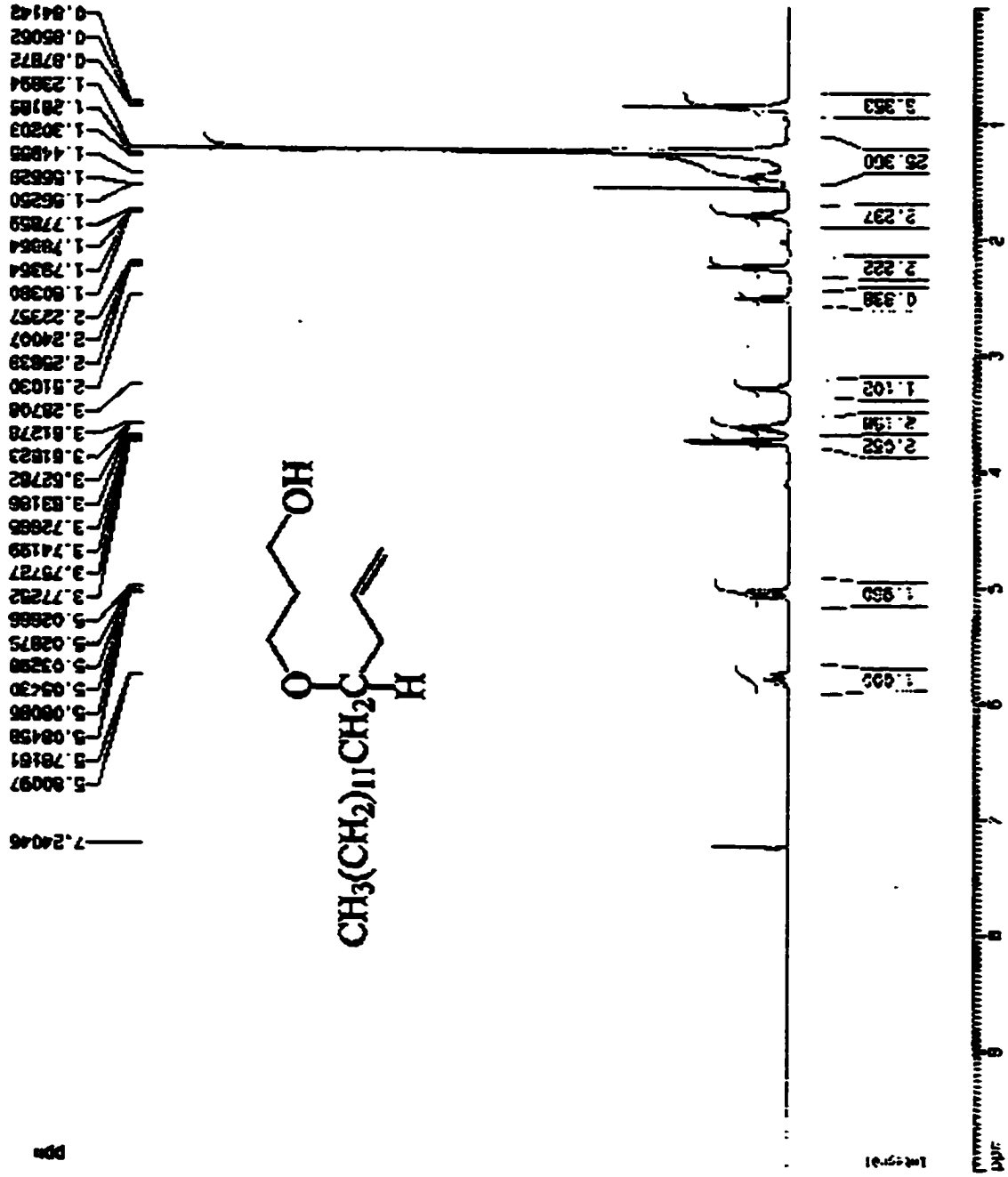

(m, 2H); CH_2OH, 2.05, (s, 1H); $CHICH_2C_{10}F_{21}$, 2.89, (m, 1H); $CH_3(CH_2)_{12}CHO$, 3.43, (m, 1H); $HOCH_2CH_2CH_2O$, 3.61, (m, 2H); CH_2OH, 3.75, (t, 2H); CHI, 4.27, (m, 1H), see Figure 4.6.

4.5.9 *3-[14-(1,1,1,2,2,3,3,4,4,5,5,6,6,7,7,8,8,9,9,10,10-heneicosylfluorotridecyl) tetradecoxy]propanol*, (**6**). The iodide (**5**) (250 mg, 0.260 mmol) in 20 mL of THF was added to a slurry of $LiAlH_4$ (20 mg, 0.52 mmol) in 3 mL of THF at 0 °C, and the mixture was brought to reflux for 3 h.[13] After cooling to room temperature, 0.2 mL of water, 0.2 mL of 3.75 M NaOH solution, and 0.6 mL of water were added. The gray granular side-product was filtered off, and the filtrate was concentrated by rotary evaporation to dryness. The resulting alcohol was purified by column chromatography (silica) using hexanes/ethyl acetate (10:1) as an eluent. The isolated yield was 50%. ^{1}H NMR: $CH_3(CH_2)_{12}$, 0.86, (t, 3H); $CH_3(CH_2)_{12}$ and $C_{10}F_{21}CH_2CH_2CH_2$, 1.20~1.57, (m, 28H); $HOCH_2CH_2$, 1.68, (m, 2H); $C_{10}F_{21}CH_2$, 2.07, (m, 2H); CH_2OH, 2.28, (t, 1H); $CH_3(CH_2)_{12}CHO$, 3.24, (m, 1H); $HOCH_2CH_2CH_2O$, 3.60, (m, 2H); CH_2OH, 3.77, (t, 2H), see Figure 4.7.

4.5.10 *3-[14-(1,1,1,2,2,3,3,4,4,5,5,6,6,7,7,8,8,9,9,10,10-heneicosylfluorotridecyl) tetradecoxy]propyl methanesulfonate*, (**7**). To a stirred solution of the alcohol (**6**) (330 mg, 0.400 mmol) in 20 mL THF were added triethylamine (160 mg, 1.60 mmol) and methylsulfonyl chloride (136 mg, 1.20 mmol). After a couple of minutes of stirring, a white precipitate formed. The mixture was stirred overnight at room temperature and then poured into water and extracted with methylene chloride. The organic phase was washed with water three times and then dried with Na_2SO_4. The solvents were removed

Figure 4.6. The nuclear magnetic resonance spectrum of (*1,1,1,2,2,3,3,4,4,5,5,6,6,7,7,8,8,9,9,10,10*-heneicosylfluoro)-*12*-iodo-*14*-(3-hydroxylpropoxy)heptacosane, (5).

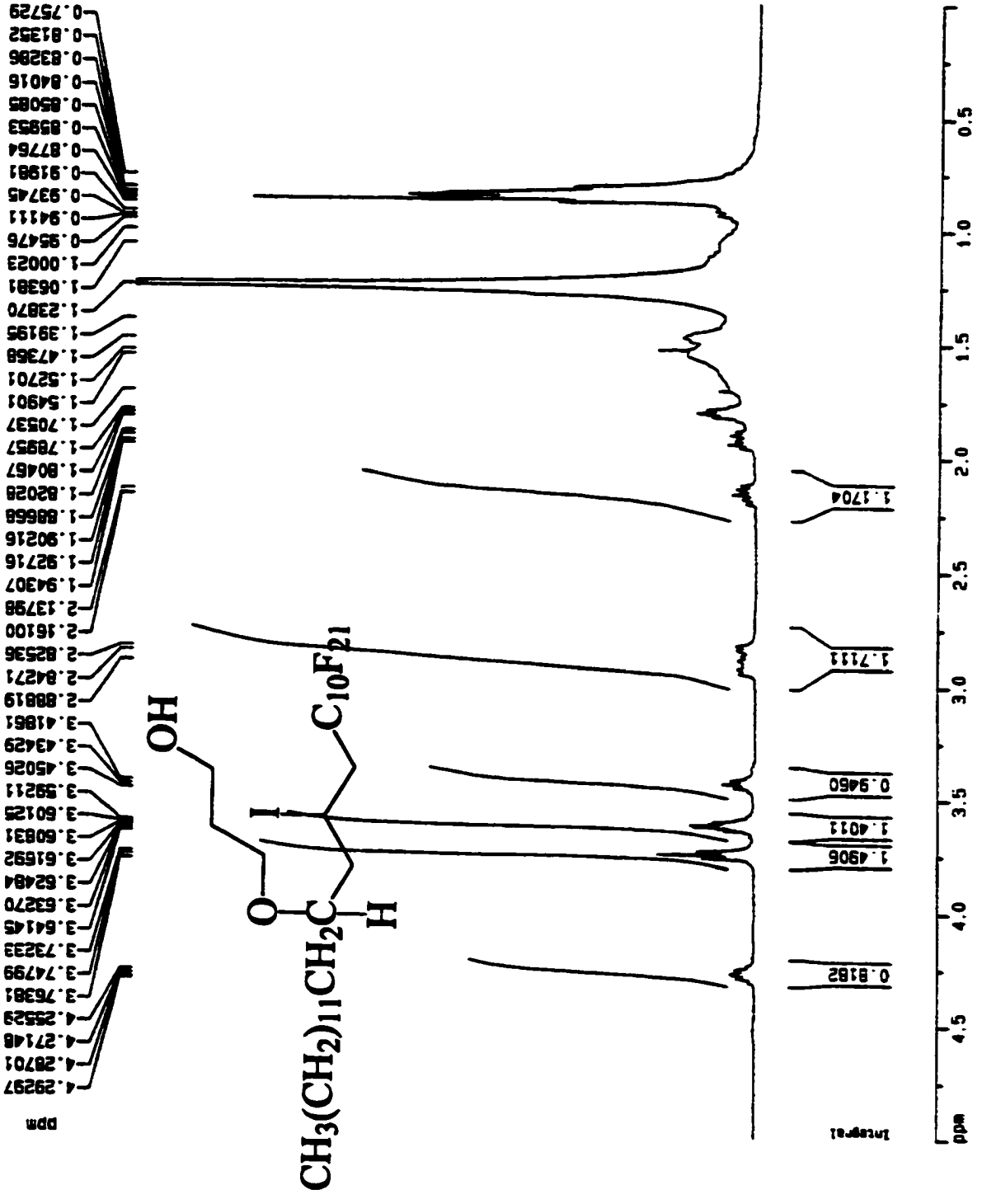

Figure 4.7. The nuclear magnetic resonance spectrum of *3*-[*14*-(*1,1,1,2,2,3,3,4,4,5,5,6,6,7,7,8,8,9,9,10,10*-heneicosylfluorotridecyl)tetradecoxy]propanol, (6).

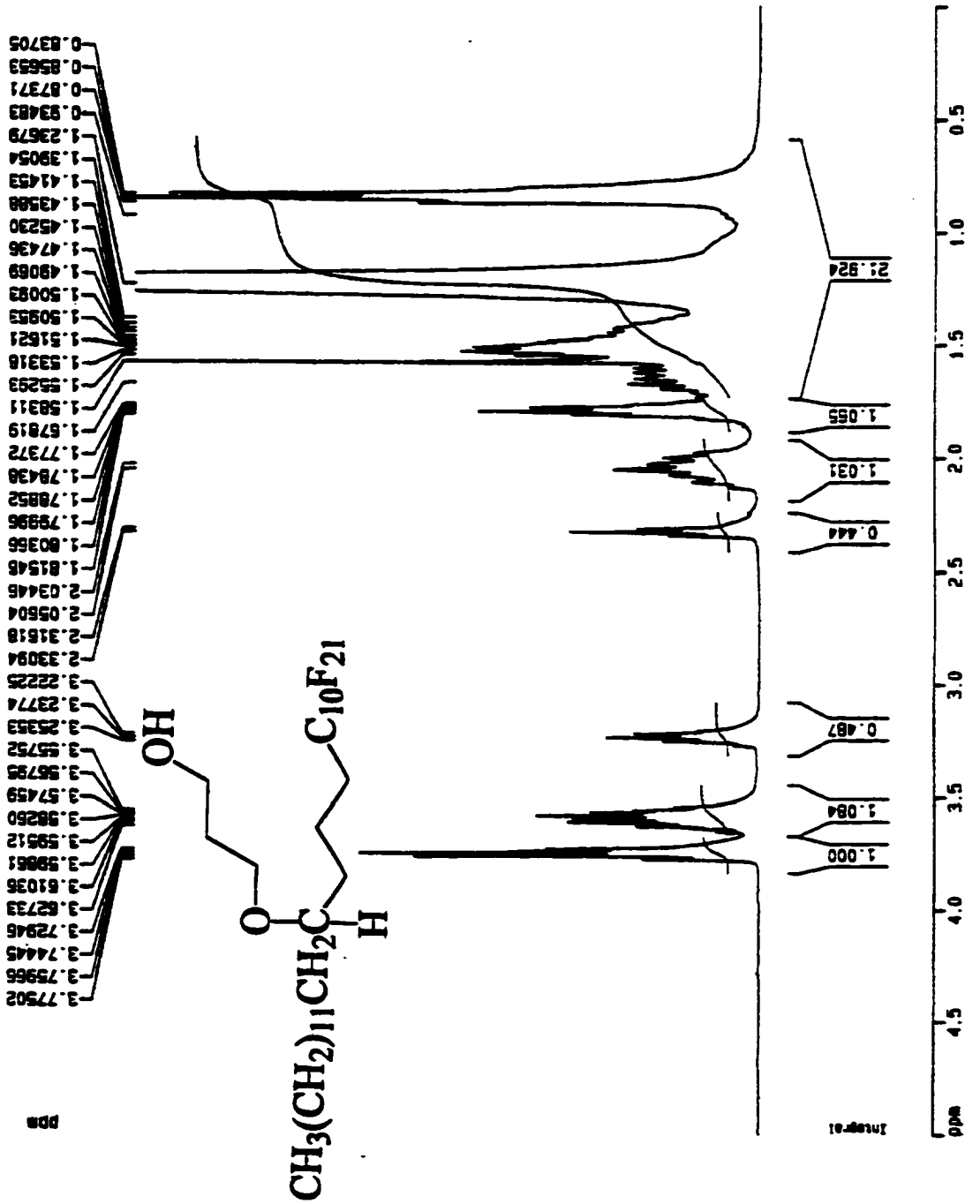

by rotary evaporation. The mesylate (7) was used without further purification. ^{1}H NMR: $CH_3(CH_2)_{12}$, 0.86, (t, 3H); $CH_3(CH_2)_{12}$ and $C_{10}F_{21}CH_2CH_2CH_2$, 1.20~1.57, (m, 28H); $CH_3O_2SOCH_2CH_2$, 1.97, (m, 2H); $C_{10}F_{21}CH_2$, 2.07, (m, 2H); $CH_3O_2SOCH_2$, 2.97, (s, 3H); $CH_3(CH_2)_{12}CHO$, 3.24, (m, 1H); $CH_3O_2SOCH_2CH_2CH_2O$, 3.52, (m, 2H); $CH_3O_2SOCH_2$, 4.33, (t, 2H), see Figure 4.8.

4.5.11 *1-Bromo-3-[14-(1,1,1,2,2,3,3,4,4,5,5,6,6,7,7,8,8,9,9,10,10-heneicosylfluoro tridecyl)tetradecoxy]propane*, (**8**). The mesylate (**7**) (200 mg, 0.200 mmol) was converted to corresponding bromide by refluxing for 12 h with lithium bromide (55 mg, 0.6 mmol) in 20 mL of acetone. Purification by column chromatography (silica) using hexanes/ethyl acetate (20:1) produced the corresponding bromide (8) in 80% yield. ^{1}H NMR: $CH_3(CH_2)_{12}$, 0.86, (t, 3H); $CH_3(CH_2)_{12}$ and $C_{10}F_{21}CH_2CH_2CH_2$, 1.20~1.57, (m, 28H); $BrCH_2CH_2$, 2.05, (t, 2H); $C_{10}F_{21}CH_2$, 2.07, (m, 2H); $CH_3(CH_2)_{12}CHO$, 3.24, (m, 1H); CH_2Br, 3.49, (t, 2H); $BrCH_2CH_2CH_2O$, 3.56, (m, 2H), see Figure 4.9.

4.5.12 *3-[14-(1,1,1,2,2,3,3,4,4,5,5,6,6,7,7,8,8,9,9,10,10-heneicosylfluorotridecyl) tetradecoxy]propanethiol*, (**9**). The branched bromide (**8**) (150 mg, 0.167 mmol) and potassium thioacetate (35 mg, 0.36 mmol) were dissolved in a degassed mixture of THF and methanol (10 mL/30 mL), and the solution was allowed to reflux for 3 h under argon, then cooled to room temperature and 3 mL of 3 N HCl was added.[15] The mixture was refluxed for an additional 24 h and then poured into water. The product was extracted with ether, and the ethereal layer was washed with water, dried with Na_2SO_4, and concentrated to dryness. Purification by column chromatography (silica) using

Figure 4.8. The nuclear magnetic resonance spectrum of *3*-[*14*-*(1,1,1,2,2,3,3,4,4,5,5,6,6,7,7,8,8,9,9,10,10*-heneicosylfluorotridecyl)tetradecoxy]propylethanesulfonate, (7).

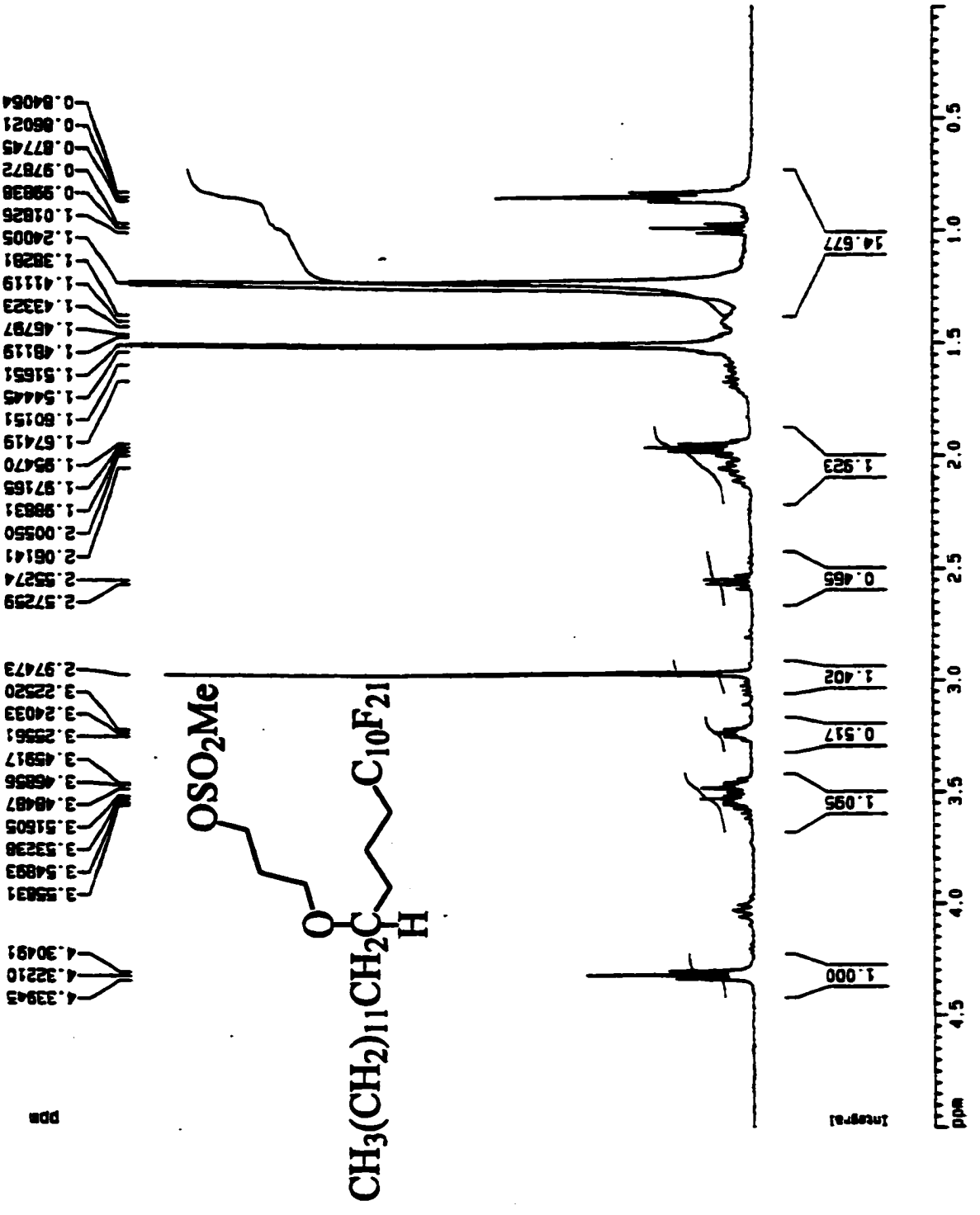

Figure 4.9. The nuclear magnetic resonance spectrum of *1*-bromo-*3*-[*14*-*(1,1,1,2,2,3,3,4,4,5,5,6,6,7,7,8,8,9,9,10,10*-heneicosylfluorotridecyl)tetradecoxy]propane, (8).

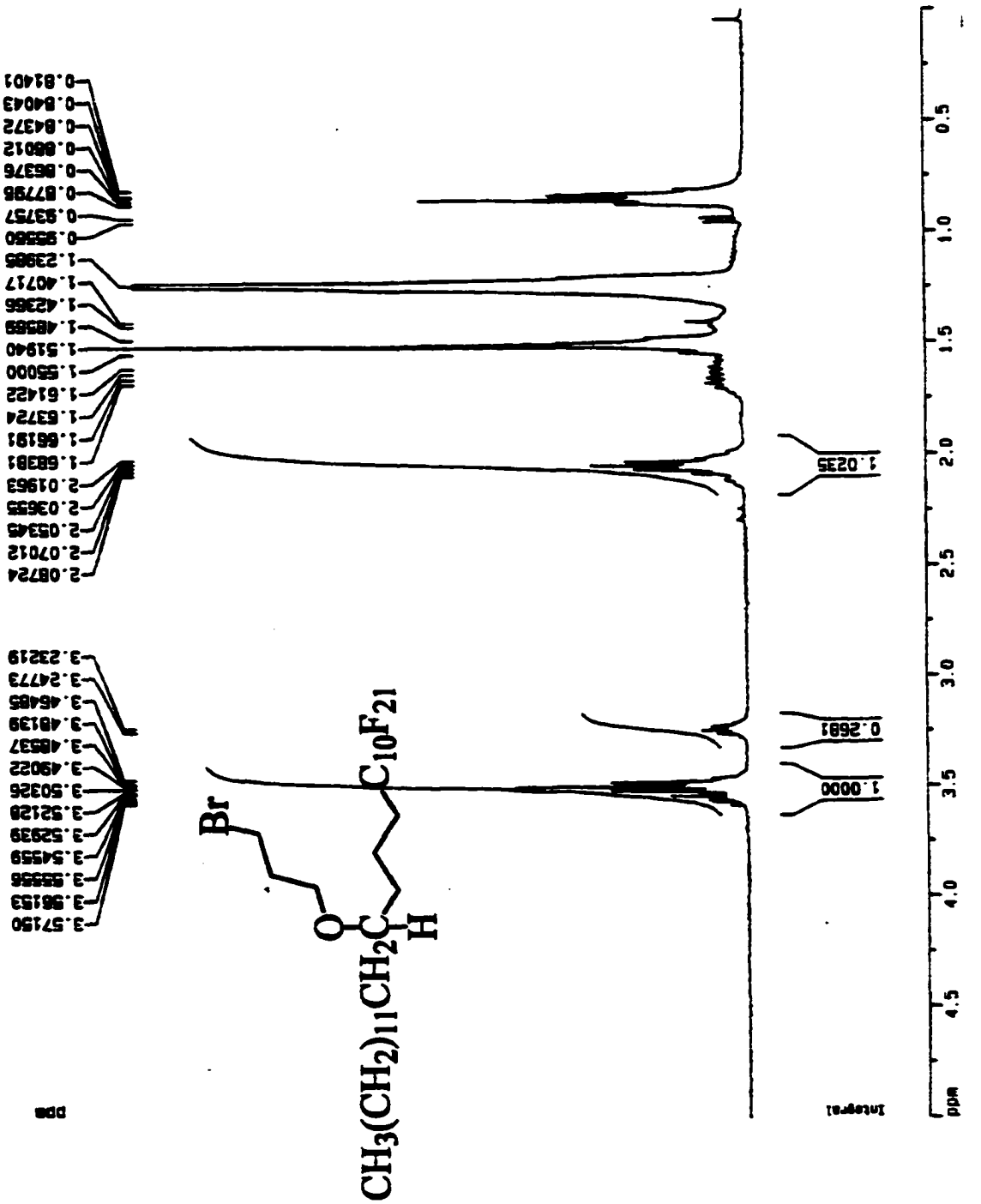

hexanes/methylene chloride (15:1) as an eluent gave the product 1 as a white solid in 50% yield. ^{1}H NMR: C*H*$_3$(CH$_2$)$_{12}$, 0.86, (t, 3H); CH$_3$(C*H*$_2$)$_{12}$ and C$_{10}$F$_{21}$CH$_2$C*H*$_2$C*H*$_2$, 1.28~1.57, (m, 28H); HSCH$_2$C*H*$_2$, 1.82, (m, 2H); C$_{10}$F$_{21}$C*H*$_2$, 2.07, (m, 2H); C*H*$_2$SH, 2.60, (q, 2H); CH$_3$(CH$_2$)$_{12}$C*H*O, 3.24, (m, 1H); HSCH$_2$CH$_2$C*H*$_2$O, 3.49, (m, 2H). Anal. Calcd for C$_{30}$F$_{21}$H$_{41}$OS: C, 42.45%; H, 4.87%. Found C, 42.46%; H, 4.67%, Figure 4.10.

Figure 4.10. The nuclear magnetic resonance spectrum of *3*-[*14*-(*1,1,1,2,2,3,3,4,4,5,5,6,6,7,7,8,8,9,9,10,10*-heneicosylfluorotridecyl) tetradecoxy]propanethiol, (9).

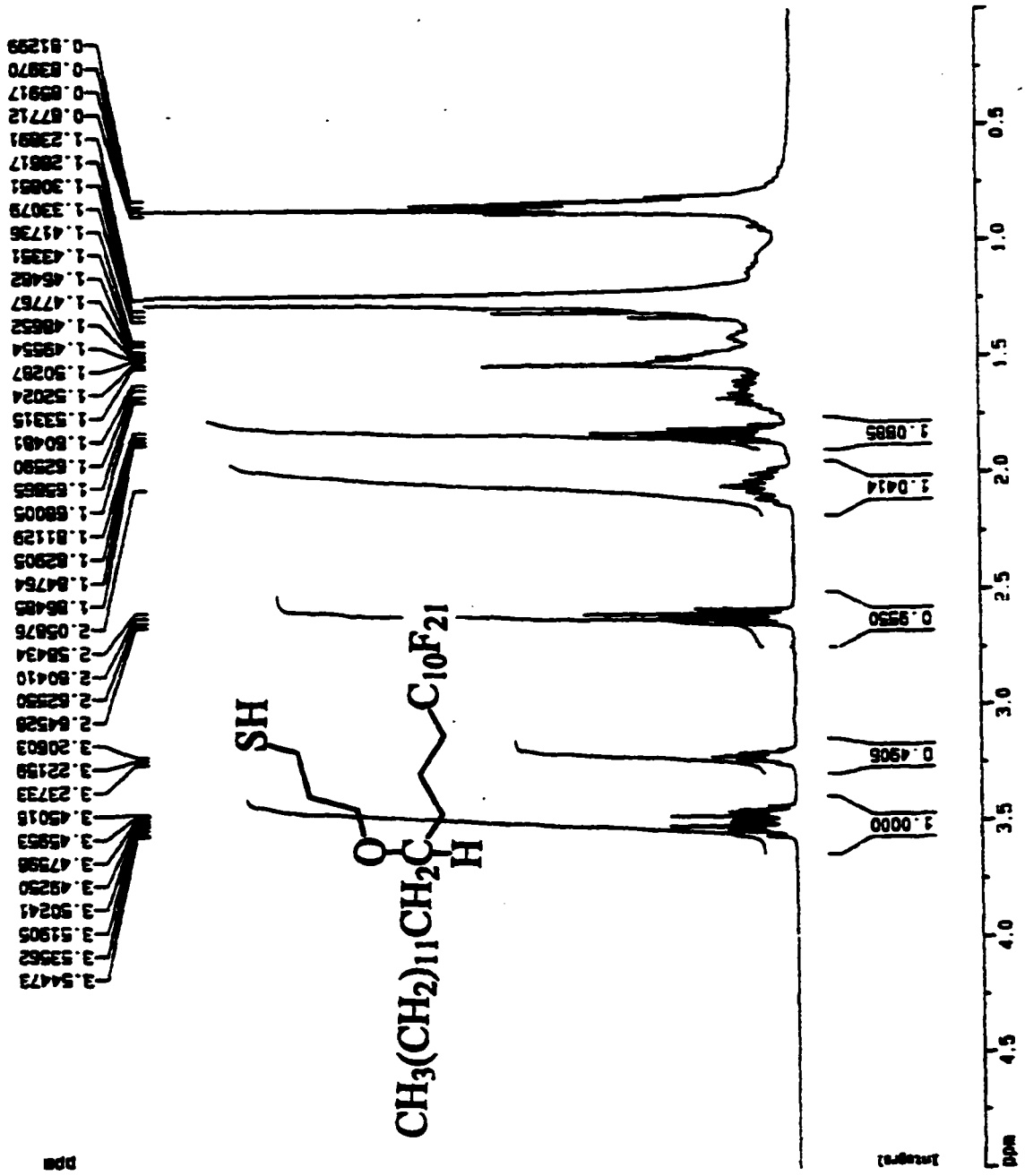

4.6 Acknowledgements

We gratefully acknowledge the National Science Foundation and industrial partners for support of this research through the Polymer Interfaces Center, an Industry/University Cooperative Research Center at Lehigh University. In addition, we thank Steve Grunzinger for helpful discussions.

4.7 Reference

1. Zhulina, E; Balazs, A. C. *Macromolecules* **1996**, *29*, 2667.
2. Brace, N. O.; Marshall, L. W.; Pinson, C. J.; van Wingerden, G., *J. Org. Chem.* **1984**, 49, 2361-2368.
3. Laibinis, P. E.; Bain, C. D.; Nuzzo, R. G.; Whitesides, G. M. *J. Phys. Chem.* **1995**, *99*, 7663-7676.
4. Sinniah, K.; Cheng, J.; Terrettaz, S.; Reutt-Robey, J. E.; Miller, C. J. *J. Phys. Chem.* **1995**, *99*, 14500-14505.
5. Ong, T. H.; Davies, P. B.; Bain, C. D. *Langmuir* **1993**, *9*, 1836-1845.
6. Ratcliffe, R.; Rodehost, R. *J. Org. Chem.* **1970**, *35*, 4000-4002.
7. Corey, E. J.; Schmidt, G. *Tetrahedron Lett.* **1979**, *5*, 399-402.
8. Mori, I.; Ishihara, K.; Flippin, L. A.; Noraki, K.; Yamamoto, H.; Bartlett, P. A.; Heathcock, C. H. *J. Org. Chem.* **1990**, *55*, 6107-6115.
9. (a) Hosomi, A.; Endo, M.; Sakurai, H. *Chem. Lett.* **1976**, 941-942. (b) Denmark, S. E.; Almstead, N. G. *J. Org. Chem.* **1991**, *56*, 6458-6467. (c) Maeda, K.; Shinokubo, H.; Oshima, K. *J. Org. Chem.* **1997**, *62*, 6429-6431.

10. (a) Ishihara, T.; Huroboshi, M.; Okada, Y. *Chem. Lett.* **1986**, 1895-1896. (b) Chen, Q.-Y.; Yang, Z.-Y.; Zhao, C.-X.; Qiu, Z.-M. *J. Chem. Soc. Perkin Trans. I.* **1988**, 563-567.

11. Greiner, J.; Milius, A.; Riess, J. *J. Fluorine Chem.* **1992**, *56*, 285-293.

12. (a) Hein, M.; Miethchen, R.; Schwäbisch, D. *J. Fluorine Chem.* **1999**, *98*, 55-60. (b) Liu, J.-T.; Sui, G.-D.; Chen, G.; Huang, W.-Y. *J. Fluorine Chem.* **1999**, *93*, 49-51. (c) Cornelia, Z.; Miethchen, R. *Eur. J. Org. Chem.* **1998**, 531-539. (d) Long, Z.-Y.; Chen, Q.-Y. *J. Org. Chem.* **1999**, *64*, 4775-4782. (e) Guo, X.-C.; Chen, Q.-Y. *J. Fluorine Chem.* **1999**, *93*, 81-86.

13. Marra, K.; Chapman, T. M. *Polym. Preprint* **1996**, *37*, 286-287.

14. (a) Nguyen, B. V.; Yang, Z.-Y.; Burton, D. J. *J. Org. Chem.* **1998**, *63*, 2887-2891. (b) Yang, Z.-Y.; Burton, D. J. *J. Org. Chem.* **1991**, *56*, 5125-5132.

15. Graupe, M.; Koini, T.; Wang, V. Y.; Nassif, G. M.; Colorado, R. Jr.; Villazana, R. J.; Dong, H.; Miura, Y. F.; Shmakova, O. E.; Lee, T. R. *J. Fluorine Chem.* **1999**, *93*, 107-115.

Chapter 5

Unusual Reconstruction at an EPDM/Air Interface

We will publish this work in a scientific journal and the copyright assigned to the publisfer.

5.1 Abstract

The surface of the crosslinked terpolymer of ethylene, propylene, and diene (EPDM) was oxidized using a water plasma. This hydrophilic surface became hydrophobic when heated against air, thus minimizing its interfacial free energy. However, the surface showed an unusual reconstruction, becoming more hydrophilic when the substrate was equilibrated against air at room temperature, contrary to the behavior of most other modified polymer surfaces. These changes in surface wettability depended on the extent of modification, annealing temperature, cooling temperature, and bulk crosslinking density.

5.2 Introduction

The use of polymers in technology is growing because of the combination of light weight, high strength, toughness and durability that polymers can provide. Less attention, however, has been paid to the interfaces of polymer with other materials than to their bulk properties.

Our research group has demonstrated that the architecture of a polymer can influence the composition and dynamics at its surface. It is well known that when polymers are heated against liquids or gases, their surfaces reorganize (if possible) to minimize the interfacial free energy.[1] Early work by Dr. Deborah Carey showed that the hydrophilicity of the surface-oxidized 1,2-polybutadiene changed as a function of temperature, with the polymer surface becoming more hydrophobic as the temperature of the water was increased. This result was the opposite of what would be expected if enthalpic forces governed the reconstruction, and indicated that entropy was responsible for the temperature dependence.[2,3]

Sureurg Khongtong demonstrated that the oxidized surface of chemically crosslinked 1,4-polybutadiene also reconstructed entropically against water,[4] as well as against aluminum.[5] We believe that this unusual behavior is due to the entropic forces associated with rubber elasticity: the migration of polar groups to the polymer/water or polymer/metal interfaces requires extension of polymer chains out of their entropically favored random-coil conformations. As the temperature of the water increases, for example, a change in entropy causes the stretched chains to recoil and rebury the polar

groups. This temperature-dependent change in surface hydrophilicity depends upon the bulk properties, such as crystallinity and levels of crosslinking, and the degree of oxidation of the surface.

Recently, Steve Grunzinger used a water plasma to modify the surface of polyisoprene to produce oxygen-containing functionality (PI-ox).[6] When the PI-ox was annealed at elevated temperature, the surface became hydrophobic. Upon cooling in air, however, the surface became hydrophilic again, contrary to the behavior that polymer surfaces will reorganize to minimize the interfacial free energy. Surprisingly, over time in air the reconstruction reversed direction and again the surface became hydrophobic. A possible explanation of these results would be that the reconstruction is a three-state, rather than the conventional two-state, process.

In this Chapter, we report a similar behavior on a chemically crosslinked EPDM surface (terpolymer of ethylene, propylene, and diene) that had been oxidized with a water-vapor plasma. After modification, the EPDM surface initially was hydrophilic due to the introduction of polar groups and became more hydrophobic after annealing overnight at 60 °C or higher temperature. The surface became hydrophilic again, however, when cooled down to room temperature against air. As with PI-ox, the direction of the reconstruction then reversed and the surface ultimately became hydrophobic again.

5.3 Results and Discussion

Films of the terpolymer of ethylene, propylene, and diene (EPDM) were formed by chemical crosslinking using dicumyl peroxide (DCP). The DCP crosslinked films were

cured for eight half-lives at 150 °C. The amount of crosslinking, estimated by measuring the average molecular weight between crosslinks (M_c), was varied systematically and measured using the swelling method and the Flory-Rehner equation.[7,8] using Flory-Huggins interaction parameter, χ, as 0.4.[9,10]

The data in Figure 5.1 shows that the molecular weight between crosslinks (M_c) changed as a function of the amount of DCP added in the films. As the amount of DCP increased from 0.2 to 1 phr (parts per hundred rubber), the value of M_c fell from 43,100 to 3200 g/mol. The value of M_c then decreased from 3200 g/mol to 1200 g/mol, when the concentration of DCP was more than 2 phr (up to 8 phr) of dicumyl peroxide was used. The unbound fraction (about ~4 wt%), which could complicate surface reconstruction, was also removed during this swelling.[11] A 36-h swelling time was sufficient to remove the unbound fraction from the EPDM network. Thus, in this study, all samples were swollen in hexanes at least 2 d to ensure the samples were free of mobile chains.

The EPDM surface was modified using a water-vapor plasma (0.1 Torr) for various amounts of time. Figure 5.2 shows the advancing contact angles of water on DCP-crosslinked (M_c=3200 g/mol) samples that had been plasma treated. Advancing contact angles (θ_a) of water (pH1) were used to monitor the surface modification: the contact angle of water decreased as the period of plasma treatment increased. We found that the contact angles were insensitive to the pH of the water (i.e., pH 13), indicating that the water plasma produced mainly hydroxyl groups or other non-ionizable functional groups. We also noticed that EPDM samples initially annealed at 60 °C showed bigger changes of wettability under the same plasma treatment, compared to non-annealed

Figure 5.1. Average molecular weight between crosslinks (M_c) for EPDM films cured with DCP.

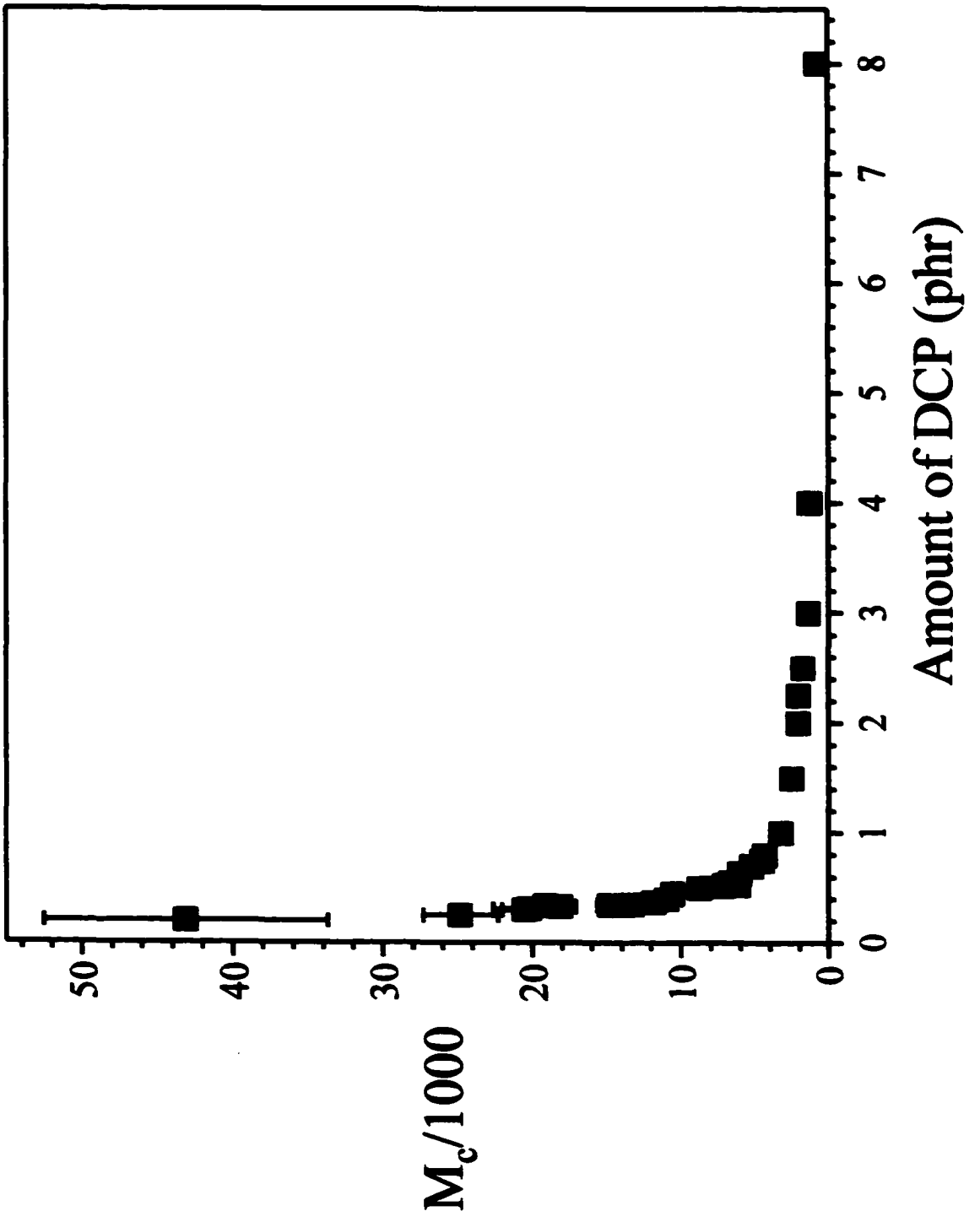

Figure 5.2. A plot of the degree of reconstruction of the EPDM surface (M_c = 3200 g/mol) as a function of the plasma treatment time. The squares represent the modified EPDM samples that had not been pre-annealed, and the circles represent the modified EPDM samples that had been pre-annealed. The measurements were carried out using water at pH 1.

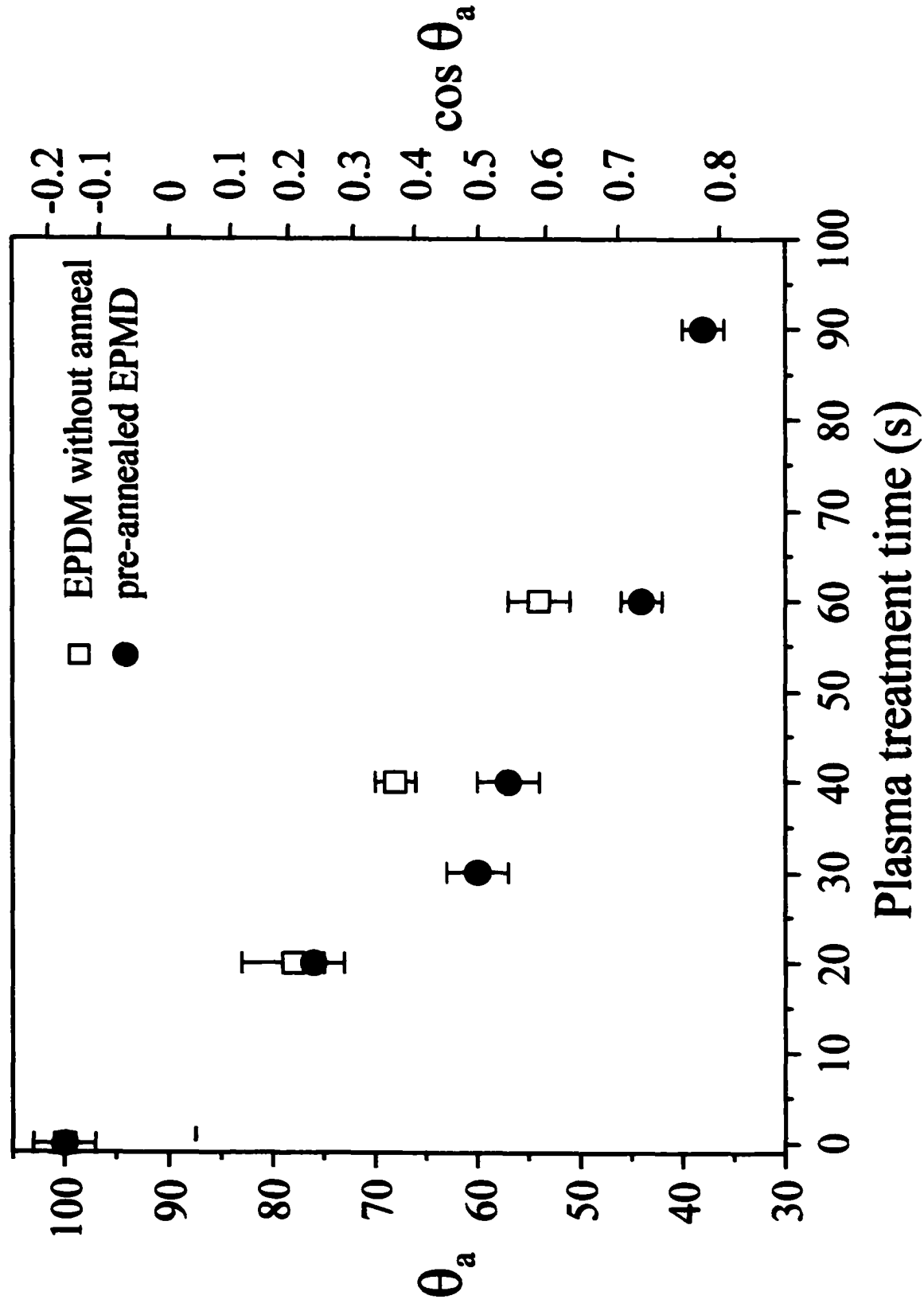

samples. A possible explanation is that more propylene repeat units may migrate to the EPDM surface to minimize the surface energy at high temperature. Others have reported that these groups are more easily to functionized, while ethylene groups tend to crosslink, during plasma treatment.[12]

We used X-ray photoelectron spectroscopy (XPS) to analyze the surface before and after plasma modification (Figure 5.3). The XPS spectra (15° take-off angle) of unmodified EPDM contained only a small amount of oxygen, likely due to the by-product of the dicumyl peroxide used in the crosslinking reaction. The significant increase in the O 1s photoemission in the survey spectrum of the modified EPDM is consistent with oxidation by the water plasma. A high-resolution spectrum in the C 1s region of the modified EPDM showed the appearance of high-binding-energy photoemission that could be fit with peak at 286.5 eV (C-O).[13] Based on the photoemission of C1s at 285 eV and at 286.5 eV, approximately 15% of the carbon was functionalized.

Thermal Reconstruction of EPDM-ox against Air.

As expected, a functionalized EPDM surface became more hydrophobic upon annealing in air at 60 °C, consistent with the system minimizing its surface energy. To our surprise, however, the advancing contact angles of water (pH1) on the annealed EPDM-ox decreased when the samples were then equilibrated in air at room temperature, and then gradually increased again over several days. Figure 5.4 shows a typical change of contact angle on this annealed EPDM-ox surface (M_c = 6000 g/mol) as a function of time.

Figure 5.3. Survey XPS spectrum of a crosslinked EPDM (M_c = 7000 g/mol) before and after surface treatment. The inset shows the high-resolution spectrum of this sample in the carbon 1s region.

Figure 5.4. Advancing contact angles of water (pH 1) on plasma-oxidized EPDM (M_c = 6000 g/mol) upon cooling in air from 60 °C to room temperature. The inset shows the initial changes in contact angles of water on plasma-oxidized EPDM upon cooling. The error bars indicate one standard deviation above and below the average.

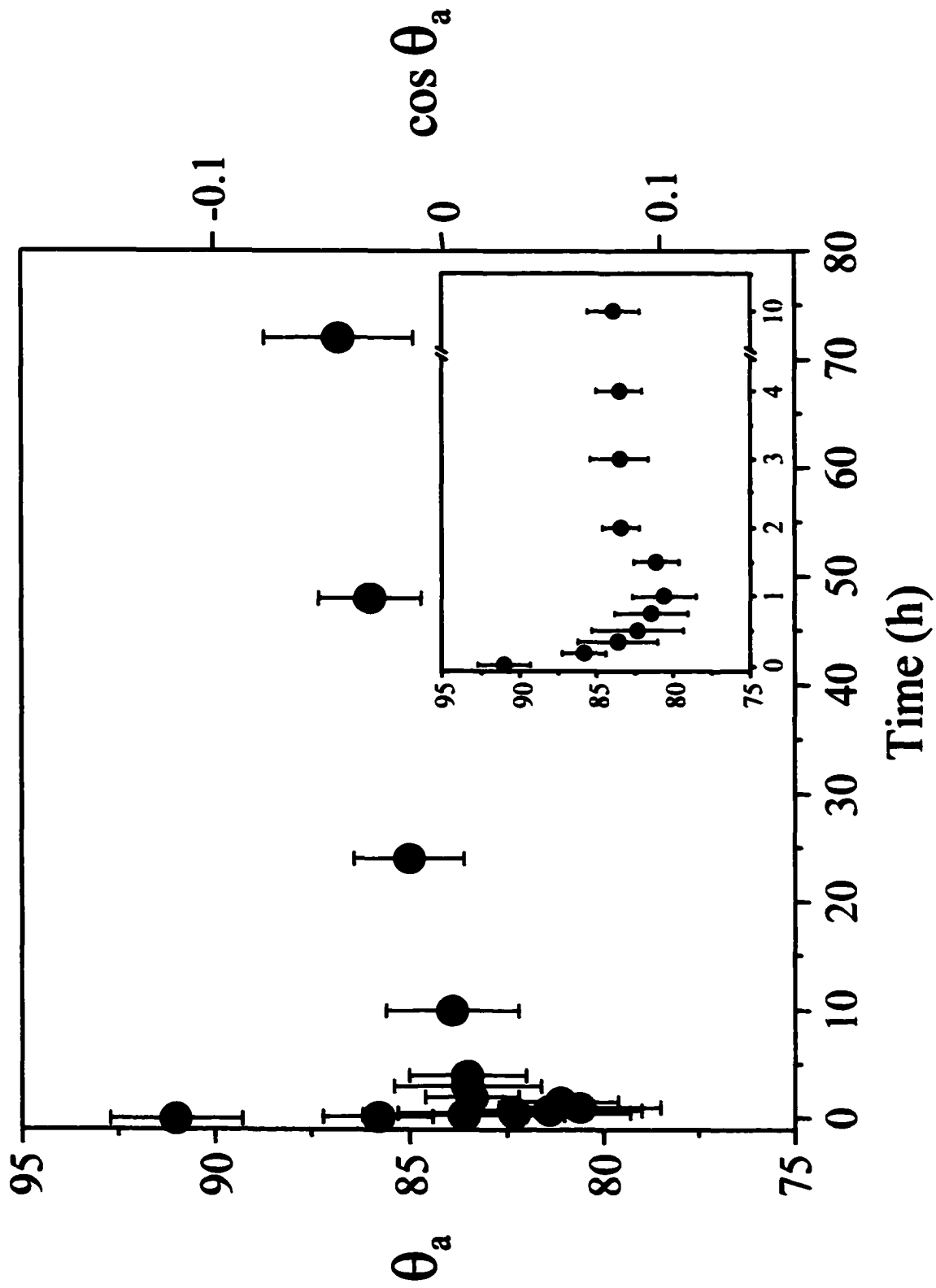

202

The observed reconstruction is analogous to that found by one of my coworkers, S. Grunzinger, for plasma-oxidized polyisoprene (PI-ox).[6] The plot in Figure 5.4 seems to be a composite curve of two consecutive reconstruction mechanisms. A reversible three-state model (A ⇆ B ⇆C) proposed by Grunzinger and Ferguson is consistent with this unusual reconstruction, where state A is the initial hydrophobic configuration of the polymer surface, state B is a hydrophilic intermediate configuration, and state C represents the final room-temperature configuration.[6] Their hypothesis is that the clustering of polar groups at lower temperature is the driving force for the surface becoming more wettable upon cooling. The polar groups tend to aggregate together at room temperature, e.g., via hydrogen bonding, a process that we propose requires chain extension. At higher temperature, this association is broken due to chains recoiling elastically, and polar groups migrate into bulk to minimize the surface energy as seen in Figure 5.5. Once the temperature is lowered, the polar groups re-aggregate at the interface, causing the surface become more hydrophilic. Meanwhile, in a second slower process, hydrophobic segments migrate to the surface to minimize the surface energy, a second process that requires chain extension. This behavior is analogous to the bulk behavior of ionomeric polymers: charged groups do not associate at elevated temperature due to entropically driven coiling of the polymer chains.

Figure 5.6 shows the magnitude of reconstruction, $|\Delta\theta_a|$, the difference of initial and minimum advancing contact angles of water, of EPDM-ox (M_c=3200 g/mol) as a function of plasma-treatment time. A 20-s treatment gave the maximum change in the wettability. A possible explanation is that longer oxidation times resulted in more chain

Figure 5.5. Schematic illustration of a possible mechanism for reconstruction of EPDM-ox upon annealing/cooling to initially become more hydrophilic.

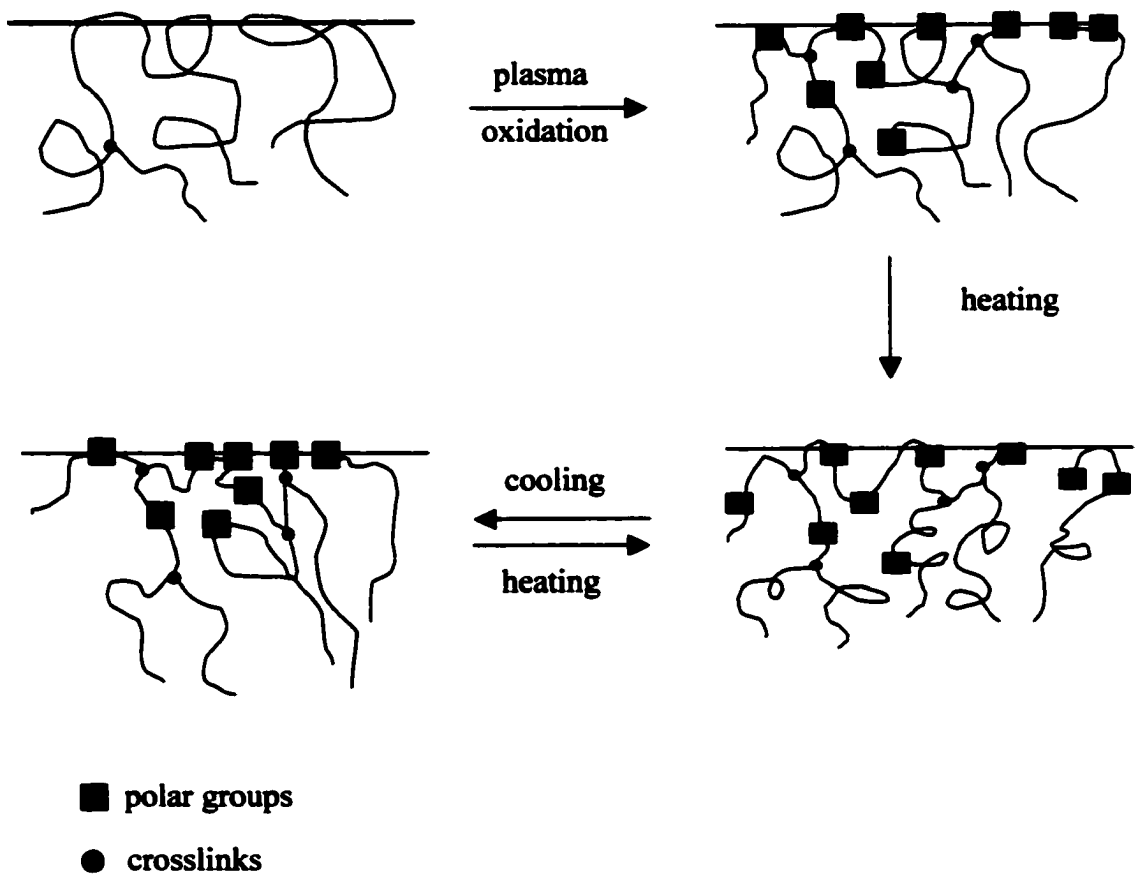

Figure 5.6. A plot of the degree of reconstruction of the EPDM surface as a function of the plasma time.

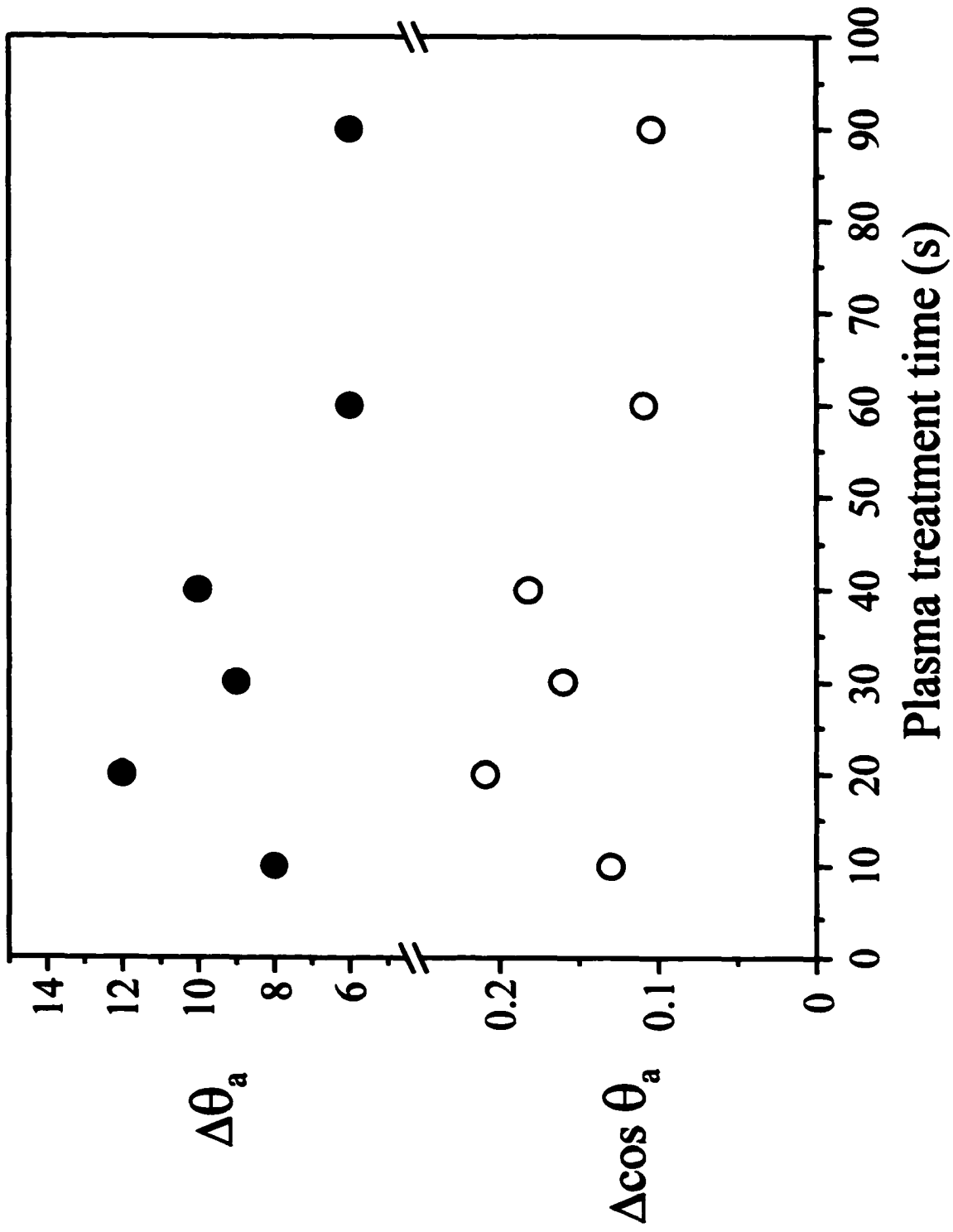

scission, so that migration of polar groups became irreversible.

Figure 5.7 shows the magnitude of reconstruction, $|\Delta\theta_a|$, as a function of crosslinking density in the bulk. The magnitude of reconstruction was insignificant, $|\Delta\theta_a| \leq 6°$, when the M_c is below 1700 g/mol and increased dramatically when M_c reached 2000 g/mol and then reached a plateau. The limited chain mobility at high levels of crosslinking would be expected to inhibit migration of polar groups near the surface, and thus lower $\Delta\cos\theta$. As with entropic reconstructions in the polybutadiene and polyisoprene systems,[4,6] the magnitude of reconstruction reached a plateau at 1900 g/mol, near the chain-entanglement length[14] We followed a published procedure to determine the chain-entanglement length (M_e) in the uncrosslinked films. Uncrosslinked samples (25 mm x 10 mm x 1 mm) were prepared by casting a film from solution. The average storage modulus G' is the averaged value of G' from –26 to 26 °C in Figure 5.8. Using the rubber elasticity theory (equation 5.1)[15]

$$G' = \rho RT/M_e \qquad (5.1)$$

where ρ is the density, R is the gas constant, T is the absolute temperature, and M_e is the molecular weight between entanglements. Based on this calculation, M_e is around 1400 g/mol, consistent with reports by others.[14]

To optimize the entropic effects in this surface, we systemically changed the heating temperature of the EPDM-ox. Our expectation was that at higher temperatures, annealing would produce a more hydrophobic surface than at lower-temperature because the polymer chains would be more mobile. Figure 5.9 shows the reconstruction of EPDM-ox (M_c = 7700 g/mol) as a function of time after having been annealed at various

Figure 5.7. Magnitude of the limiting change in θ_a and cos θ_a (H_2O, pH 1) on surface-modified EPDM upon cooling to room temperature from 60 °C as a function of molecular weight between crosslinks (M_c). The error bars indicate one standard deviation above and below the average. The dotted vertical line shows the approximate chain entanglement molecular-weight for this polymer.

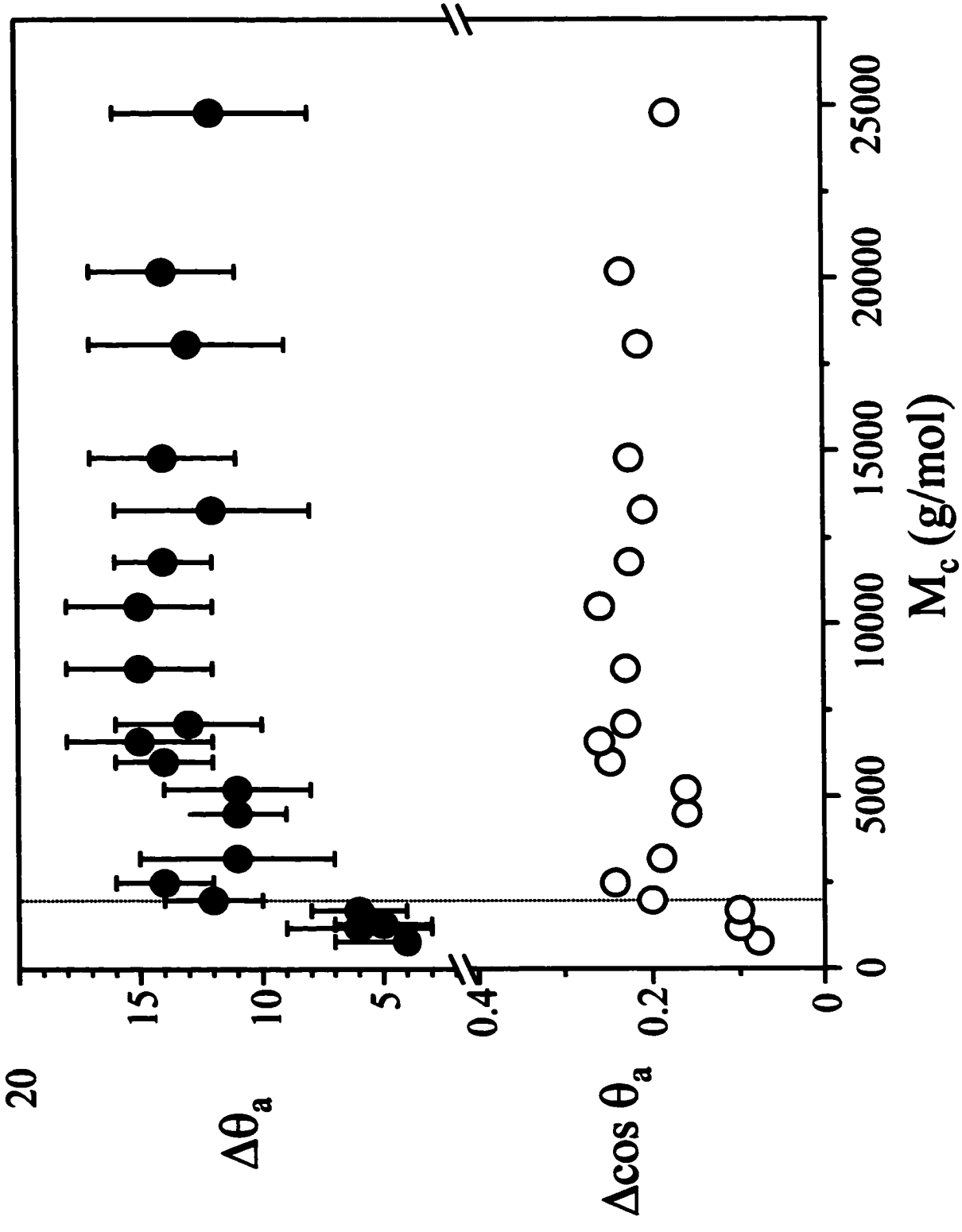

Figure 5.8. Dynamic modulus for uncrosslinked EPDM as a function of temperature.

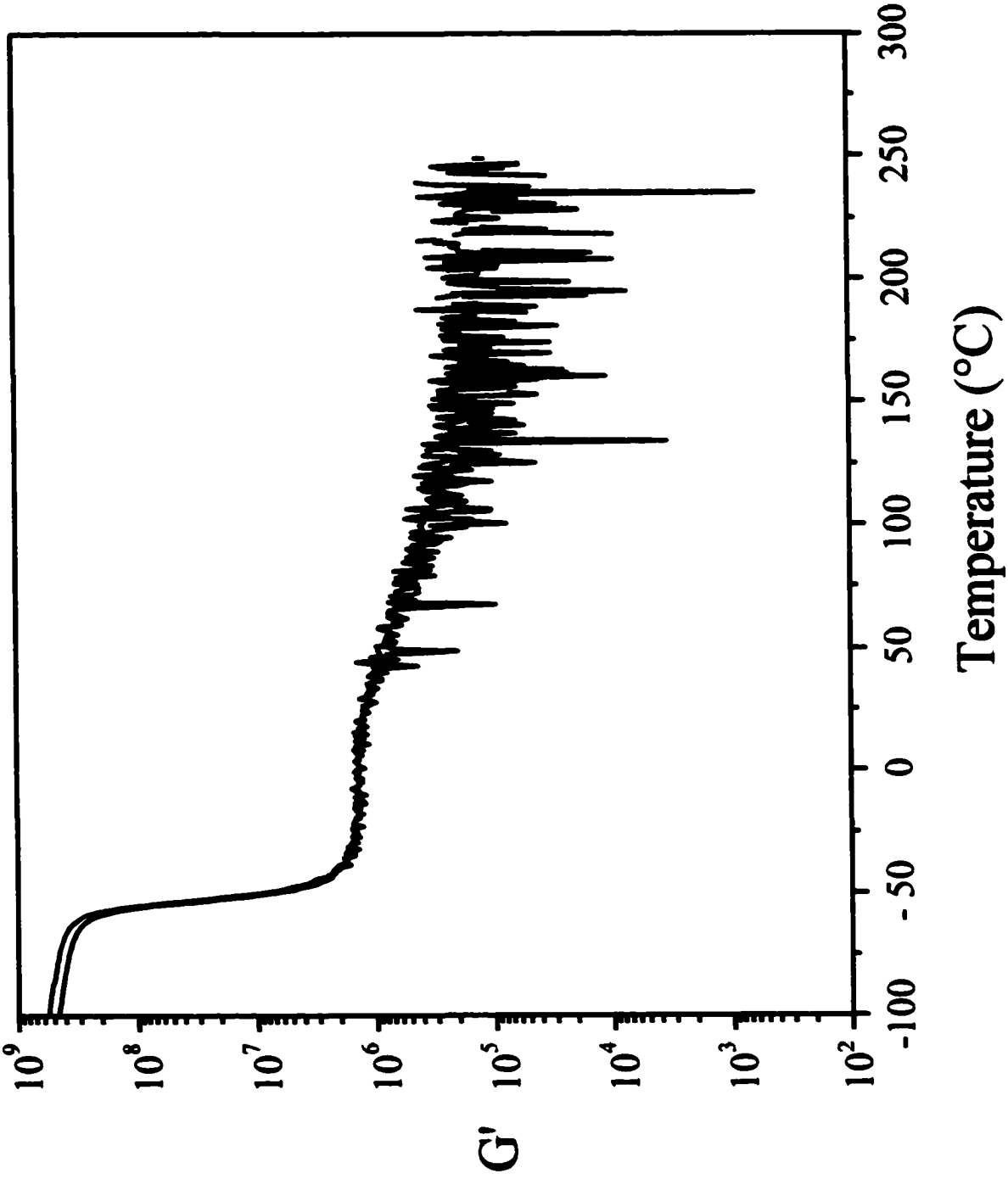

Figure 5.9. Advancing contact angles of water (pH 1) on plasma-oxidized EPDM upon cooling to room temperature after having been annealed to 100 °C (■), 80 °C (○), and 60 °C (◆). Open squares represent reconstruction of the EPDM-ox at room temperature. The error bars indicate one standard deviation above and below the average.

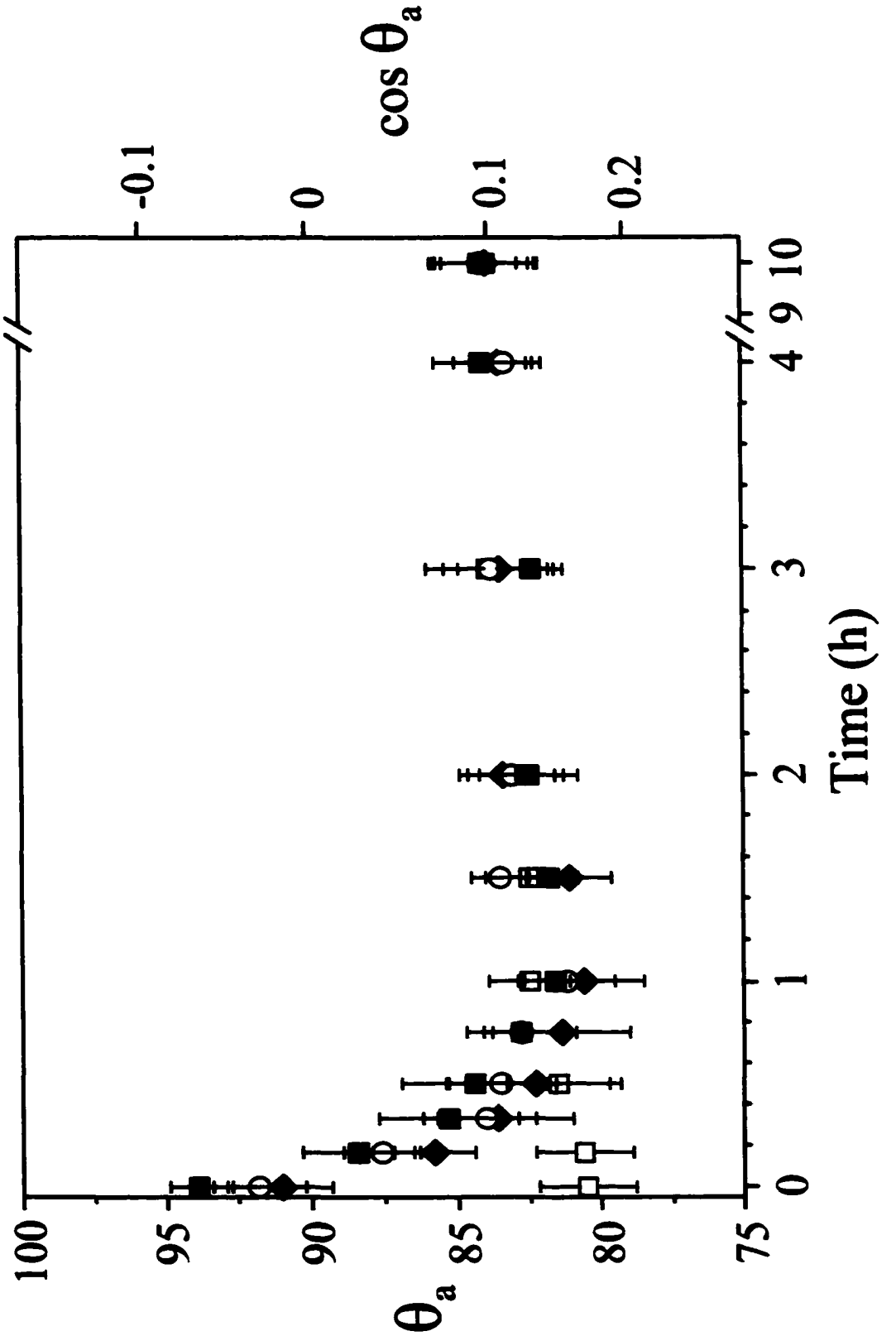

temperatures. As expected, a larger change in wettability was observed for samples annealed at higher temperature, consistent with our hypothesis. The sample annealed at 100 °C had the highest initial contact angle of water (~ 94°). No differences in the minimum contact angle of water were observed for the EPDM-ox samples after the subsequent reconstructions when the sample were cooled to room temperature.

We also systematically studied the influence of temperature in the cooling phase of the reconstruction. Figure 5.10 shows the reconstruction of EMPD-ox (M_c = 7700 g/mol) at various temperatures, for samples that had been annealed at 100 °C under N_2 overnight. As expected, no significant change in wettability, $|\Delta\theta_a|$ = 3°, was observed when EMDP-ox was equilibrated at 60 °C. At 40 °C and 30 °C, the extent of reconstruction became finite, with $|\Delta\theta_a|$ increasing to 5° and 6°, respectively. The reconstruction became significant when EPDM-ox samples were cooled against air at room temperature. A value of $|\Delta\theta_a|$ of 12° resulted after 1 h in the air. An even more significant reconstruction was observed when the EPDM-ox was cooled against N_2 at 15 °C. In this experiment, the EPDM-ox was placed under N_2 in a sealed pressure tube in a 15 °C water bath to cool from 100 °C. As shown in Figure 5.10, the advancing contact angle of water on this surface dropped from 94° to 77° in 10 min and reached a limiting value of 73 °C after 20 min. When samples were cooled in N_2 to 0 °C, the contact angle of water reached an even lower value of 72°. Similar results were obtained for a sample with an M_c of 7000 g/mol (Figure 5.11).

To test the influence of water condensation during the reconstruction, we conducted repeated runs of reconstruction of EPDM-ox (M_c = 7000 g/mol) with the

Figure 5.10. Advancing contact angles of water (pH 1) on plasma-oxidized EPDM (M_c = 7700 g/mol) upon cooling to 60 °C (●), 40 °C (◇), 30 °C (●), room temperature (□), 15 °C (◆), 10 °C (○) and 0 °C (■) having been annealed to 100 °C. The error bars indicate one standard deviation above and below the average.

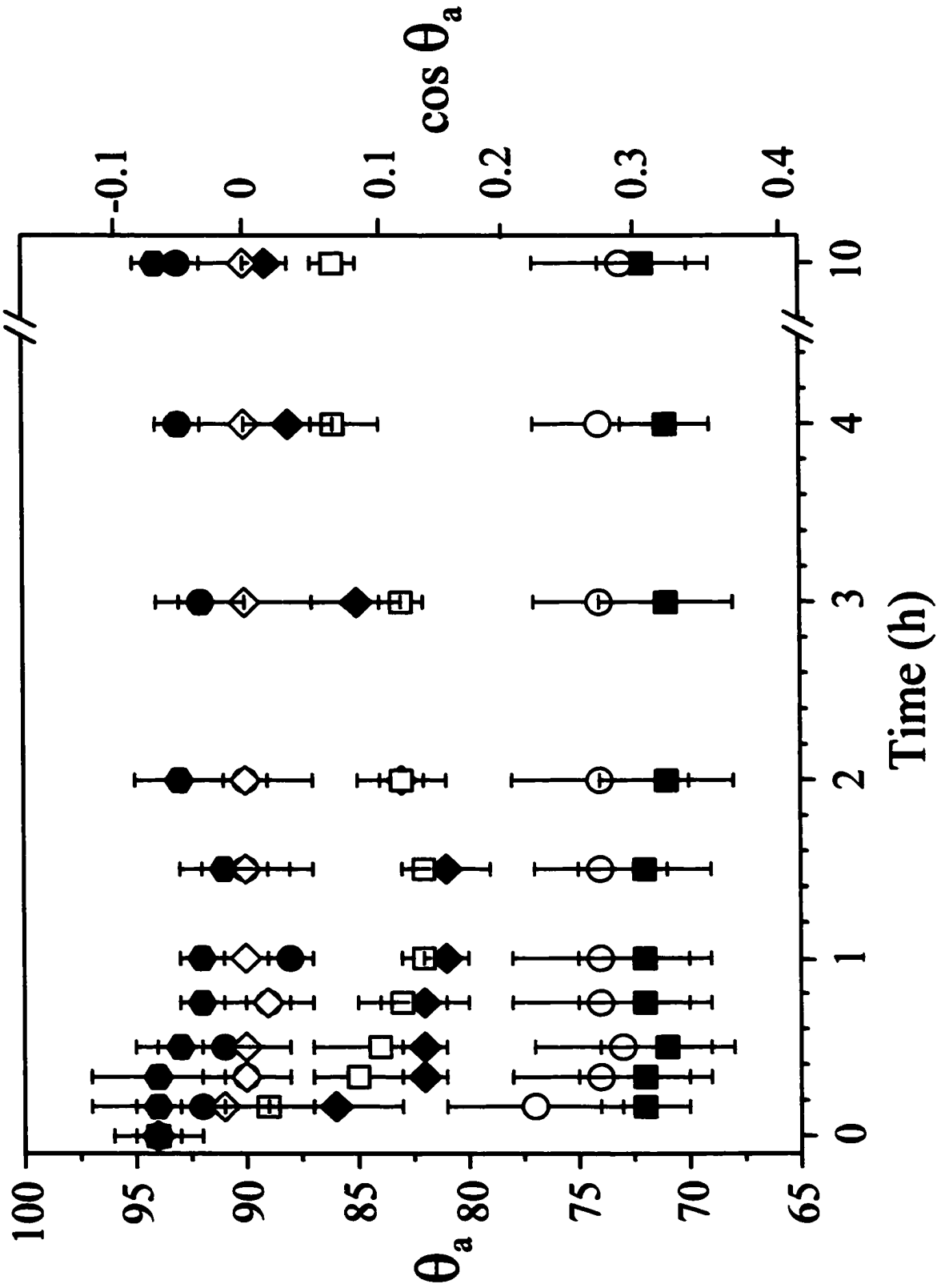

Figure 5.11. Advancing contact angles of water on plasma-oxidized EPDM (M_c = 7000 g/mol) upon cooling to 60 °C (■), room temperature (○), and 0 °C (□) after havng been annealed to 100 °C. Diamonds (filled) presents contact angles taken from individual samples at 0 °C as a function of time. The error bars indicate one standard deviation above and below the average.

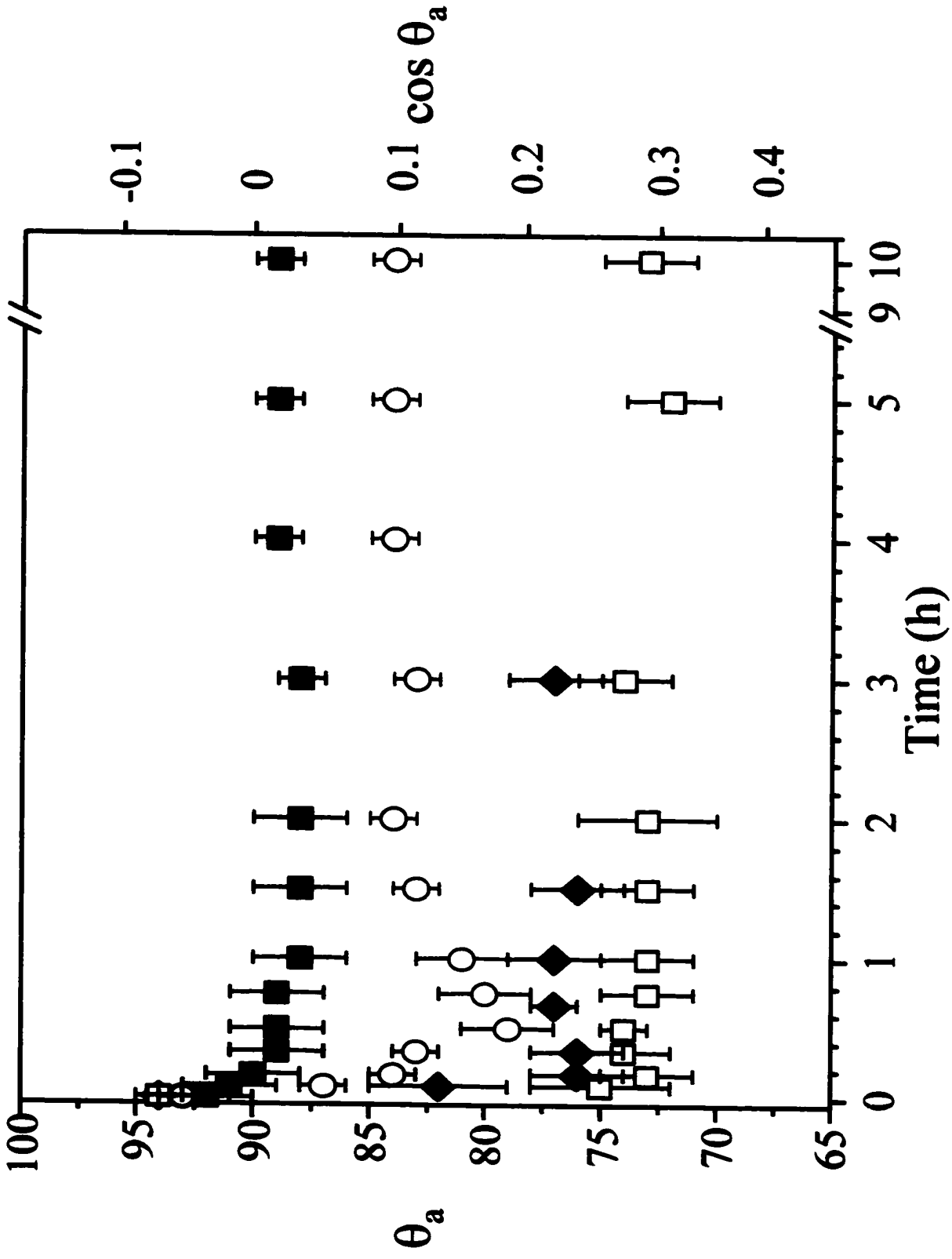

samples equilibrated in pressure tubes at 0 °C, this measurement of wettability was done using a separate sample for times at 5, 10, 30, 40, 60, and 180 min. As shown in Figure 5.11, the EPDM-ox did not reach the limiting values until 10 minutes at 0 °C. No significant difference was

observed between contact angles of water on a single sample compared with individual samples at various period of time. The advancing contact angle of water (pH1) indicated that the reconstruction should not be affected by cooling the pressure tube in a 0 °C water bath.

5.4 Conclusions

The water-plasma treatment on EPDM produced a surface with oxygen-containing functionality. These polar groups were buried when the substrate was heated at elevated temperature, resulting in a hydrophobic surface. Upon cooling, the surface became more hydrophobic due to these polar groups initially migrating to the surface, before again becoming slightly more hydrophobic. The magnitude of changes in wettability depended on the crosslinking density and on temperature. These results complement those of Steve Grunzinger with polyisoprene.[6]

5.5 Experimental Methods

5.5.1 *Materials.* EPDM (Vistalon 6505, M_n = 90,000 and M_w = 234,000) was obtained from Exxon. Absolute ethanol (McCormick Distilling Co.), dicumyl peroxide (98%, Aldrich) and hexanes (Fisher, 99.9+%) were used as received.

5.5.2 *Sample Preparation.* 10.0 grams of EPDM (Vistalon 6505 from Exxon, M_n =

90,000 and M_w = 234,000) were dissolved in 200 mL of hexanes and stirred overnight. For crosslinking, the required amount of dicumyl peroxide was added to the polymer solution, and the solution was stirred for another 6 h. The solvent was then removed under vacuum until a constant weight was observed, and the mixture was pressed within an hour. Two polished aluminum plates (10 cm x 10 cm) were cleaned by soaking in hexanes overnight. A cardboard frame with a thickness of ~1 mm was cut to the dimensions of the plates, and a hole (8 cm x 8 cm) was cut in the frame to serve as a mold. The EPDM with dicumyl peroxide was then cured at 150 °C using a Tetrahedron press set at 1.0 klb of force. The curing time was set to 84 min (8 half-lives).[16] The cured film was peeled away from the aluminum plates and then cut into pieces (~1.0 cm x 2.5 cm). The samples were then soaked in 20 mL of hexanes for at least 2 d to extract the unbound fraction (~ 4 wt%). The solvent was the removed under vacuum at room temperature until the sample reached a constant weight.

5.5.3 *Surface Modification.* The EPDM surface was first annealed at 60 °C for overnight and then modified by water-plasma oxidation. Samples were treated for 20 s with a water-vapor (0.1 Torr) plasma, produced in a 250-mL round bottom flask with a Tesla coil. Advancing contact angles of water (pH 1) were used to monitor the surface modification.

5.5.4 *Surface Reconstruction.* After water-vapor-plasma treatment, the samples were then heated in a sealed tube under N_2 at 60 °C for overnight to allow the reconstruction to a steady state. Contact angle of water (pH 1) was again used to monitor the reconstruction when the samples were cooled to room temperature in air (or nitrogen,

as noted).

5.5.5 *X-ray Photoelectron Spectroscopy.* The XPS spectra in this paper were obtained using a Scienta ESCA-300 spectrometer, equipped with a rotating anode (Al Kα) source producing 6.0 kW of x-ray power, a monochromator, and 300-mm (diameter) hemispherical analyzer. All spectra were collected at a take-off angle of 15° and 90° between the plane of the surface and the detector, a slit width of 0.8 mm, and were referenced to the C 1s peak set at 285.0 eV. The background pressure in the sample chamber was $2x10^{-9}$ Torr. Survey scans were collected with a pass energy of 300 eV and a step energy of 1.0 eV, and took 5.5 min to complete. High-resolution spectra were the sum of two scans collected with a pass energy of 150 eV and a step energy of 0.05 eV. Under these conditions, a single scan took 4.6 min to complete. For quantitative analysis, the sensitivity factors used to correct the number of counts under each peak (or envelope) were: O 1s, 2.8370 and C 1s, 1.000. The sensitivity factors for oxygen and carbon are based on data in reference 13 and were verified by A. C. Miller with the Scienta ESCA-300 at Lehigh University.

5.5.6 *Contact-Angle Measurements.* Contact-angle measurements were made with water (pH 1 or pH 13) using a Rame-Hart NRL Model 100 goniometer at room temperature. A minimum of eight measurements on four independent drops were made for each sample. For annealed samples, the measurement was done within 2 min after moving from the oven. For comparison contact angle measurements were also taken on annealed samples without cooling. The difference between a 2-min cooled sample and an uncooled sample was within 2°.

5.5.7 *Dynamic Mechanical Measurements.* Dynamic mechanical testing was carried out using a Rheometric Dynamic Analyzer (RDA-II). Samples were cut to rectangular geometry (30 mm x 10 mm x 1 mm) for tensional measurements. The entanglement modulus was measured at a frequency of 1.0 Hz while sweeping the temperature from −100 to 200 °C with a ramp rate of 5 °C/min at a constant strain of 0.1%. The manufacturer's software was used to control the test and to analyze the data.

5.6. Acknowledgements

We gratefully acknowledge the support for these Studies from the Office of Research (ONR). We also thank National Science Foundation and industrial partners for support of this research through the Polymer Interfaces Center, an Industry/University Cooperative Research Center at Lehigh University. In addition, we thank Lehigh University for support of the Scienta ESCA facility and A. C. Miller for technical assistance and helpful discussions.

5.7 References and Notes

1. For a review, see Ferguson, G. S.; Whitesides, G. M. in *Modern Approaches to Wettability: Theory and Applications*; M. Schroeder, G. Loeb, Eds., Plenum: New York, 1992, and references therein.
2. Carey, D. H.; Ferguson, G. S. *Macromolecules*, **1994**, *27*, 7254.
3. Carey, D. H.; Grunzinger, S. J. ; Ferguson, G. S. *Macromolecules*, **2000**, *33*, 8802.
4. Khongtong, S.; Ferguson, G. S, *J. Am. Chem. Soc.* **2001**, *123*, 3588-3594.
5. Khongtong, S.; Ferguson, G. S, submitted to *J. Am. Chem. Soc.*

6. Grunzinger, S. J.; Ferguson, G. S., *J. Am. Chem. Soc.*, ASAP.

7. Sperling, L. H. *Introduction to Physical Polymer Science,* 2nd ed.; John Wiley & Sons: New York, 1992.

8. Queslel, J. P.; Mark, J. E. *J. Chem. Phys.* **1985**, *82*, 3449-3452.

9. Hrnjak-Murgić, Z. ; Jelenčić, J.; Bravar, M. *Kautsch. Gummi, Kunstst.* **1990**, 43, 940-942.

10. Hrnjak-Murgić, Z. ; Jelenčić, J.; Bravar, M. Marović, M. *Kautsch. Gummi, Kunstst.* **1990**, 43, 940-942.

11. Mong-Tung Lee, Particia L. Kennedy, Lori E. Stephans, and Gregory S. Ferguson, paper in preparation.

12. (a) Morra, M.; Occhiello, E.; Gila, L.; Garbassi, F. *J. Adhesion* **1990**, *33*, 77-88. (b) Yao, Y.; Liu, X.; Zhu, Y. *J. Adhes. Sci. Technol.* **1993**, *7*, 63-75.

13. Peak assignments were made with reference to: Beamson, G.; Briggs, D., High-Resolution XPS of organic Polymers, The Scienta ESCA300 Database; John Wiley and Sons: New York, 1992.

14. Litvinov, V. M.; Barendswaard, W.; van Duin, M. *Rubber Chem. Technol.* **199?**, *71*, 105-118.

15. (a) Flory, P. J. Proc. R. Soc. London, Ser. A. 1976, 351, 351. (b) Sperling, L. H. *Introduction to Physical Polymer Science,* 2nd ed.; John Wiley & Sons: New York, 1992, p401.

16. Branddrup, J.; Immergut, E. H. Grulke, E. Polymer handbook, 4th ed.; John Wiley & Sons: New York, 1999.

Vita

Mong-Tung Lee was born in Taipei, Taiwan, R. O. C. on the 7th of April 1969. He is the first son of Kung-Ching Lee and Ky Cheng.

After graduating from Taipei Cheng-Kung Senior High School in 1987, he attended Tamkang University, where he received his Bachelor of Science degree in Applied Chemistry in June 1991. In August 1993, after he worked two years as a research associate in the Academia Sinica, he joined the Department of Chemistry of University of Massachusetts at Lowell and received his Master of Science degree in 1995.